

# Molecular interactions of archazolid with the V-ATPase

## Dissertation

zur Erlangung des akademischen Grades

**Doctor rerum naturalium**

(Dr. rer. nat.)



Fachbereich Biologie/Chemie der Universität Osnabrück

vorgelegt von

**Svenja Bockelmann**

Wallenhorst, August 2011



**Table of contents**

1.	Introduction.....	1
1.1	Ion translocating ATPases.....	1
1.2	The structure and function of V-ATPases.....	2
1.2.1	Subunit composition of the V <sub>1</sub> complex .....	4
1.2.2	Subunit composition of the V <sub>O</sub> complex .....	5
1.2.3	The mechanism of ion translocation .....	7
1.3	Assembly and targeting of V-ATPases .....	8
1.4	Regulation of V-ATPases by reversible dissociation.....	9
1.5	The role of V-ATPases in physiology and pathophysiology .....	10
1.5.1	The V-ATPase in the midgut of <i>Manduca sexta</i> .....	11
1.5.2	The V-ATPase of <i>Saccharomyces cerevisiae</i> .....	11
1.5.3	The mammalian V-ATPase and its impact on human pathophysiology.....	13
1.6	Inhibitors of the V-ATPase .....	14
1.6.1	Plecomacrolide inhibitors: The beginning of V-ATPase inhibitor studies..	15
1.6.2	Benzolactone enamides: Species specific V-ATPase inhibition .....	17
1.6.3	Archazolids: A novel class of V-ATPase inhibitors .....	18
1.7	Objective of the thesis .....	19
2.	Material and Methods .....	20
2.1	Material .....	20
2.1.1	Chemicals and reagents.....	20
2.1.2	Culture media.....	20
2.1.3	<i>Escherichia coli</i> strains .....	21
2.1.4	<i>Saccharomyces cerevisiae</i> strains .....	21
2.1.5	Plasmids .....	22
2.1.6	Oligonucleotides .....	22
2.1.7	Animals .....	25
2.1.8	Inhibitors .....	25
2.2	Molecular biological and genetic methods.....	26
2.2.1	Transformation of DNA in chemical competent <i>Escherichia coli</i> .....	26
2.2.2	Preparation of plasmid DNA from <i>Escherichia coli</i> .....	27
2.2.3	Restriction and ligation of DNA .....	27
2.2.4	Agarose gel-electrophoresis and DNA extraction .....	27
2.2.5	Amplification of DNA .....	27
2.2.6	Preparation of genomic DNA from <i>Saccharomyces cerevisiae</i> .....	27

## Table of contents

---

2.2.7	Transformation of DNA in <i>Saccharomyces cerevisiae</i> .....	28
2.2.8	Spotting growth assay .....	28
2.2.9	Construction of a <i>vma3</i> deletion strain .....	28
2.2.10	Site-directed mutagenesis .....	28
2.2.11	Other methods .....	29
2.3	Biochemical methods .....	30
2.3.1	Preparation of vacuoles from <i>Saccharomyces cerevisiae</i> .....	30
2.3.2	Purification of <i>Manduca sexta</i> V <sub>1</sub> V <sub>O</sub> holoenzyme and V <sub>O</sub> complex .....	30
2.3.3	Determination of protein concentration .....	31
2.3.4	V-ATPase activity assay and determination of inorganic phosphate .....	31
2.3.5	Protein precipitation with trichloric acid .....	32
2.3.6	SDS-PAGE and Coomassie staining .....	32
2.3.7	Electroblotting and immunostaining .....	33
2.3.8	Vacuolar staining in <i>Saccharomyces cerevisiae</i> .....	33
2.3.9	Labeling of the <i>Manduca sexta</i> V-ATPase with NCD-4 .....	34
2.3.10	Photo affinity labeling of the <i>Manduca sexta</i> V-ATPase .....	34
2.4	Electron paramagnetic resonance (EPR) spectroscopy .....	35
2.4.1	Protein preparation for EPR measurements .....	35
2.4.2	Continuous wave ( <i>cw</i> ) EPR spectroscopy .....	36
2.4.3	Distance measurements via four-pulse double electron electron resonance (DEER) .....	36
2.5	Computational methods .....	37
3.	Results .....	38
3.1	Site-directed mutagenesis of the <i>VMA3</i> gene in <i>Saccharomyces cerevisiae</i> .....	38
3.1.1	Site-directed mutagenesis of <i>VMA3</i> .....	38
3.1.2	Influence of mutations on cell growth and vacuolar acidification .....	39
3.1.3	Assembly and activity of the mutant V-ATPase .....	40
3.1.4	Influence of mutations on inhibitor binding .....	41
3.2	Photo affinity labeling of the <i>Manduca sexta</i> V-ATPase .....	44
3.2.1	PAL derivatives of archazolid .....	44
3.2.2	Binding of PAL derivatives to subunit c of the V-ATPase .....	45
3.3	Fluorescent labeling of the <i>Manduca sexta</i> V-ATPase .....	47
3.3.1	Binding competition of archazolid with NCD-4 at subunit c .....	47
3.3.2	Suppression of archazolid binding monitored with NCD-4 labeling .....	48
3.4	Influence of further mutations within the proposed archazolid binding site .....	50
3.4.1	Selection of amino acid residues for site-directed mutagenesis .....	50
3.4.2	Influence of mutations on cell growth and vacuolar acidification .....	50

3.4.3	Assembly and activity of the mutant V-ATPase.....	51
3.4.4	Influence of mutations on inhibitor binding .....	52
3.5	Double mutation in <i>VMA3</i> and mutagenesis of <i>VMA11</i> .....	54
3.5.1	Selection of amino acid residues for site-directed mutagenesis .....	54
3.5.2	Influence of mutations on cell growth and vacuolar acidification.....	54
3.5.3	Assembly and activity of the mutant V-ATPase.....	55
3.5.4	Influence of mutations on inhibitor binding .....	56
3.6	Inhibition of mutant V-ATPases by derivatives of archazolid.....	58
3.6.1	Selection of archazolid derivatives .....	58
3.6.2	Influence of structural differences on inhibition of the yeast V-ATPase ....	58
3.7	Biological activity of novel archazolid derivatives.....	61
3.8	EPR spectroscopy as a tool for the study of inhibitor binding to the V-ATPase	62
3.8.1	Binding properties of spin-labeled V-ATPase inhibitors.....	62
3.8.2	Binding of spin-labeled inhibitors to the <i>Saccharomyces cerevisiae</i> V-ATPase.....	64
3.9	Distance measurements on the c ring of the V-ATPase.....	66
4.	Discussion.....	69
4.1	Inhibitor binding to the V-ATPase $V_O$ complex .....	69
4.2	The plecomacrolide binding site in <i>Saccharomyces cerevisiae</i> .....	70
4.3	The binding site of archazolid.....	73
4.3.1	Location of the binding site within the $V_O$ ring.....	73
4.3.2	Contribution of single amino acid residues .....	75
4.3.3	Involvement of the essential glutamate.....	78
4.3.4	Contribution of the inhibitor structure .....	79
4.4	A proposed binding mechanism.....	81
4.4.1	Archazolid interferes with the proton translocation mechanism .....	81
4.4.2	Does archazolid prevent rotation of the c ring?.....	83
4.5	Design of more specific derivatives .....	84
4.6	Toward the structure of the c ring .....	85
4.6.1	Using V-ATPase inhibitors to elucidate the c ring stoichiometry .....	85
4.6.2	Considerations about the physiological impact of the c ring stoichiometry	86
5.	Summary.....	89
6.	References.....	91
7.	Appendix.....	102
7.1	Abbreviations .....	102
7.2	Vector maps.....	103
7.3	Curriculum Vitae.....	104

***Table of contents***

---

7.4	Publications .....	105
7.5	Erklärung über die Eigenständigkeit der erbrachten wissenschaftlichen Leistung .....	106
8.	Acknowledgements.....	107

## 1. Introduction

The development of highly efficient drugs is a fundamental challenge for progress in modern medicine. A detailed understanding of how drugs interact with their biological target molecules extends the possibilities to optimize drug efficiency and minimize harmful side effects. Furthermore, growing knowledge of the molecular basis of severe diseases uncovers novel promising therapeutic target molecules. Throughout the past years the vacuolar H<sup>+</sup>-ATPase (V-ATPase), besides its fundamental role in normal cellular processes, has been shown to be involved in a variety of severe diseases such as cancer and osteopetrosis (Hinton *et al.*, 2009; Sennoune and Martinez-Zaguilan, 2007). For this reason the research on the suitability of the V-ATPase as a new target for disease therapy is emerging (Bowman and Bowman, 2005; Fais *et al.*, 2007; Niikura, 2006). One aspect of this research is the discovery and development of highly efficient, tissue specific inhibitors of the V-ATPase and a detailed understanding of the enzyme-inhibitor interaction at the molecular level.

### 1.1 Ion translocating ATPases

Vacuolar ATPases belong to the class of ion-translocating ATPases which also comprises the A-, F- and P-type ATPases. All these enzymes are molecular machines that use the ubiquitous energy storage molecule ATP to create ion motive force, or in some cases vice versa.

Compared to the other representatives of this protein class, the P-ATPases are quite small and simple in structure consisting of one major catalytic subunit ( $\alpha$ -subunit) which is in some cases combined with additional subunits without catalytic function (Chan *et al.*, 2010). P-ATPases are a large and versatile protein family which contributes to a variety of membrane transport processes in eukaryotes and prokaryotes. One major example of this family is the Na<sup>+</sup>/K<sup>+</sup>-ATPase in plasma membranes of mammalian cells which consists of an  $\alpha$ -subunit associated with an auxiliary  $\beta$ -subunit, and can be modulated by an additional  $\gamma$ -subunit under stress conditions (Chan *et al.*, 2010). The Na<sup>+</sup>/K<sup>+</sup>-ATPase extrudes three Na<sup>+</sup> ions in exchange for two K<sup>+</sup> ions at the expense of one ATP molecule, thereby creating an electrochemical gradient that is necessary for e.g. electric excitability and secondary transport processes (Kühlbrandt, 2004; Morth *et al.*, 2007). Other important examples of P-ATPases are the sarcoplasmic reticulum Ca<sup>2+</sup>-ATPase that contributes to the contraction of muscle cells and the H<sup>+</sup>/K<sup>+</sup>-ATPase that is responsible for the acidification of the stomach (Kühlbrandt, 2004).

In contrast to P-ATPases, the F-type ATPases are large, multi-subunit enzymes that use the transmembrane ion motive force, generated for example by respiratory complexes in mitochondrial and bacterial membranes, to produce ATP from ADP and inorganic phosphate. Therefore these enzymes are also called ATP synthases (Junge and Nelson, 2005; Stock *et al.*, 2000). The ATP synthases are organized in two complexes, a cytosolic F<sub>1</sub> part and a membrane-embedded F<sub>0</sub> complex. In the case of the comparatively simple *Escherichia coli* enzyme, F<sub>1</sub> comprises five different subunits with the stoichiometry  $\alpha_3\beta_3\gamma_1\delta_1\epsilon_1$  and F<sub>0</sub> is composed of three subunits with the stoichiometry  $a_1b_2c_{9-12}$  (Stock *et al.*, 2000). The synthesis of ATP is first of all driven by the F<sub>0</sub> complex that

translocates either protons or, in some bacteria, sodium ions across the membrane via rotation of a ring of c subunits. This rotational movement is then mechanically transferred to the F<sub>1</sub> complex via a central stalk built up by the subunits  $\gamma$  and  $\epsilon$  (in *E. coli*) and finally results in the synthesis of ATP at the catalytic  $\beta$  subunits that are arranged in an alternating hexamer with the  $\alpha$  subunits in F<sub>1</sub> (Junge and Nelson, 2005; Stock *et al.*, 2000). Besides the central stalk, a peripheral one (subunits b and  $\delta$  in *E. coli*) is present which is proposed to prevent rotation of the  $\alpha/\beta$ -hexamer during ATP synthesis (Stock *et al.*, 2000).

Because of a quite similar overall structure and mechanism of action, the F- and V-type ATPases are proposed to originate from a common ancestor (Mulikidjanian *et al.*, 2007; Müller and Grüber, 2003). Likewise, the two major protein complexes present in the V-ATPases are denoted as V<sub>1</sub> (cytosolic) and V<sub>O</sub> (membrane-bound) complex. V-ATPases are mainly found in membranes of intracellular compartments such as vacuoles, lysosomes or secretory vesicles of eukaryotic cells, playing a key role in pH regulation and membrane energization. In addition, V-ATPases sorted to the plasma membrane contribute to special functions of various cell types such as bone resorption mediated by osteoclasts (Beyenbach and Wieczorek, 2006; Forgac, 2007). Despite general similarities, V-ATPases exhibit many unique features that distinguish them from F-ATPases (Mulikidjanian *et al.*, 2007; Müller and Grüber, 2003). One main difference is that V-ATPases function as ATP-driven proton pumps under normal cellular conditions, as opposed to ATP synthesis observed for F-ATPases. Another fundamental difference is the regulation of V-ATPases by reversible dissociation of the V<sub>1</sub> and the V<sub>O</sub> complex (see paragraph 1.4) which has not been observed in F-ATPases (Müller and Grüber, 2003).

In addition to the enzyme types presented above, another group of ATPases that resemble the general structure and function of the F- and V-ATPases is described. These enzymes were first identified in archaea and are therefore referred to as A-ATPases, composed of an A<sub>1</sub> and an A<sub>O</sub> complex (Müller and Grüber, 2003). Nevertheless, these enzymes are also found in a variety of bacteria like e.g. *Enterococcus hirae* or *Thermus thermophilus* (Iwata *et al.*, 2004; Murata *et al.*, 2005). In addition, some authors argue that these enzymes represent more a subclass of the V-ATPases rather than a distinct family and therefore they are in some cases also referred to as prokaryotic V-type ATPases (Yokoyama and Imamura, 2005). The main difference between the A- and V-ATPases is that the A-ATPases synthesize ATP *in vivo* similar to F-ATPases and that they do not seem to be regulated by reversible dissociation (Grüber and Marshansky, 2008; Müller and Grüber, 2003).

### 1.2 The structure and function of V-ATPases

During the past ten years the fragmentary picture of the structure of V-ATPases became more and more clear mainly due to improved electron microscopy techniques (Muench *et al.*, 2009; Zhang *et al.*, 2008) and an increasing number of crystal structures of single subunits (Drory *et al.*, 2004; Murata *et al.*, 2005; Sagermann *et al.*, 2001). Since a detailed picture of the structural composition of V-ATPases is a prerequisite to explain the



functional mechanism of these enzymes, the understanding of the complexity of V-ATPase function is emerging.

To date, the most accurate model of the whole V-ATPase complex comes from cryo-electron microscopic studies on the V-ATPase isolated from the midgut of the tobacco hornworm, *Manduca sexta* (Muench *et al.*, 2009), which is a frequently used model organism for biochemical studies on this enzyme (Wieczorek *et al.*, 2000). The three-dimensional reconstruction of this enzyme at a resolution of 16.5 Å clearly shows the distinct  $V_1$  and  $V_O$  complexes with four stalk structures (Muench *et al.*, 2009; Fig. 1.1A and B). One of these stalks is located in the center of the enzyme and resembles the central stalk described also for F-ATPases. The other stalks (S1, S2 and S3, see Fig. 1.1B) reside at the periphery. Two of them extend from the  $V_1$  to the  $V_O$  complex while the third one (S2) ends up halfway down from the  $V_1$  to the  $V_O$  complex where it joins a collar-like structure that surrounds part of the V-ATPase and connects all three peripheral stalks (Muench *et al.*, 2009; Fig. 1.1A and B). Three peripheral stalks are also expected from a model of the yeast V-ATPase at a resolution of 25 Å obtained by negative stain electron microscopy (Zhang *et al.*, 2008; Fig. 1.1C), while reconstructions of the bovine (34 Å resolution) and the *Neurospora crassa* (20 Å resolution) V-ATPase could resolve only two of them (Gregorini *et al.*, 2007; Venzke *et al.*, 2005). The presence of multiple peripheral stalks in V-ATPases again distinguishes them from F-ATPases where only one outer stalk is observed.

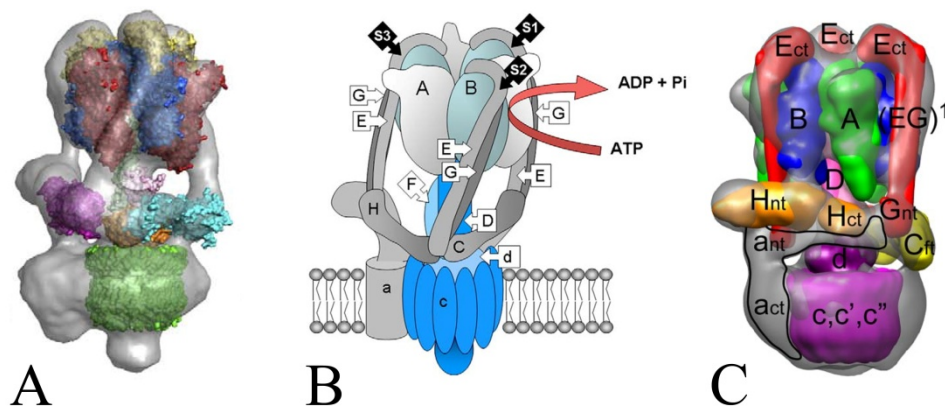


**Figure 1.1: Three-dimensional models of the V-ATPase from *Manduca sexta* and *Saccharomyces cerevisiae*.**

(A) 3D reconstruction of the *M. sexta* V-ATPase at a resolution of 16.5 Å obtained by cryo-electron microscopy with known crystal structures of V- and A-type ATPase subunits fitted (Muench *et al.*, 2009). (B) Schematic model of the V-ATPase from Muench *et al.* (2009). Capital letters,  $V_1$  subunits; lower case letters,  $V_O$  subunits; S1 to S3 indicating the three peripheral stalks formed by EG dimers. Red arrow indicates the site of ATP hydrolysis at the A/B interfaces. (C) 3D model of the V-ATPase from *S. cerevisiae* at a resolution of 25 Å derived from negative stain electron microscopy (Zhang *et al.*, 2008). Capital letters,  $V_1$  subunits; lower case letters,  $V_O$  subunits; ct, C terminal; nt, N terminal; ft, foot domain; (EG)<sup>1</sup> indicating one EG dimer. Colored regions represent yeast homology models and crystal structures of subunits fitted to the 3D reconstruction.

**Table 1.1: Subunit composition of rotary ATPases.**

Summarized are examples for the subunit composition of all three different types of rotary ATPases. Molecular masses of the subunits are given exemplarily for the *M. sexta* and *S. cerevisiae* V-type ATPase. n. f. = not found. The A-ATPase proteolipid subunits are referred to as c, K and L, respectively. For clarity, in this study the label “c subunit” will also be used for the A-ATPase proteolipids. Adapted according to Forzac (2007) and Muench *et al.* (2011).

Subunit	Molecular Mass (kDa) <i>M. sexta</i> / <i>S. cerevisiae</i>	Subunit names and composition			
		V-ATPase <i>M. sexta</i>	V-ATPase <i>S. cerevisiae</i>	A-ATPase <i>Prokaryotic</i>	F-ATPase <i>E. coli</i>
<b>V<sub>1</sub> complex</b>	<b>741 / 666</b>			<b>A<sub>1</sub></b>	<b>F<sub>1</sub></b>
A	69 / 70	A	Vma1	A	β
B	55 / 55	B	Vma2	B	α
C	44 / 40	C	Vma5		
D	28 / 34	D	Vma8	D	γ
E	26 / 33	E	Vma4	E	δ
F	14 / 14	F	Vma7	F	ε
G	13 / 13	G	Vma10	H	b
H	50 / 55	H	Vma13		
<b>V<sub>0</sub> complex</b>	<b>176 / 253</b>			<b>A<sub>0</sub></b>	<b>F<sub>0</sub></b>
a	100 / 100	a	Vph1, Stv1	I	a
c	16 / 17	c	Vma3	c, K, L	c
c′	n. f. / 17		Vma11		
c″	n. f. / 21		Vma16		
d	40 / 38	d	Vma6	C	
e	20 / 9	e	Vma9		

### 1.2.1 Subunit composition of the V<sub>1</sub> complex

The V<sub>1</sub> complex consists of eight different subunits with the proposed stoichiometry A<sub>3</sub>B<sub>3</sub>C<sub>1</sub>D<sub>1</sub>E<sub>3</sub>G<sub>3</sub>H<sub>1</sub> (Kitagawa *et al.*, 2008). The structure of the V<sub>1</sub> complex of the *M. sexta* V-ATPase was already resolved at high resolution by Radermacher *et al.* (2001) using electron microscopy of single particles. The resulting three-dimensional model clearly visualizes a hexagonal shape of the V<sub>1</sub> headpiece representing the alternating arrangement of the catalytic A and the noncatalytic B subunits (Radermacher *et al.*, 2001). In analogy to the structure of F<sub>1</sub> in F-ATPases, the cleavage of ATP is proposed to occur at the A/B interface (subunit B oriented clockwise to A) with major contributions from amino acid residues in subunit A (Abrahams *et al.*, 1994; Muench *et al.*, 2009).

In the current model of the *M. sexta* V-ATPase the B subunits are the anchor points for the three peripheral stalks that consist of one copy of subunits E and G each (Muench *et al.*, 2009; Fig. 1.1A and B). All three EG-stalks merge with the collar structure composed of subunits C and H that is located just above the membrane bilayer. The whole stalk construct is on the one hand presumed to prevent rotation of the V<sub>1</sub> complex during proton transport as it has been proposed for the single stalk structure in F-ATPases (Muench *et al.*, 2009; Stock *et al.*, 2000). On the other hand, it probably places the subu-

nits C and H in their appropriate positions (Muench *et al.*, 2009) and therefore, it is proposed to assist in the process of reversible dissociation (Muench *et al.*, 2011).

The central stalk that is responsible for energy transduction from the  $V_1$  to the  $V_O$  complex, is composed of subunits F and D plus the  $V_O$  subunit d that probably forms a link between F/D and the  $V_O$  rotor ring (Muench *et al.*, 2009).

### 1.2.2 Subunit composition of the $V_O$ complex

The  $V_O$  complex of *M. sexta* consists of subunits a, d, e and the ring-forming subunit c. The latter, commonly also called proteolipid, is the only subunit present in more than one copy. However, the number of copies in the  $V_O$  ring is still not determined exactly for any known V-ATPase. Regarding the cryo-electron microscopic model of the *M. sexta* V-ATPase, the fitting of different crystal structures revealed the best correlation for the proteolipid ring of the sodium A-ATPase from *Enterococcus hirae* that contains 10 copies of the bacterial homologue of subunit c (Muench *et al.*, 2009; Murata *et al.*, 2005).

It is commonly accepted that the A-, F- and V-ATPase proteolipid subunits derive from a common ancestral gene that underwent gene duplication and fusion in the case of the V-ATPases (Mandel *et al.*, 1988). Accordingly, while the F-ATPases retained two transmembrane helices (TM), each of the V-ATPase c subunits has four and A-ATPases exhibit two to even six TMs (Mandel *et al.*, 1988; Müller and Grüber, 2003). All c subunits contain a highly conserved acidic amino acid residue that is essential for proton translocation. In case of the V-ATPase an essential glutamate residue is located in TM4 (E137 in *S. cerevisiae*; Fig. 1.2A and B) while a second glutamate in TM2 was lost during evolution (Mandel *et al.*, 1988). The essential glutamate within subunit c is a target for *N,N'*-dicyclohexyl-carbodiimide (DCCD; Fig. 1.6E), which is a covalently binding inhibitor widely used for enzyme-inhibitor studies (Finbow *et al.*, 1992; Harrison *et al.*, 2000; Páli *et al.*, 2004b).

In the  $V_O$  ring of fungi, two additional isoforms of subunit c,  $c'$  and  $c''$ , are present in one single copy each (Hirata *et al.*, 1997; Umemoto *et al.*, 1991). Subunit  $c'$  seems to be a unique feature of fungal V-ATPases (Chavez *et al.*, 2006). Like subunit c,  $c'$  also contains four transmembrane helices with the essential glutamate located in TM4 (E145 in *S. cerevisiae*) (Hirata *et al.*, 1997). In contrast, subunit  $c''$  is proposed to possess five transmembrane helices with the essential glutamate located in TM3 (E108 in *S. cerevisiae*) (Powell *et al.*, 2000). The function of the additional helix in  $c''$  (TM1) still remains enigmatic, particularly because it is not required for V-ATPase activity (Nishi *et al.*, 2003). The orientation of helices within the c subunits has been assigned by epitope-tagging and chimeric fusion of proteolipid subunits, revealing that the C and N termini in subunits c and  $c'$  are directed toward the luminal side of the membrane while the N terminus of  $c''$  resides in the cytoplasm (Flannery, 2004). Chimeric fusion proteins were also constructed to elucidate the arrangement of c subunits in the ring, showing that subunit  $c'$  is located adjacent to  $c''$  in counterclockwise direction as viewed from the luminal side of the membrane (Wang *et al.*, 2007; Fig. 1.2C). The overall stoichiometry of the c ring in yeast is proposed to be  $c_4, c'_1, c''_1$  (Nishi *et al.*, 2003; Powell *et al.*, 2000).

In the bovine V-ATPase an accessory subunit (Ac45) of unknown function is described that is proposed to be located at the extra-cytosolic end of the c ring (Gregorini *et al.*, 2007; Supek *et al.*, 1994). This subunit has to date neither been found in fungi, nor in the *M. sexta* V-ATPase (Huss and Wieczorek, 2007; Wilkens *et al.*, 2005). Nevertheless, the *M. sexta* enzyme exhibits a knob-like structure at the extra-cytoplasmic side of the c ring which is similar to the structure observed in the bovine V-ATPase, and could arise from the presence of Ac45 or an equivalent accessory subunit (Muench *et al.*, 2009; Fig. 1.1A and B).

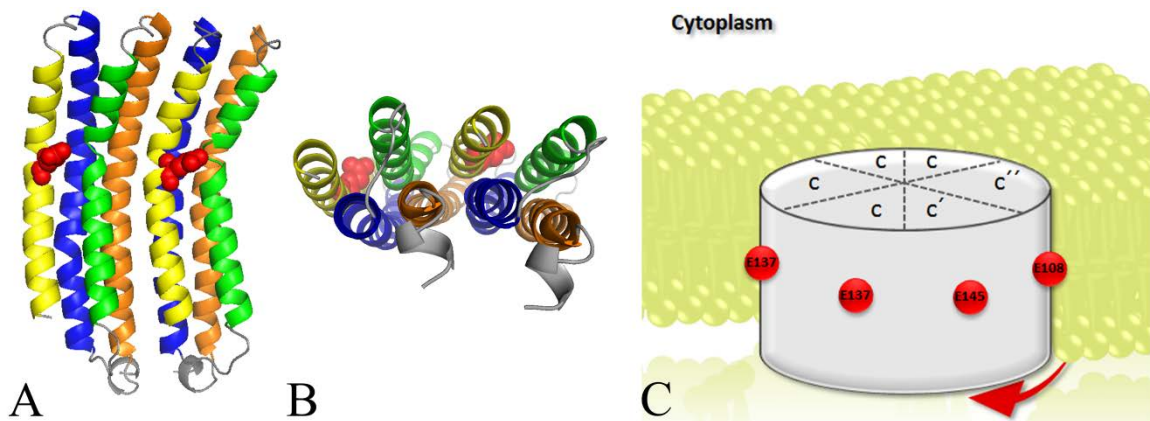


**Figure 1.2: Arrangement of V-ATPase proteolipid subunits.**

(A) and (B) The amino acid sequence of the *S. cerevisiae* c subunit was modeled onto the *E. hirae* c ring structure (Murata *et al.*, 2005) as described in Bockelmann *et al.* (2010). Helical representations of two adjacent c subunits in the ring are presented in a side view (A) and a view from the extra-cytoplasmic side of the membrane (B), respectively. The C and N termini of the c subunits are oriented toward the extra-cytoplasmic side of the membrane (A). An outer ring of helices is formed by transmembrane helices (TM) 4 (yellow) and 2 (green) with TM4 of one c subunit following clockwise to TM2 of the preceding subunit (B). TM3 (blue) and TM1 (orange) form an inner ring with TM3 of one subunit following clockwise to TM1 of the other. The crucial E137 in TM4 is depicted in red spheres. (C) Arrangement of c subunits in the  $V_O$  ring of *S. cerevisiae* according to Wang *et al.* (2007). Simplified representation of the yeast c ring (gray) comprising four c subunits and a single copy of c' and c'', each. Subunit c' is located adjacent and counter-clockwise to c'' as viewed from the extra-cytoplasmic side (red arrow). The glutamate residues essential for proton transport (red) are: E137 (subunit c), E145 (subunit c') and E108 (subunit c'').

Next to the proteolipid subunits, subunit a is also directly involved in proton translocation. The main structural characteristics of this subunit are a hydrophilic N-terminal domain oriented towards the cytoplasm and a C-terminal domain presumably comprising eight TMs (Wang *et al.*, 2008). Subunit a contains a conserved arginine residue, probably located within TM7 in the C-terminal domain, that is essential for proton transport (Kawasaki-Nishi *et al.*, 2001).

Subunits d and e do not seem to be directly involved in proton transport but however, they are indispensable for V-ATPase function (Bauerle *et al.*, 1993; Sambade and Kane, 2004). The eubacterial homologue of subunit d from *Thermus thermophilus* has been shown to form a socket-like structure at the cytoplasmic surface of the  $V_O$  rotor ring (Iwata *et al.*, 2004). The crystal structure of this subunit also fits into the cryo-electron

microscopic model of the *M. sexta* and the yeast enzyme (Fig. 1.1), implying that V-ATPase subunit d connects the  $V_O$  ring to the  $V_1$  subunits F and D, therefore being part of the central rotor (Muench *et al.*, 2009). The function and localization of the membrane-integral subunit e is still not known despite the fact that it was found in the mammalian, insect and yeast V-ATPase (Ludwig *et al.*, 1998; Merzendorfer *et al.*, 1999; Sambade and Kane, 2004).

### 1.2.3 The mechanism of ion translocation

According to their structural similarity, F- and V-ATPases are both thought to function as rotary motors that couple ion transport to ATP synthesis or hydrolysis, respectively (Junge and Nelson, 2005). Evidence for the rotation of V-ATPase subcomplexes came from experiments where beads were attached to either subunit D or F of the central stalk (Imamura *et al.*, 2003) or to subunit c of the proteolipid ring (Yokoyama *et al.*, 2003). After immobilization of either the  $V_1$  complex or the holoenzyme on a glass surface, rotation of the beads was detected, clearly showing that V-ATPases function by rotation of the central stalk and the c ring of the  $V_O$  complex.

Under normal cellular conditions V-ATPases use the energy of ATP hydrolysis to translocate protons across the membrane through rotation of the c ring. Due to the lack of high resolution structures, the detailed mechanism of rotation and energy transmission in V-ATPases is not yet known, but the functional model proposed for the analogous F-ATPase family is widely accepted to be valid also for V-ATPases (Junge and Nelson, 2005; Junge *et al.*, 2009). When adopting this model for V-ATPases, ATP hydrolysis occurs at the A/B interfaces through a “binding change mechanism” (Boyer, 1997), which means that the three equivalent catalytic sites have different alternating states. One of the catalytic sites binds ATP while the second one cleaves ATP and the third one releases ADP and inorganic phosphate ( $P_i$ ). The energy released by hydrolysis of ATP induces conformational changes that are transmitted to the  $V_O$  complex via rotation of the central stalk in steps of  $120^\circ$  per ATP molecule. Rotation of the central stalk finally results in rotation of the c ring that transduces protons via its essential glutamate residues through interaction with subunit a. During rotation of the central stalk and the c ring, also referred to as the “rotor complex”, accompanying movement of the A/B hexamer is prevented by the peripheral stator network, likewise referred to as “stator complex” (Junge and Nelson, 2005).

The current concept of proton translocation suggests that subunit a contains two half-channels, one opening toward the cytoplasmic side of the membrane and, clockwise to the first one as viewed from the extra-cytoplasmic side, a second channel facing the lumen or extracellular space (Junge *et al.*, 2009; Fig. 1.3). A deprotonated glutamate residue of the c ring is kept in the cytoplasmic channel as it can only enter the membrane in its protonated i.e. uncharged state. Meanwhile a protonated glutamate resides in the extra-cytoplasmic half-channel in order to be deprotonated via interaction with the essential arginine residue in subunit a. Upon protonation of the first and deprotonation of the second glutamate one proton is transported from the cytoplasm to the extra-cytoplasmic space with one counterclockwise step of rotation of the c ring.

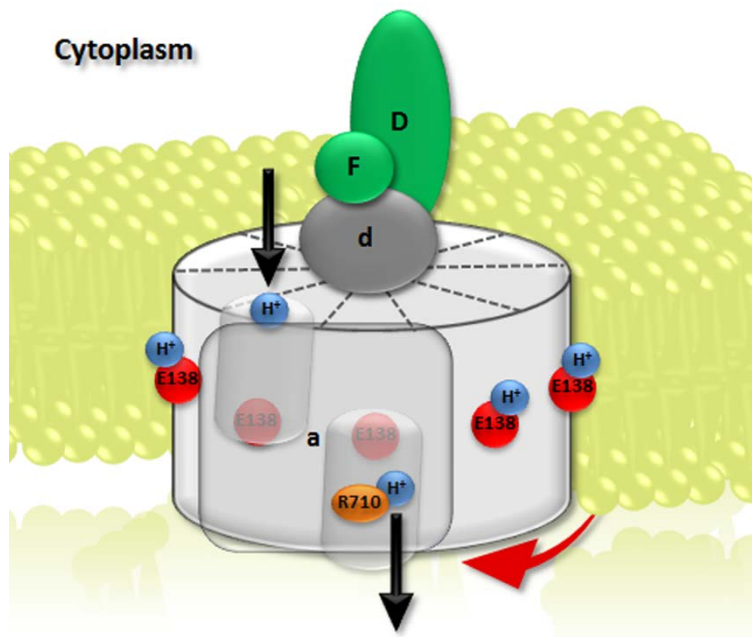


**Figure 1.3: Simplified model of proton translocation via the V-ATPase rotor ring.**

Schematic representation of the c ring with adjacent subunits important for rotation of the V-ATPase. The energy obtained from ATP hydrolysis at the catalytic sites in  $V_1$  is transduced via rotation of the central stalk subunits (D, F (green) and d (dark gray)) to the c ring in the  $V_0$  complex (gray). Counterclockwise rotation of the c ring, as viewed from the extra-cytoplasmic side (red arrow), drives proton translocation from the cytoplasm to either the lumen of intracellular compartments or the extracellular space mediated by two half-channels within subunit a (transparent gray). An essential glutamate of one c subunit (E138 in *M. sexta*; red) is loaded with a proton (blue) in the cytoplasmic half-channel while another glutamate releases a proton to the extra-cytoplasmic space with the aid of a conserved arginine residue in the second half-channel of subunit a (R710 in *M. sexta*; orange) (black arrows). Adopted from Forgac (2007).

### 1.3 Assembly and targeting of V-ATPases

Due to the ease of genetic modification, the assembly and targeting of V-ATPases is to date best studied in the yeast *S. cerevisiae*. By using V-ATPase subunit knock-out strains it was shown that the  $V_1$  and  $V_0$  complexes are assembled independently (Doherty and Kane, 1993). In addition, three proteins, Vma12, Vma21 and Vma22, are crucial for proper V-ATPase assembly and function but are not part of the mature protein complex (Hirata *et al.*, 1993; Ho *et al.*, 1993). These three proteins are located in the membrane of the endoplasmic reticulum (ER) and act as chaperons that promote assembly of the  $V_0$  complex via interaction with either subunit a (Vma12 and Vma22) or subunit c' (Vma21) (Forgac, 2007). The mature  $V_0$  complex, still comprising Vma21, is then transferred to the Golgi network where the chaperon is released and  $V_1$  subunits are added to finally form the  $V_1V_0$  complex. Assembly of  $V_1$  onto  $V_0$  can either occur by the addition of smaller sub-complexes or whole  $V_1$  complexes without subunit C that is always added separately. Alternatively, the V-ATPase subunits might also undergo another pathway where they are assembled to form the holoenzyme without prior formation of  $V_1$  and  $V_0$  complexes (Forgac, 2007).

The specific targeting of the mature V-ATPases to their dedicated location is mediated by organelle or tissue specific isoforms of subunit a (Toei *et al.*, 2010). Yeast exhibits only two isoforms, Vph1 for vacuolar localization and Stv1 for localization to the Golgi, while in mammalian cells four isoforms (a<sub>1</sub>-a<sub>4</sub>) and some splice variants are known. The mammalian isoforms occur for example in nerve cells (a<sub>1</sub>), renal proximal tubule cells (a<sub>2</sub>), osteoclasts (a<sub>3</sub>) or renal intercalated cells (a<sub>4</sub>). Nevertheless, the isoforms do not constrain V-ATPases to a specific membrane within their target cells, neither do all cells types contain only one isoform of subunit a.

#### 1.4 Regulation of V-ATPases by reversible dissociation

As described in detail in the preceding paragraphs, V-ATPases function as energy-consuming rotary motors. The high expense of ATP by these enzymes demands for regulatory mechanisms that connect V-ATPase function to the physiological state of the cell or the whole organism, thus preventing unnecessary consumption of chemical energy. One major regulatory mechanism of V-ATPases is silencing the enzyme by reversible dissociation of the V<sub>1</sub> from the V<sub>O</sub> complex instigated by energy limitation (Fig. 1.4). The dissociation was first described for V-ATPases in the midgut of molting and starving *M. sexta* larvae, respectively (Gräf *et al.*, 1996; Sumner *et al.*, 1995), and likewise found to occur in the vacuolar ATPase of *S. cerevisiae* upon glucose deprivation (Kane, 1995). It was also shown that this process can be reversed by refeeding and restoring glucose levels, respectively (Gräf *et al.*, 1996; Kane, 1995). In addition, it was found that the dissociated V<sub>1</sub> complex is not capable of hydrolysis of Mg<sup>2+</sup>-ATP (Gräf *et al.*, 1996). Likewise, the sole V<sub>O</sub> complex does not translocate protons across the membrane (Beltran and Nelson, 1992; Zhang *et al.*, 1992). *In vitro* experiments using the purified *M. sexta* V-ATPase revealed that the dissociation of the V<sub>1</sub> is induced by a low ATP/ADP ratio, representing a low energy state of the cell, with bound ADP destabilizing the holoenzyme (Huss and Wiczorek, 2007).

Due to the finding that subunit C and the remaining V<sub>1</sub> complex dissociate and reassociate independently (Kane, 1995; Merzendorfer *et al.*, 2000), and because of the central position of subunit C within the collar structure, connecting the peripheral stators of the V-ATPase (Fig. 1.1), this subunit is thought to play a crucial role in the regulation of reversible dissociation (Muench *et al.*, 2009; Zhang *et al.*, 2008). In addition, it was found that subunit C is able to interact directly with the actin cytoskeleton and that it can be phosphorylated by PKA *in vitro*, implicating further possibilities to modulate V-ATPase function via this subunit (Vitavska *et al.*, 2005; Vitavska *et al.*, 2003; Voss *et al.*, 2007). Besides subunit C, subunit H is probably also crucial for the modulation of V-ATPase function, as it is proposed to block rotation of the central stalk in the detached V<sub>1</sub> complex via interaction of its C-terminal domain with subunit F (Diab *et al.*, 2009; Jefferies and Forgac, 2008; Parra *et al.*, 2000). Subunit H is thus presumed to permit the “resting state” of the V<sub>1</sub> complex which prevents futile consumption of ATP and allows rapid reassembly of the holoenzyme if necessary (Diepholz *et al.*, 2008; Muench *et al.*, 2011).

In yeast it was found that dissociation and reassociation are two distinct pathways with different regulatory mechanisms. Dissociation upon glucose deprivation for example only occurs at acidic extracellular pH (Diakov and Kane, 2010) and requires intact microtubules, while reassociation does not (Xu and Forgac, 2001). Glucose-induced reassociation of  $V_1$  and  $V_0$  is mediated by the RAVE (Regulator of the  $H^+$ -ATPase of Vacuolar and Endosomal membranes) complex that binds to free  $V_1$  and seems to play a general role in the assembly of the V-ATPase (Smardon *et al.*, 2002). Additionally, the assembly of the holoenzyme is promoted by the glycolytic enzyme aldolase that probably stabilizes  $V_1$ - $V_0$  interaction via binding to subunits B, E and a (Lu *et al.*, 2004). In this context, aldolase is presumed to couple the assembly state of V-ATPases to the ATP-producing glycolytic pathway. A broad overview of the current knowledge of regulatory mechanisms for V-ATPases is given in Forgac (2007).

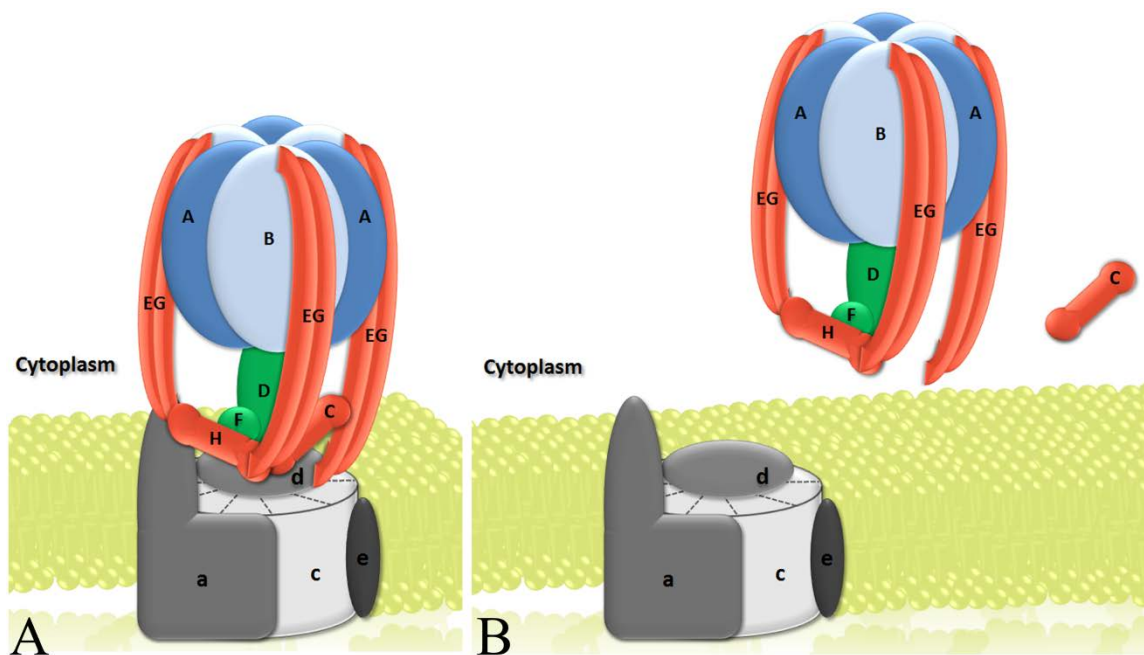


**Figure 1.4: Regulation of V-ATPases by reversible dissociation.**

Upon nutrient depletion the V-ATPase holoenzyme (A) undergoes reversible dissociation (B). During this process the  $V_1$  complex detaches from the membrane-bound  $V_0$  complex with subunit C being released separately. Capital letters,  $V_1$  subunits A-H; lower case letters,  $V_0$  subunits a, c, d and e. According to Forgac (2007).

### 1.5 The role of V-ATPases in physiology and pathophysiology

Because of their special function as energy converters, V-ATPases are involved in nearly all physiological processes of eukaryotic cells, in most cases representing the primary energizer of diverse membrane transport systems. In fulfilling this substantial role, these enzymes maintain the function of single cells, as well as of specialized tissues and whole organisms. In this regard, it is not surprising that malfunction of the V-ATPase leads to severe pathological defects.



### 1.5.1 The V-ATPase in the midgut of *Manduca sexta*

Insects living on a tannin-rich plant diet have to overcome the tendency of tannins to bind proteins at low pH values which would result in a reduced digestion efficacy (Dow, 1984). This problem is commonly solved by a very high pH in the digestive midgut lumen. Thus, in the *M. sexta* larvae an extremely alkaline pH ( $> 11$ ) is generated in the midgut (Dow, 1984). The midgut epithelium in these larvae is composed of two major cell types, (1) the goblet cells that are responsible for  $K^+$  secretion into and  $H^+$  depletion from the midgut lumen, and (2) the columnar cells that surround the goblet cells and function in nutrient uptake (Fig. 1.5A) (Baldwin and Hakim, 1991; Dow, 1984).

In 1986, Wieczorek *et al.* described a  $K^+$ -stimulated ATPase activity in the *M. sexta* goblet cell apical membrane (GCAM) indicating the presence of an ATP driven  $K^+$  pump in these cells (Wieczorek *et al.*, 1986). A few years later, it was found that a V-type ATPase in combination with a  $K^+/H^+$  antiporter is responsible for potassium transport into the midgut lumen. This V-ATPase pumps protons into the goblet cell cavity thereby driving the electrogenic exchange of  $H^+$  against  $K^+$  out of the cell (Fig. 1.5A) (Schweickl *et al.*, 1989; Wiecezorek *et al.*, 1991; Wiecezorek *et al.*, 1989). The stoichiometry of the transport was assigned to be  $K^+/2H^+$  thus providing the explanation for the extremely high pH found in *M. sexta* midgut lumen (Azuma *et al.*, 1995). In addition, the potassium motif force generated by the two transporters energizes the uptake of amino acids from the midgut lumen via an amino acid/ $K^+$  symporter in the apical membrane of the columnar cells (Hennigan *et al.*, 1993). Today, it is widely accepted that the V-ATPase in the *M. sexta* GCAM is the sole energizer, driving all ion and metabolite transport processes in the whole midgut epithelium of the lepidopteran larvae (Harvey *et al.*, 1998; Wiecezorek *et al.*, 2000). Due to the vast amount of V-ATPases in the GCAM and a very efficient purification method, the *M. sexta* exhibits an excellent system for biochemical research on the V-ATPase (Huss *et al.*, 2002; Wiecezorek *et al.*, 1990; Wiecezorek *et al.*, 2000).

### 1.5.2 The V-ATPase of *Saccharomyces cerevisiae*

While *M. sexta* provides a system for the biochemical study of V-ATPases, the yeast *S. cerevisiae* has emerged as a genetic model for eukaryotic V-ATPases. This is mainly due to the fact that all V-ATPase subunits, except subunit a, are only present in a single isoform in yeast (Tab. 1.1) thus allowing facile genetic modification. In particular, knock-out strains of *S. cerevisiae* deficient in one V-ATPase subunit exhibit a characteristic *vma<sup>-</sup>* phenotype which means that these strains fail to grow at alkaline pH ( $> 6.5$ ) or elevated  $CaCl_2$  concentration (100 mM) in the medium (Nelson and Nelson, 1990; Ohya *et al.*, 1991). This distinct phenotype arises from the physiological function, namely vacuolar acidification, which V-ATPases fulfill within the yeast cell (Fig. 1.5B).

In *S. cerevisiae* V-ATPases are located in either the vacuolar or the Golgi membrane (paragraph 1.3), and in both compartments they are responsible for luminal acidification, hence providing the optimal pH for e.g. the proper function of proteases. The vacuole of *S. cerevisiae* functions on the one hand as a digestive compartment and is involved in metabolite storage, on the other hand, it is also highly important for the ion and pH homeostasis of the cell (Klionsky *et al.*, 1990). By pumping protons from the cyto-

plasm into the vacuolar lumen the V-ATPase generates an electrochemical membrane potential that drives all secondary transport systems. One of these transporters is Vcx1, a  $\text{Ca}^{2+}/\text{H}^+$  antiporter that transports  $\text{Ca}^{2+}$  into the vacuolar lumen and thus protects the cell from harmful excess of calcium ions in the cytoplasm (Miseta *et al.*, 1999). Consequently, yeast cells defective in V-ATPase function cannot cope with high extracellular calcium concentrations and thus do not grow on the respective media.

The loss of Vcx1 function can partially be compensated by the activation of the  $\text{Ca}^{2+}$ /calmodulin-dependent protein phosphatase calcineurin and subsequent upregulation of additional  $\text{Ca}^{2+}$  transporters (Pmr1 and Pmc1) (Kane, 2006). The pH component of the *vma*<sup>-</sup> phenotype in general can be overcome by growth of the defective yeast cells on media with low pH ( $\leq 6.5$ ), possibly because this allows vacuolar acidification via endocytosis of protons from the extracellular medium or passive uptake of weak acids (Munn and Riezman, 1994; Plant *et al.*, 1999). Furthermore, the *vma*<sup>-</sup> phenotype can be complemented by transformation of the mutant strain with a plasmid expressing the respective subunit (Nelson and Nelson, 1990). In some cases, it was even shown that the expression of c subunits from other organisms provided complementation of a *S. cerevisiae* subunit c deletion strain (Harrison *et al.*, 1994; Ikeda *et al.*, 2001). The possibility of phenotype complementation is also a very useful tool for mutagenesis studies as the influence of amino acid exchanges on V-ATPase function can easily be tested by monitoring cell growth of yeast strains that express mutant subunits.

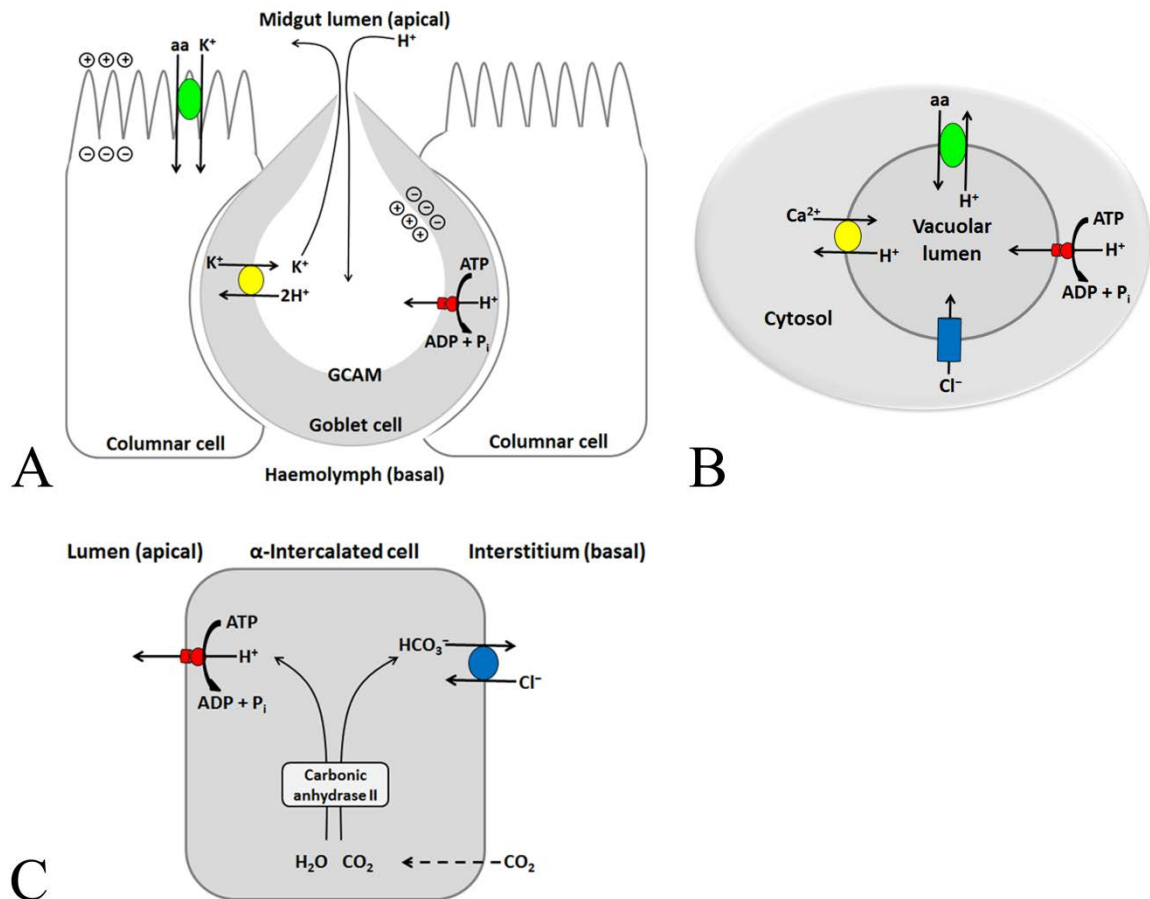


**Figure 1.5: Physiological functions of the V-ATPase.**

(A) Function of the V-ATPase in the *M. sexta* midgut epithelium. By transporting protons out of the goblet cell lumen, the V-ATPase (red) in the goblet cell apical membrane (GCAM) drives the electrogenic  $K^+/2H^+$ -antiporter (yellow), thereby energizing the whole midgut epithelium and thus driving all secondary ion and metabolite transport processes. According to Wieczorek *et al.* (2000). (B) In *S. cerevisiae* the V-ATPase in the vacuolar membrane provides optimal conditions for digestive enzymes via acidification of the vacuolar lumen. In addition, the electrochemical gradient sustained by the V-ATPase drives secondary transporters responsible for ion homeostasis and metabolite transport. According to Klionsky *et al.* (1990). (C) V-ATPases in the apical membrane of human kidney  $\alpha$ -intercalated cells contribute to the acid-base homeostasis of the whole organism. Upon diffusion of  $CO_2$  into the cell, protons are generated by carbonic anhydrase II and subsequently secreted into the urine via the V-ATPase. Concurrently produced  $HCO_3^-$  is transported back to the blood via a basolateral  $HCO_3^-/Cl^-$ -antiporter. Exemplarily depicted membrane channels and transporters are colored in green (amino acid-transporter), blue ( $Cl^-$ -channel/exchanger) and yellow (cation-exchanger), respectively. aa, amino acid.

### 1.5.3 The mammalian V-ATPase and its impact on human pathophysiology

For V-ATPases in mammalian cells acidification of intracellular compartments is one major task. These enzymes provide the optimal pH for e.g. digestive enzymes in lysosomes or receptor-mediated endocytosis. Furthermore, the importance of V-ATPases at the plasma membrane of different cell types becomes more and more evident (Hinton *et al.*, 2009). Because of the multitude of V-ATPase functions in mammalian cells, the focus in this paragraph will be on specific roles of the plasma membrane V-ATPase that are implicated in some severe diseases. An extensive overview on functions of mammalian V-ATPases is given in Hinton *et al.* (2009).

The human kidney  $\alpha$ -intercalated cells in the late distal tubule and the collecting duct are responsible for acid secretion into the urine, thereby contributing to the acid-base balance of the whole organism (Wagner *et al.*, 2004). These cells contain a large amount of V-ATPases in their apical membrane that transport protons into the tubule lumen while  $\text{HCO}_3^-$  is secreted into the blood via a  $\text{Cl}^-/\text{HCO}_3^-$  antiporter in the basolateral membrane (Fig. 1.5C). In patients suffering from inherited renal tubular acidosis the proton excretion via the  $\alpha$ -intercalated cells is abolished, resulting in sometimes severe metabolic acidosis with respective clinical features. One cause of this failure of proton secretion can be mutations in the V-ATPase subunit isoforms B1 and a4, respectively (Karet *et al.*, 1999; Smith *et al.*, 2000).

V-ATPases are also located in the plasma membrane of osteoclast cells which promote bone degradation via acidification of the extracellular space and subsequent release of bone dissolving enzymes (Hinton *et al.*, 2009). In healthy organisms osteoclasts and their counterpart, the bone forming osteoblasts, maintain equilibrium of bone resorption and bone formation. In osteopetrosis, a genetic defect caused by mutations in the osteoclast a3 isoform of the V-ATPase, acid secretion is abolished, resulting in hindered bone resorption followed by pathological bone thickening (Fratini *et al.*, 2000; Hinton *et al.*, 2009).

During the past years V-ATPases were shown to play an important role in metastasis of tumor cells. For example, in breast cancer cells it was demonstrated that a large amount of V-ATPases is present in the plasma membrane of highly metastatic cells and that these V-ATPases also exhibit higher activity when compared to V-ATPases from lowly metastatic cells (Sennoune *et al.*, 2004). It was proposed that V-ATPases provide an acidic extracellular pH that allows proteolytic digestion of the extracellular space and thus favors tumor invasiveness and migration. Importantly, tumor migration of highly metastatic cells in these experiments was significantly reduced by the addition of the specific V-ATPase inhibitor bafilomycin. In view of the important role V-ATPases play in some severe diseases, this enzyme is currently emerging as a promising therapeutic target with inhibitors of the V-ATPase arising as potential drugs.

### 1.6 Inhibitors of the V-ATPase

To date, a variety of specific V-ATPase inhibitors is known which can be divided into three major classes by means of structural similarities (Fig. 1.6). Firstly, the long known and well characterized plecomacrolide inhibitors (paragraph 1.6.1), secondly, the benzolactone enamides which were discovered in the late 1990ties (paragraph 1.6.2) and thirdly, the archazolids which form a novel inhibitor class first described by Sasse *et al.* (2003) (paragraph 1.6.3). Besides these three classes, other V-ATPase inhibitors are known but will be mentioned only briefly herein. (1) Destruxins are secondary metabolites from fungi primarily found in *Metarhizium anisopliae*. These cyclic hexadepsipeptides inhibit the V-ATPase of *S. cerevisiae* with low micromolar  $\text{IC}_{50}$  values (Muroi *et al.*, 1994; Vazquez *et al.*, 2005). (2) Chondropsins are large macrolide lactams from the marine sponge *Chondropsis* sp. (Cantrell *et al.*, 2000; Rashid *et al.*, 2001). They exhibit 10-fold higher efficacy against fungal V-ATPase compared to the bovine one, with  $\text{IC}_{50}$  values of 0.04-

0.7  $\mu\text{M}$  and 0.4 to more than 10  $\mu\text{M}$ , respectively (Bowman *et al.*, 2003). (3) Diphyllin is a plant-derived lignan that was shown to be highly efficient against bovine V-ATPase with an  $\text{IC}_{50}$  value of 17 nM (Sørensen *et al.*, 2007).

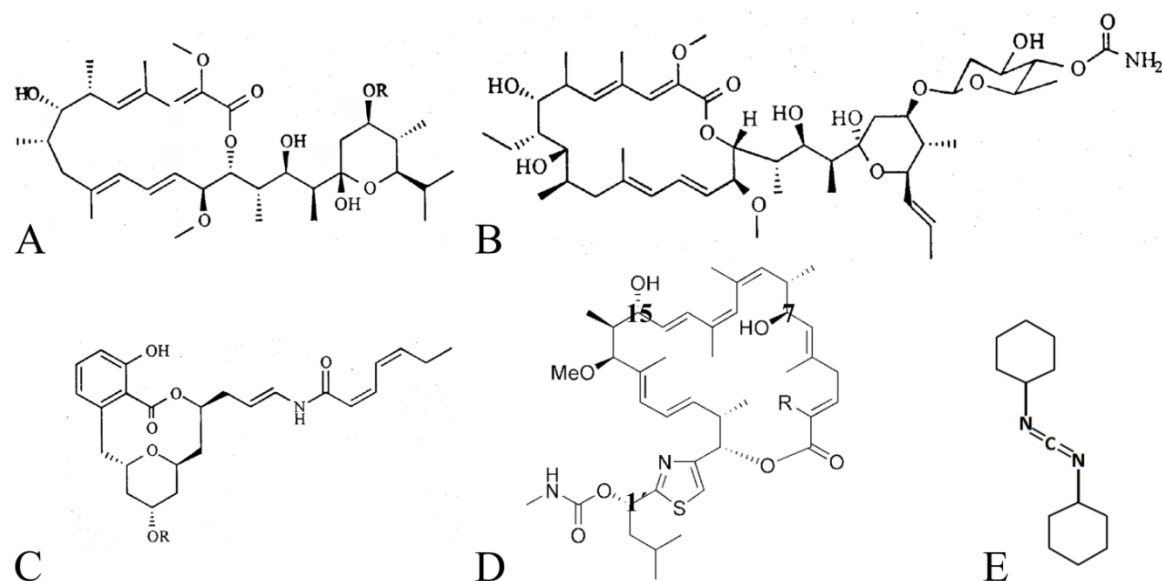


**Figure 1.6: Structures of selected V-ATPase inhibitors.**

Depicted are the structures of main representatives of all three major V-ATPase inhibitor classes. The established plecomacrolide inhibitors bafilomycin A1 (A) and concanamycin A (B), the benzolactone enamide apicularen A (C; R = H) and the recently discovered macrolactone archazolid A (D). Numbers in (D) indicate crucial carbon atoms (see paragraph 1.6.3; R =  $\text{CH}_3$ ). (E) Structure of the inhibitor *N,N'*-dicyclohexylcarbodiimide (DCCD) which covalently binds to the essential glutamate within V- and F-ATPase proteolipid subunits (paragraph 1.2.2). (A), (B) and (C) Modified from Beutler and McKee (2003). (D) Modified from Menche *et al.* (2007b).

### 1.6.1 Plecomacrolide inhibitors: The beginning of V-ATPase inhibitor studies

The plecomacrolides bafilomycin and concanamycin are long established V-ATPase inhibitors with  $\text{IC}_{50}$  values in the low nanomolar range (Bowman *et al.*, 1988; Dröse *et al.*, 1993), and up to now they are used in a variety of assays to identify V-ATPases or novel V-ATPase inhibitors. Both compounds are macrolide antibiotics from *Streptomyces* sp. composed of a macrolactone and a hemiketal ring (Dröse and Altendorf, 1997; Fig. 1.6 A and B). Compared to bafilomycin, concanamycin is somewhat larger as it comprises an 18-membered instead of a 16-membered lactone ring and an additional sugar moiety. Intensive structure-function studies revealed that both, the macrolactone and the hemiketal ring, are involved in inhibitor binding to the V-ATPase (Dröse and Altendorf, 1997; Dröse *et al.*, 1993; Dröse *et al.*, 2001; Gagliardi *et al.*, 1998a; Gagliardi *et al.*, 1999).

Based on the structural components of bafilomycin that are important for target inhibition, synthetic derivatives of this compound (shortly named indoyls) have been designed, in order to obtain tissue specific V-ATPase inhibitors (Gagliardi *et al.*, 1998a; Gagliardi *et al.*, 1998b). Indeed, one of these substances, (2*Z*,4*E*)-5-(5,6-dichloro-2-indolyl)-2-methoxy-*N*-(1,2,2,6,6-pentamethylpiperidin-4-yl)-2,4-pentadienamide (INDOLO), exhibited an  $\text{IC}_{50}$  value of 30 nM against the V-ATPase of human osteoclasts which was approximately 40-fold more efficient when compared to the kidney V-ATPase

(Gagliardi *et al.*, 1998b; Nadler *et al.*, 1998). Derivatives of INDOL0 have been used frequently to monitor the V-ATPase-inhibitor interaction using electron paramagnetic resonance (EPR) spectroscopy (Dixon *et al.*, 2003; Dixon *et al.*, 2008; Dixon *et al.*, 2004; Páli *et al.*, 2004a).

In the 1990-ties it was already suggested in different studies that the plecomacrolides might bind to the V-ATPase  $V_O$  complex (Crider *et al.*, 1994; Hanada *et al.*, 1990; Zhang *et al.*, 1994). Nevertheless, at this time the binding site could not be assigned, and both, subunits a and c, were proposed as potential binding partners (Rautiala *et al.*, 1993; Zhang *et al.*, 1994). In 2002 two studies came out that clearly revealed the  $V_O$  subunit c as plecomacrolide binding partner (Bowman and Bowman, 2002; Huss *et al.*, 2002). In the first instance, Bowman *et al.* performed random mutagenesis studies in *N. crassa* and found four exchanges within subunit c that conferred notable resistance of the V-ATPase against bafilomycin, thereby revealing three amino acid positions in subunit c that participate in inhibitor binding. In the second instance, Huss *et al.* identified subunit c as the binding partner for concanamycin A with photo affinity labeling (PAL) experiments using a radioactively labeled diazirinyl-derivative of concanamycin A, 9-O-[p-(trifluoroethyldiaziriny)-benzoyl]-21,23-dideoxy-23-[ $^{125}$ I] iodoconcanolide A ( $^{125}$ I-concanolid). Few years later, site-directed mutagenesis studies in *S. cerevisiae* implicated a minor contribution of subunit a in plecomacrolide binding (Wang *et al.*, 2005).

Finally, further mutagenesis studies in *N. crassa* and *S. cerevisiae* (Bowman *et al.*, 2006; Bowman *et al.*, 2004), in combination with the crystal structure of the c ring from the A-type ATPase of *E. hirae* (Murata *et al.*, 2005), resulted in the first model of a V-ATPase inhibitor binding site (Bowman *et al.*, 2006; Fig. 1.7). In this model, the plecomacrolide binding site, displayed in the  $V_O$  ring of *N. crassa*, resides at the interface of two adjacent c subunits, and amino acid residues of helices 1 and 2 of one subunit and helix 4 of the adjacent subunit contribute to the enzyme-inhibitor interaction. Since the binding site was localized between two c subunits, it was proposed that the plecomacrolides inhibit V-ATPase function either by blocking rotation of the c ring because of steric hindrance at subunit a or by preventing internal torsion of the transmembrane helices within the c ring (Bowman *et al.*, 2004; Forgac, 2007).

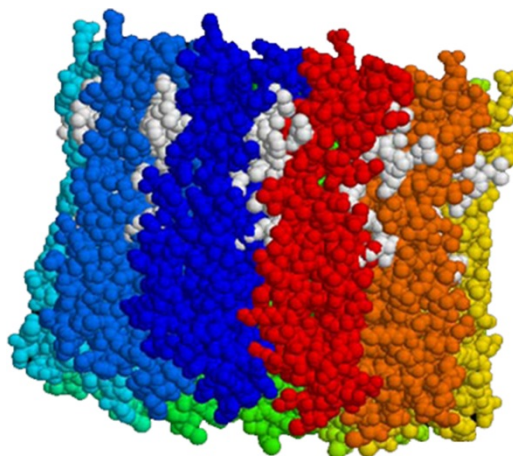


**Figure 1.7: Proposed binding site of the plecomacrolide inhibitors.**

The sequence of the *N. crassa* c subunit was fitted on the *E. hirae* c ring structure from Murata *et al.* (2005) as described in Bowman *et al.* (2006). Single subunits are displayed in a different color, each. Amino acid residues contributing to the plecomacrolide binding site (gray spheres) reside at the interface of two adjacent c subunits and at the cytoplasmic half of the ring. Picture modified from Bowman *et al.* (2006).

### 1.6.2 Benzolactone enamides: Species specific V-ATPase inhibition

The benzolactone enamides comprise a variety of compounds isolated from different organisms such as the tunicate *Aplidium lobatum* (lobatamides) (Galinis *et al.*, 1997), the marine sponge *Haliclona* sp. (salicylihalamides) (Erickson *et al.*, 1997) or the myxobacteria *Chondromyces* sp. (apicularens) (Fig. 1.6C; Kunze *et al.*, 1998). In a multitude of experiments using whole cell assays as well as isolated V-ATPases from different species, the benzolactone enamides were shown to be highly efficient V-ATPase inhibitors with nanomolar IC<sub>50</sub> values (reviewed in Huss and Wieczorek, 2009). Such assays also revealed that benzolactone enamides are not effective against V-ATPases from fungal sources, and therefore these compounds represent the first known class of V-ATPase inhibitors that exhibits species-dependent target selectivity (Bockelmann, S., Wieczorek, H. and Huss, M., unpublished results, Boyd *et al.*, 2001). This special feature evidently draws the attention to the investigation of the benzolactone enamides as potential lead compounds to develop specific drugs. Accordingly, throughout the past years the *in vivo* effects of e.g. apicularen on diverse cancer and osteoclast cell lines have been investigated to uncover the molecular basics of inhibitor-induced cell death (Hong *et al.*, 2005a; Hong *et al.*, 2007; Hong *et al.*, 2003; Hong *et al.*, 2005b; Hong *et al.*, 2006; Kim *et al.*, 2007).

The binding site of the benzolactone enamides is also believed to reside in the V<sub>O</sub> complex, since salicylihalamide, a prominent member of this inhibitor class, was shown to prevent proton transport in the isolated V<sub>O</sub> complex from bovine clathrin coated vesicles (Xie *et al.*, 2004). In contrast, both, salicylihalamide and apicularen A, were not able to prevent binding of the radioactive PAL compound <sup>125</sup>I-concanolid A to the c subunit (Huss *et al.*, 2002; Huss *et al.*, 2005). Thus, it was proposed that the benzolactone enamide binding site has to be significantly different from the plecomacrolide binding site. Since salicylihalamide, but not bafilomycin, promoted the redistribution of cytosolic V<sub>1</sub>

complex to the membrane bound  $V_O$ , it was also proposed that these compounds possess different inhibition mechanisms and that the binding of salicylhalamide to the V-ATPase might stabilize the holoenzyme (Xie *et al.*, 2004).

### 1.6.3 Archazolids: A novel class of V-ATPase inhibitors

The archazolids were first described in 2003, when Sasse *et al.* isolated novel antibiotic compounds, archazolid A and B, from the myxobacteria *Archangium gephyra* and *Cystobacter violaceus*. These antibiotics exhibit a characteristic structure that comprises a large 24-membered macrolactone ring and a thiazol side chain (Fig. 1.6D). From the beginning, the archazolids were proposed to be specific V-ATPase inhibitors as their inhibition profile in a mammalian cell line assay resembled the profile of the established V-ATPase inhibitors bafilomycin and concanamycin (Sasse *et al.*, 2003). The addition of such inhibitors to kidney cells resulted in the formation of vacuoles in the endoplasmic reticulum and in the loss of lysosomal acidification (Huss *et al.*, 2005; Sasse *et al.*, 2003). In activity assays with different isolated ATPases the archazolids were confirmed to be specific V-ATPase inhibitors, as they neither affected the P-type  $Na^+/K^+$ -ATPase nor the mitochondrial F-ATPase, but strongly inhibited the V-ATPase from *M. sexta* midgut with a low nanomolar  $IC_{50}$  value (Huss *et al.*, 2005). Since whole fungal cells were shown to be only moderately affected by archazolid (Sasse *et al.*, 2003), this inhibitor was also tested on the V-ATPase in isolated vacuoles from *S. cerevisiae* (Bockelmann, S., Wieczorek, H. and Huss, M., unpublished results). These assays revealed a low nanomolar  $IC_{50}$  value for the inhibition of the fungal V-ATPase, suggesting that the inefficiency of archazolid on whole cells was due to hindered uptake of the compound across the cell wall. Thus the archazolids were proven to be novel highly specific inhibitors of V-ATPases from different species including mammals, insects and yeast. Throughout the past years further natural archazolid derivatives have been isolated, adding to the diversity of this inhibitor class (Menche *et al.*, 2007c; Menche *et al.*, 2007d).

The three-dimensional structure and stereochemistry of archazolid was assigned recently by various NMR techniques in combination with molecular modeling and confirmed by total synthesis (Fares *et al.*, 2008; Hassfeld *et al.*, 2006; Menche *et al.*, 2007a). Based on these data, synthetic analogues of archazolid were designed in order to reveal the structural features of the inhibitor that define its biological activity (Menche *et al.*, 2007b). Examination of these analogues in cell lines and with purified *M. sexta* V-ATPase showed that modifications of the C-7 hydroxyl group of archazolid (Fig. 1.6D) lead to a striking loss of the inhibitor function (approximately 1000-fold higher  $IC_{50}$  value), suggesting a participation of this area of the molecule in the enzyme-inhibitor interaction. Furthermore, changes at the C-15 hydroxyl group also revealed a 20-fold decrease in sensitivity of the V-ATPase to the inhibitor. In contrast, modifications at C-1' caused only negligible changes in the  $IC_{50}$  value indicating that the macrolactone ring but not the thiazol side chain is important for inhibitor binding to the V-ATPase.

Regarding the definite assignment of the archazolid binding site within the V-ATPase only limited information has been obtained. In addition to the structure-function analysis of archazolid itself, some hints were derived from a competition assay with dif-



ferent V-ATPase inhibitors performed with the *M. sexta* V-ATPase (Huss *et al.*, 2005). In this assay, archazolid prevented, like the plecomacrolide inhibitor bafilomycin, labeling of the V-ATPase subunit c with the radioactive concanamycin derivative  $^{125}\text{I}$ -concanolid A. Therefore, it was assumed that archazolid shares at least part of its binding site with the plecomacrolide antibiotics. Accordingly, the archazolid binding site was suggested to reside at the interface of two adjacent c subunits within the c ring of the V-ATPase (see paragraph 1.6.1.).

## **1.7 Objective of the thesis**

Since the archazolids represent a novel and structurally unique class of V-ATPase inhibitors, knowledge of their binding site and inhibition mechanism is limited. On this account, the aim of the present thesis was to gain more insights into the structure-function relationship of archazolid and its target protein in order to define the crucial features of V-ATPase inhibition. Ultimately, the detailed knowledge of these critical features should enable the design of highly efficient simplified, and ideally also isoform specific, analogues of the inhibitor as prospective pharmacological agents.

Huss *et al.* (2005) already provided hints that the binding site of archazolid might overlap with the plecomacrolide binding site within subunit c of the V-ATPase  $V_O$  ring. In this regard, one approach of this work was to unequivocally identify the V-ATPase subunits interacting with archazolid by using radioactive PAL derivatives of the inhibitor. Furthermore, since the Bowman group identified a set of amino acids participating in plecomacrolide binding (Bowman and Bowman, 2002; Bowman *et al.*, 2006; Bowman *et al.*, 2004), the contribution of these amino acids to the binding of archazolid should be investigated and additional participants should be uncovered. At the same time, the biological evaluation of novel archazolid derivatives, provided by the group of Dirk Menche (University of Heidelberg, Germany), should reveal further insights into the critical structural features of the inhibitor. In addition, spin-labeled derivatives of V-ATPase inhibitors should be used to elucidate enzyme-inhibitor interactions via EPR spectroscopy.

## 2. Material and Methods

### 2.1 Material

#### 2.1.1 Chemicals and reagents

**Table 2.1: Chemicals and reagents used in this study.**

Plastic ware was purchased from Eppendorf (Hamburg, Germany) or Sarstedt (Nümbrecht, Germany). Unless denoted otherwise, reagents were purchased from companies as follows.

Company	Chemicals
BD Biosciences	Bacto™ Yeast Extract, Difco™ Yeast Nitrogen Base w/o amino acids, Bacto™ Tryptone, Difco™ LB Broth
Biomol	Pefabloc SC
Erkol	Polyvinyl alcohol 28/20
Eurogentec	SmartLadder
Fluka	Calcium chloride, dimethyl sulfoxide, acetic acid, Ficoll PM400, potassium chloride, magnesium chloride, sodium hydroxide, phenol/chloroform/isoamyl alcohol (25:24:1), potassium dihydrogen phosphate, rubidium chloride, sucrose, sulfuric acid, trichloroacetic acid
GE Healthcare	LMW-SDS Marker Kit
Merck	Amido black, Coomassie Brilliant Blue R-250, ε-amino-n-carbonic acid, sodium molybdate, potassium acetate, potassium chloride, potassium hexacyanoferrate (III), potassium hydroxide, Triton X-100
Riedel	Acetone, ammonium hydrogen carbonate, manganese chloride
Roche	dNTP mix
Roth	Milk powder, sorbitol, Tween 20, DMF
Serva	Acrylamide, Agar Agar Serva Kobe I, ammonium persulfate, BCIP, bisacrylamide, bromphenol blue, dithiothreitol, sodium EDTA, ethidium bromide, formaldehyde, glucose, glycine, MOPS, MES, NBT, nitrocellulose, peptone, SDS, Tris
Sigma	Acetonitrile, amino acids, ATP, β-mercaptoethanol, BSA, C <sub>12</sub> E <sub>10</sub> , glycerol, malachite green, mineral oil, PonceauS, TEMED

#### 2.1.2 Culture media

All media were prepared in H<sub>2</sub>O purified with a Milli-Q Advantage A10 (Millipore) and sterilized by autoclaving. For culture plates Agar Agar SERVA Kobe I was added before autoclaving to a final amount of 2% for all LB and YPD media and 1.5% for SD media.

**Table 2.2: Bacterial and yeast culture media used in this study.**

Name	Composition
Ψb	2.0 % peptone, 0.5% yeast extract, 0.5% MgSO <sub>4</sub> , pH 7.6 with KOH
LB	0.5 % tryptone, 0.5 % yeast extract, 0.5% NaCl
LB <sup>Amp</sup>	LB medium, 100 µg/ml ampicillin
YPD	1% yeast extract, 2% peptone, 2% glucose
YPDA	YPD medium, 0.02% adenine hemisulfate
YPDA pH 5.5	YPDA medium, 50 mM MES/50 mM MOPS, pH 5.5 with NaOH
YPDA pH 7.5	YPDA medium, 50 mM MES/50 mM MOPS, pH 7.5 with NaOH
YPDA CaCl <sub>2</sub>	YPDA pH 5.5 medium, 0.1 M CaCl <sub>2</sub>

YPDA pH 7.5 CaCl <sub>2</sub>	YPDA pH 7.5, 0.1 M CaCl <sub>2</sub>
YPDAS	YPDA medium, 1 M sorbitol
SD	0.67% Yeast Nitrogen Base (w/o amino acids), 2% glucose, 1.5% agar, 10% drop-out solution, 50 mM MES/50 mM MOPS, pH 5.5 with NaOH
Drop-out solution	0.02% adenine hemisulfate, 0.02% L-arginine HCl, 0.02% L-histidine HCl, 0.03% L-isoleucine, 0.1% L-leucine, 0.03% L-lysine HCl, 0.02% L-methionine, 0.05% L-phenylalanine, 0.2% L-threonine, 0.02% L-tryptophan, 0.03% L-tyrosine, 0.02% uracil, 0.15% L-valine For selection media the respective amino acid was omitted.

### 2.1.3 *Escherichia coli* strains

**Table 2.3: *Escherichia coli* strains used in this study.**

Name	Genotype	Source
DH5 $\alpha$	F <sup>-</sup> , $\Phi$ 80dlacZ $\Delta$ M15, $\Delta$ (lacZY A-argF) U169, <i>endA1</i> , <i>recA1</i> <i>hsdR17</i> (r <sub>K</sub> <sup>-</sup> m <sub>K</sub> <sup>+</sup> ), <i>deoR</i> , <i>thi-1</i> , <i>supE44</i> , $\lambda$ <i>gyrA96</i> , <i>relA1</i>	Hanahan, 1983
XL1- Blue	<i>recA1</i> , <i>endA1</i> , <i>gyrA96</i> , <i>thi-1</i> , <i>hsdR17</i> , <i>supE44</i> , <i>relA1</i> , <i>lac</i> [F <sup>'</sup> , <i>proAB</i> , <i>lacIqZ_M15</i> , Tn10, (Tetr)]	Stratagene

### 2.1.4 *Saccharomyces cerevisiae* strains

**Table 2.4: *Saccharomyces cerevisiae* strains used in this study.**

Name	Genotype	Source
BMA64	MATa/MAT $\alpha$ <i>ura3-52/ura3-52</i> ; <i>trp1</i> $\Delta$ 2/ <i>trp1</i> $\Delta$ 2; <i>leu2-3,112/leu2-3,112</i> ; <i>his3-11/his3-11</i> ; <i>ade2-1/ade2-1</i> ; <i>can1-100/can1-100</i>	Euroscarf, Germany
BMA64-1B	MAT $\alpha$ ; <i>ura3-52</i> ; <i>trp1</i> $\Delta$ 2; <i>leu2-3,112</i> ; <i>his3-11</i> ; <i>ade2-1</i> ; <i>can1-100</i>	Euroscarf, Germany
BMA64-1B $\Delta$ <i>vma3</i>	MAT $\alpha$ , <i>ura3-52</i> , <i>trp1</i> $\Delta$ 2, <i>leu2-3-112</i> , <i>his3-11</i> , <i>ade2-1</i> , <i>can1-100</i> , <i>vma3::HIS3</i>	This study
BY4742	MAT $\alpha$ ; <i>his3</i> $\Delta$ 1; <i>leu2</i> $\Delta$ 0; <i>lys2</i> $\Delta$ 0; <i>ura3</i> $\Delta$ 0	Euroscarf, Germany
BY4742- $\Delta$ <i>vma11</i>	MAT $\alpha$ ; <i>his3</i> $\Delta$ 1; <i>leu2</i> $\Delta$ 0; <i>lys2</i> $\Delta$ 0; <i>ura3</i> $\Delta$ 0; YPL234c::kanMX4	Euroscarf, Germany

**2.1.5 Plasmids**

**Table 2.5: Plasmids used in this study.**

Name	Description	Source
pFA6a- <i>HIS3MX6</i>	Amp, <i>HIS3</i>	Laboratory stock
pRS415	CEN/ARS, Amp, <i>LEU2</i>	Laboratory stock
pRS415- <i>VMA3</i>	<i>VMA3</i> , native promoter	This study
pRS415- <i>VMA11</i>	<i>VMA11</i> , native promoter	Voss, F., Diploma thesis, University of Osnabrück, 2010

**2.1.6 Oligonucleotides**

All oligonucleotides used in the this study were designed with the help of Clone Manager Suite 7, purchased from Eurofins MWG Operon (Germany) and stored at -20°C.

**Table 2.6: Primers for cloning and sequencing.**

Name	Sequence 5'→3'	Application
TEF- <i>SpHIS</i> -for	CAAAAAGACTAATCAATTAGAATAACAAAAGAAAC ATATACATATAGATCTGTTTAGCTTGCCTCGTCCCCG	Amplification of <i>HIS3</i> for homologous recombination
TEF- <i>SpHIS</i> -rev	GTATACTCTATTCCTGCTTTAGTGATTCAGAAGCTGC CCTGGATGGCGGCGTTAGTATCGAATC	
<i>VMA3</i> -for	CTACGGCCTATTCCATTG	Verification of homologous recombination
<i>VMA3</i> -rev	CTCATCGTACCCATTGTG	
YMat-a-for	ACTCCACTTCAAGTAAGAGTTTG	Verification of yeast mating type
YMat-α-for	GCACGGAATATGGGACTACTTCG	
YMat-rev	AGTCACATCAAGATCGTTTATG	
<i>VMA3</i> -EagI-for	TACTCACGGCCGTCTACGGCCTATTC	Cloning and sequencing of <i>VMA3</i> with native promoter
<i>VMA3</i> -BamHI-rev	TACTCAGGATCCCTCATCGTACCCATTGTG	
<i>VMA11</i> -EagI-for	TAC TCA CGG CCG CAG GCT TAA AGA GCC ATT TC	Sequencing of <i>VMA11</i> with native promoter
<i>VMA11</i> -BamHI-re	TAC TCA GGA TCC CCT GAT GCC ATG GAT ACT AC	

**Table 2.7: Primers for site-directed mutagenesis of Vma3p.**

Primer names accord with the respective amino acid exchanges within transmembrane helices of Vma3p as indicated.

Name	Sequence 5' → 3'	Codon exchange
<b><i>Helix 1</i></b>		
T32A-for	GGTGCTGCTTACGGTGCTGCTAAGTCTGGTG	act → gct
T32A-rev	CACCAGACTTAGCAGCACCGTAAGCAGCACC	
T32I-for	GGTGCTGCTTACGGTATTGCTAAGTCTGGTG	act → att
T32I-rev	CACCAGACTTAGCAATACCGTAAGCAGCACC	
I39A-for	GTCTGGTGTTGGTGCCTGTGCCACTTGTGTG	atc → gcc
I39A-rev	CACACAAGTGGCACAGGCACCAACACCAGAC	
I39F-for	GTCTGGTGTTGGTTTCTGTGCCACTTGTGTG	atc → ttc
I39F-rev	CACACAAGTGGCACAGAAACCAACACCAGAC	
<b><i>Helix 2</i></b>		
I54A-for	CCAGACCTATTATTCAAGAACGCTGTTCTGTTATTATGGCTGG	att → gct
I54A-rev	CCAGCCATAATAACAGGAACAGCGTTCCTTGAATAATAGGTCTGG	
I54F-for	CCAGACCTATTATTCAAGAACTTTGTTCTGTTATTATGGCTGG	att → ttt
I54F-rev	CCAGCCATAATAACAGGAACAAAGTTCCTTGAATAATAGGTCTGG	
G61A-for	CCTGTTATTATGGCTGCTATCATTGCCATTTACGG	ggt → gct
G61A-rev	CCGTAAATGGCAATGATAGCAGCCATAATAACAGG	
G61S-for	CCTGTTATTATGGCTAGTATCATTGCCATTTACGG	ggt → agt
G61S-rev	CCGTAAATGGCAATGATACTAGCCATAATAACAGG	
Y66F-for	GTATC ATTGCCATTTTCGGTTTAGTTG	tac → ttc
Y66F-rev	CAACTAAACCGAAAATGGCAATGATAC	
Y66S-for	GTATCATTGCCATTTCCGGTTTAGTTG	tac → tcc
Y66S-rev	CAACTAAACCGAAAATGGCAATGATAC	
<b><i>Helix 4</i></b>		
I130A-for	CAAGATTATTCGTCGGTATGGCTTTGATTTTGATTTTGGCTGAAG	att → gct
I130A-rev	CTTCAGCAAAAATCAAAATCAAGAACATACCGACGAATAATCTTG	
I130F-for	CAAGATTATTCGTCGGTATGTTCTTGATTTTGATTTTGGCTGAAG	att → ttc
I130F-rev	CTTCAGCAAAAATCAAAATCAAGAACATACCGACGAATAATCTTG	
L131A-for	CAAGATTATTCGTCGGTATGATTGCGATTTTGATTTTGGCTGAAG	ttg → gcg
L131A-rev	CTTCAGCAAAAATCAAAATCGCAATCATAACCGACGAATAATCTTG	
L131F-for	CAAGATTATTCGTCGGTATGATTTTCATTTTGATTTTGGCTGAAG	ttg → ttc
L131F-rev	CTTCAGCAAAAATCAAAATGAAAATCATAACCGACGAATAATCTTG	

## Material and Methods

I134A-for	CGTCGGTATGATTTTGATTTTGGCTTTTGCTGAAGTTTTGGGTC	att → gct
I134A-rev	GACCCAAAACCTTCAGCAAAAAGCCAAAATCAAATCATACCGACG	
I134F-for	CGTCGGTATGATTTTGATTTTGTTTTTTGCTGAAGTTTTGGGTC	att → ttt
I134F-rev	GACCCAAAACCTTCAGCAAAAAACAAAATCAAATCATACCGACG	
F135A-for	CGTCGGTATGATTTTGATTTTGATTGCTGCTGAAGTTTTGGGTCTA TACGG	ttt → gct
F135A-rev	CCGTATAGACCCAAAACCTTCAGCAGCAATCAAATCAAATCAT ACCGACG	
F135L-for	CGTCGGTATGATTTTGATTTTGATTCTTGCTGAAGTTTTGGGTCTA TACGG	ttt → ctt
F135L-rev	CCGTATAGACCCAAAACCTTCAGCAAGAATCAAATCAAATCAT ACCGACG	
V138A-for	GATTTTTGCTGAAGCATTGGGTCTATACGG	gtt → gca
V138A-rev	CCGTATAGACCCAAATGCTTCAGCAAAAATC	
V138T-for	GATTTTTGCTGAAACTTTGGGTCTATACGG	gtt → act
V138T-rev	CCGTATAGACCCAAAGTTTCAGCAAAAATC	
L141F-for	GAAGTTTTGGGTTTCTACGGTTTGATTG	cta → ttc
L141F-rev	CAATCAAACCGTAGAAACCCAAAACCTTC	
L141I-for	GAAGTTTTGGGTATATACGGTTTGATTG	cta → ata
L141I-rev	CAATCAAACCGTATATACCCAAAACCTTC	
Y142A-for	GCTGAAGTTTTGGGTCTAGCCGTTTGATTGTTGC	tac → gcc
Y142A-rev	GCAACAATCAAACCGGCTAGACCCAAAACCTTCAGC	
Y142H-for	GCTGAAGTTTTGGGTCTACACGGTTTGATTGTTGC	tac → cac
Y142H-rev	GCAACAATCAAACCGTGTAGACCCAAAACCTTCAGC	
Y142N-for	GCTGAAGTTTTGGGTCTAAACGGTTTGATTGTTGC	tac → aac
Y142N-rev	GCAACAATCAAACCGTTTAGACCCAAAACCTTCAGC	
L144F-for	GGGTCTATACGGTTTCATTGTTGCTTTG	ttg → ttc
L144F-rev	CAAAGCAACAATGAAACCGTATAGACCC	
L144I-for	GGGTCTATACGGTATCATTGTTGCTTTG	ttg → atc
L144I-rev	CAAAGCAACAATGATACCGTATAGACCC	
I145F-for	GTCTATACGGTTTGTTTGTTGCTTTGTTG	att → ttt
I145F-rev	CAACAAAGCAACAACAAACCGTATAGAC	
I145L-for	GTCTATACGGTTTGCTTGTTGCTTTGTTG	att → ctt
I145L-rev	CAACAAAGCAACAAGCAAACCGTATAGAC	
Y142N- L144I-for	GGGTCTAAACGGTATCATTGTTGCTTTG	tac → aac,
Y142N- L144I-rev	CAAAGCAACAATGATACCGTTTAGACCC	ttg → atc

**Table 2.8: Primers for site-directed mutagenesis of Vma11p.**

Primer names accord with the respective amino acid exchanges in transmembrane helix 4 of Vma11p.

Name	Sequence 5' → 3'	Codon exchange
<b>Helix 4</b>		
M152A-for	GTTATATGGTGC GATTGTAGCTTTGATTTTGAACACTAGAGGCT C	atg → gcg
M152A-rev	GAGCCTCTAGTGTTCAA AATCAAAGCTACAATCGCACCATATAA C	
M152F-for	GTTATATGGTTTCATTGTAGCTTTGATTTTGAACACTAGAGGCTC	atg → ttc
M152F-rev	GAGCCTCTAGTGTTCAA AATCAAAGCTACAATGAAACCATATA AC	

### 2.1.7 Animals

*Manduca sexta* (Lepidoptera, Sphingidae) larvae were reared at 27 °C under long-day conditions (16 h of light) using a synthetic diet (Gypsy Moth Diet, MP Biomedicals).

### 2.1.8 Inhibitors

All specific V-ATPase inhibitors were solved in dimethyl sulfoxide, split into appropriate aliquots and stored at -20°C or for long term storage at -80°C. DCCD and its derivatives were solved in ethanol, aliquoted and stored at -20°C. Azide and vanadate were solved in 160 mM KCl and 30 mM MgCl<sub>2</sub>, respectively, aliquoted and stored at -20°C.

**Table 2.9: ATPase inhibitors used in this study.**

Name	Chemical denotation/formula	Source/Reference
Apicularen A		B. Kunze, HZI Braunschweig
Archazolid A		F. Sasse, HZI Braunschweig
Archazolid F		D. Menche, University of Heidelberg; Horstmann <i>et al.</i> , 2011
MD-archazolid	Mono-[4-(3-trifluoromethyldiazirin-3-yl)benzoyl]-archazolid A	D. Menche, University of Heidelberg
BD-archazolid	Bis-[4-(3-trifluoromethyldiazirin-3-yl)benzoyl]-archazolid A	D. Menche, University of Heidelberg; Bockelmann <i>et al.</i> , 2010
Bisphospho-archazolid	Bis-7,15-(monoallylphospho)-archazolid A	D. Menche, University of Heidelberg
<sup>14</sup> C-MD-archazolid	Mono-[4-(3-trifluoromethyldiazirin-3-yl)-[1- <sup>14</sup> C] benzoyl]-archazolid A	D. Menche, University of Heidelberg
<sup>14</sup> C-BD-archazolid	Bis-[4-(3-trifluoromethyldiazirin-3-yl)-[1- <sup>14</sup> C]benzoyl]-archazolid A	D. Menche, University of Heidelberg; Bockelmann <i>et al.</i> , 2010
Archazolid C	archazolid-7- <i>O</i> -β-D-glucopyranoside	D. Menche, University of Heidelberg; Menche <i>et al.</i> , 2007c

Descarb-archazolid	1'-descarbamoyl-archazolid A	D. Menche, University of Heidelberg; Menche <i>et. al.</i> , 2007b
Oxo-archazolid	15-dehydro-archazolid A	D. Menche, University of Heidelberg; Menche <i>et. al.</i> , 2007b
SL-archazolid	7-2,2,6,6-tetramethyl-piperidine-1-oxyl-Archazolid	D. Menche, University of Heidelberg
Azide	Sodium azide, NaN <sub>3</sub>	Sigma
Bafilomycin A <sub>1</sub>		LC Laboratories
Concanamycin A		S. Grond, University of Tübingen
Concanolid A	21,23-didesoxy-concanolide A	S. Grond, University of Tübingen
<sup>14</sup> C-concanolid A	23-O-(3-trifluoromethyl-diazirin-3-yl)-[1- <sup>14</sup> C]benzoyl-21-desoxy-concanolide A	S. Grond, University of Tübingen
DCCD	<i>N,N'</i> -dicyclohexylcarbodiimide	Sigma
NCD-4	<i>N</i> -cyclohexyl- <i>N'</i> -(4-(dimethylamino)naphthyl)-carbodiimide	Invitrogen
NCCD	<i>N</i> -2,2,6,6-tetramethyl-piperidine-1-oxyl- <i>N'</i> -(cyclohexyl)carbodiimide	D. Menche, University of Heidelberg; Azzi <i>et al.</i> , 1973
Vanadate	Sodium orthovanadate, Na <sub>3</sub> VO <sub>4</sub>	Merck

## 2.2 Molecular biological and genetic methods

### 2.2.1 Transformation of DNA in chemical competent *Escherichia coli*

To obtain competent *E. coli*, the cells were treated according to Hanahan (1983). Five ml of Ψb medium were inoculated and incubated overnight at 37°C and 220 rpm. This pre-culture was then transferred to 100 ml pre-warmed, fresh Ψb medium and incubated at 37°C and 220 rpm up to an OD of A<sub>600</sub> ≈ 0.5. The culture was then cooled on ice for 5 min and the cells were harvested by centrifugation at 5,000 x g and 4°C for 5 min. The pellet was resuspended in 20 ml ice cold TfbI (30 mM KAc pH 5.8, 100 mM RbCl, 10 mM CaCl<sub>2</sub>, 50 mM MnCl<sub>2</sub>, 15% glycerol) and the suspension was incubated on ice for 5 min. Subsequently the cells were again pelleted as described above and finally suspended in 4 ml ice cold TfbII (10 mM MOPS pH 6.5, 75 mM CaCl<sub>2</sub>, 10 mM RbCl, 15% glycerol). The suspension was incubated on ice for 15 min, aliquotted, frozen in liquid nitrogen and stored at -80°C.

For transformation of DNA, 200 μl competent cells were thawed quickly and incubated on ice for 10 min. Following addition of DNA (max. 100 ng), the cells were further incubated on ice for 30 min. The cells were then heat-shocked at 42°C for 90 s and again cooled on ice. Four volumes of LB medium were added and the cells were incubated at 37°C and 140 rpm for 60 min. Finally, the cells were plated on LB medium containing the appropriate antibiotic.



### **2.2.2 Preparation of plasmid DNA from *Escherichia coli***

The QIAprep Miniprep Kit (Qiagen) was used to isolate plasmid DNA from *E. coli* following the manufacturer's instructions. First the bacterial cells were lysed under alkaline conditions to release the plasmid DNA. After neutralization of the lysate and adjustment to high-salt conditions the chromosomal DNA and cell debris were removed by centrifugation. The cleared lysate containing the plasmid DNA was then applied on QIAprep spin columns where it is selectively bound to a silica membrane at high-salt conditions. After washing, the plasmid DNA was eluted at low-salt conditions with H<sub>2</sub>O and stored at -20°C.

### **2.2.3 Restriction and ligation of DNA**

To digest DNA, restriction endonucleases (New England Biolabs) in a final concentration of 1 U/μg DNA were used. The reactions were performed in a total volume of 30 μl for 2 h at 37°C using the manufacturer's buffer system. Digested vector DNA was additionally incubated with 10 U of calf intestine alkaline phosphatase (CIP, New England Biolabs) for 1 h at 37°C to remove the 5' phosphate groups.

For ligation of DNA fragments, vector and insert DNA were mixed in a molar ratio of 1:3 together with T4 DNA ligase and buffer (New England Biolabs) in a final volume of 30 μl. The reaction was carried out overnight at 16°C.

### **2.2.4 Agarose gel-electrophoresis and DNA extraction**

Prior to separation of DNA fragments fivefold loading buffer was added to the probe. The DNA fragments were then size-separated at 95 V using 1% agarose gels in TAE running buffer (40 mM Tris, 10 mM NaAc, 1 mM EDTA, pH 8.0). Next the DNA was stained in ethidium bromide (2 μg/ml) for 20 min and the gel was then washed with H<sub>2</sub>O. The VersaDoc System (Bio-Rad) was used for documentation. To extract DNA fragments from agarose gels, the QIAquick Gel Extraction Kit (Qiagen) was used following a similar principle as described in paragraph 2.2.2.

### **2.2.5 Amplification of DNA**

Standard amplification of DNA fragments was carried out with *Taq* DNA polymerase (New England Biolabs) according to the manufacturer's recommendations using either plasmid or genomic yeast DNA as template. PCR for homologous recombination was done with Phusion High-Fidelity DNA Polymerase (New England Biolabs) and site-directed mutagenesis with PfuUltra high-fidelity DNA polymerase (Stratagene) as described in paragraph 2.2.9 and 2.2.10, respectively.

### **2.2.6 Preparation of genomic DNA from *Saccharomyces cerevisiae***

One single colony of yeast cells was suspended in 200 μl extraction buffer (10 mM Tris-HCl pH 8.0, 1 mM EDTA, 50 mM NaCl, 0.5% Triton X100), then approximately 0.2 g glass beads (Ø 0.4 mm) were added and the cells were mechanically disrupted by vor-

texting. To extract the genomic DNA, 100  $\mu$ l phenol/chloroform/isoamyl alcohol (25:24:1) were added and the probe was vortexed for 10 min at 4°C followed by centrifugation at 17,000 x g and 4°C for 15 min to separate genomic DNA and cell debris. The resulting aqueous phase containing the genomic DNA was diluted with H<sub>2</sub>O and stored at -20°C.

### 2.2.7 Transformation of DNA in *Saccharomyces cerevisiae*

Yeast cell transformation was done by electroporation. For this purpose 50 ml YPD medium were inoculated with a single yeast cell colony and incubated at 30°C and 230 rpm until early logarithmic phase. The cells were harvested by centrifugation, washed twice with sterile, ice cold H<sub>2</sub>O and then washed with 5 ml 1 M sorbitol and finally resuspended in the appropriate volume of 1 M sorbitol. Fifty  $\mu$ l of this suspension were transformed with approximately 5  $\mu$ g of DNA via electroporation using a GenePulserXcell (BioRad) at 1.5 kV, 25  $\mu$ F, 200 Ohms. Immediately afterwards 1 ml of YPDS was added and the cells were incubated at 30°C for 2 h with gentle shaking. The cells were then washed with sterile H<sub>2</sub>O and streaked onto plates with the appropriate SD selection medium.

### 2.2.8 Spotting growth assay

To confirm the V-ATPase function in yeast strains *in vivo* (paragraph 1.5.2), spotting growth assays were performed. Yeast cells were grown in 5 ml YPDA medium to early stationary phase and then diluted to 10<sup>5</sup> cells/ml in H<sub>2</sub>O. Serial tenfold dilution from 10<sup>4</sup> cells/ml to 10<sup>0</sup> cells/ml was performed in H<sub>2</sub>O and 5  $\mu$ l of each dilution were pipetted onto plates with different growth media. The plates were incubated at 30°C for 3 days and the VersaDoc System (Bio-Rad) was used for documentation.

### 2.2.9 Construction of a *vma3* deletion strain

The *vma3* deletion mutant BMA64-1B $\Delta$ *vma3* used throughout this study was constructed by exchanging the native *VMA3* gene against the *HIS3* gene via homologous recombination. A DNA fragment containing the *HIS3* gene with *tef1* promoter and terminator flanked by 40 bp homologous to the regions upstream and downstream of the *VMA3* gene was amplified using the vector pFA6a-*HIS3*MX6, primers TEF-Sp*HIS*-for/rev (Tab. 2.6) and Phusion High-Fidelity DNA Polymerase (New England Biolabs) following the manufacturer's recommendations. The resulting fragment was transformed into the diploid yeast strain BMA64. The cells were selected on SD medium without histidine and sporulated on potassium acetate plates (2% potassium acetate, 1.5% agar). The haploid spores were again selected on SD plates without histidine, and the successful exchange of the *VMA3* gene and the mating type were verified by PCR on genomic DNA (primers in Tab. 2.6).

### 2.2.10 Site-directed mutagenesis

For mutagenesis of the *VMA3* gene, the coding sequence flanked by 300 bp upstream and downstream, containing its native promoter and terminator, was amplified using the pri-

mer pair *VMA3*-EagI-for/*VMA3*-BamHI-rev (Tab. 2.6) and cloned into the yeast CEN vector pRS415 using the respective restriction sites. The plasmid was checked by sequencing and is in the following referred to as pRS415-*VMA3*. Mutagenesis on pRS415-*VMA3* was carried out using the QuikChange II Site-Directed Mutagenesis Kit (Stratagene) according to the manufacturer's instructions. Therefore mutant plasmids were generated by PCR with primers bearing specific base pair exchanges in *VMA3* (Tab. 2.7), followed by digestion of the parental plasmids with DpnI which specifically cleaves methylated DNA. The mutant plasmids were replicated in super-competent XL1-Blue cells supplied by the manufacturer and the base pair exchanges were verified by sequencing using primers *VMA3*-EagI-for and *VMA3*-BamHI-rev complementary to the endings of the insert. To express mutant versions of Vma3p in *S. cerevisiae*, the plasmids bearing specific mutations were transformed into the *vma3* deletion strain BMA64-1B $\Delta$ *vma3* and cells were selected on SD plates without leucine. With positive transformants spotting growth assays were performed to check V-ATPase function *in vivo*.

Mutagenesis of *VMA11* on the plasmid pRS415-*VMA11* was performed as described above using primers listed in Tab. 2.8. Primers for sequencing were *VMA11*-EagI-for and *VMA11*-BamHI-rev (Tab. 2.6). The mutant plasmids were then transformed into the *vma11* deletion strain BY4742- $\Delta$ *vma11*. Following selection of transformants and testing of V-ATPase function was performed as described above.

### **2.2.11 Other methods**

Spectroscopic determination of cell density at 600 nm was carried out using a Spectra-Max Plus (Molecular Devices). DNA concentrations were determined using a NanoPhotometer (Implen) and DNA sequencing was carried out at Seqlab (Sequence Laboratories Göttingen GmbH, Germany).

## 2.3 Biochemical methods

### 2.3.1 Preparation of vacuoles from *Saccharomyces cerevisiae*

Yeast vacuoles were basically purified following the protocols of Uchida *et al.* (1985) and Kane (1995). A 5 ml pre-culture of yeast cells in YPDA medium was incubated overnight at 30°C and then transferred to 1 l fresh YPDA medium. The next day the cells were harvested by centrifugation at 4,500 x g and 25°C for 5 min and washed once with sterile H<sub>2</sub>O. Then the cells were resuspended in 100 ml 1 M sorbitol containing 20 mM DTT, and approximately 500 U of zymolyase 100T (100 U/mg; MP Biomedicals), dissolved in 1 ml zymolyase buffer (50 mM Tris-HCl pH 7.7, 1 mM EDTA, 50% glycerol), were added. Digestion of cell walls was allowed to proceed for 60-90 min and the digestion efficiency was checked by lysis of a small amount of spheroplasts in buffer A (10 mM Tris-MES pH 6.9, 0.1 mM MgCl<sub>2</sub>, 12% Ficoll-400). To optimize the yield of assembled V-ATPase, the spheroplasts were additionally incubated for 30 min in 100 ml YPDAS at 30°C with gentle shaking. After recovery, the spheroplasts were lysed in 15 ml ice cold buffer A containing 50 µl protease inhibitor cocktail (Calbiochem), and the lysate was centrifuged at 2,200 x g and 4°C for 10 min. The supernatant was evenly distributed to two centrifuge tubes for a SW41Ti rotor (Beckman) and each fraction was covered with 6 ml of buffer A. Ultracentrifugation was carried out at 107,000 x g and 4°C for 1 h with slow acceleration and deceleration. Upon centrifugation in the self-forming continuous ficoll density gradient the yeast vacuoles form a white layer on top. Subsequent to resuspension of the vacuoles in 6 ml buffer A, 6 ml buffer B (10 mM Tris-MES pH 6.9, 0.5 mM MgCl<sub>2</sub>, 8% Ficoll-400) were layered on top and the probe was centrifuged for another 30 min as described above. Finally, the vacuoles were suspended in 1 ml buffer C (10 mM Tris-MES pH 6.9, 5 mM MgCl<sub>2</sub>, 25 mM KCl) with 10 µl protease inhibitor cocktail, aliquotted and stored at -80°C.

### 2.3.2 Purification of *Manduca sexta* V<sub>1</sub>V<sub>O</sub> holoenzyme and V<sub>O</sub> complex

The V<sub>1</sub>V<sub>O</sub> holoenzyme and the V<sub>O</sub> complex from the *M. sexta* larval midgut were purified according to Wieczorek *et al.* (1990) and Huss *et al.* (2002). For the holoenzyme preparation, midguts from 16-32 fifth instar larvae were collected in ice cold SET buffer (5 mM Tris-HCl pH 8.1, 5 mM EDTA, 250 mM sucrose) and washed for three times with the same buffer. Per every four midguts, 5 ml SET/P (SET containing 5 mM Pefabloc SC (biomol)) were added and the midguts were homogenized at 20,500 rpm for 30 s using a T25 ULTRA-TURRAX (IKA, Germany). The membranes were pelleted at 12,000 x g and 4°C for 5 min (Beckman Avanti-J25, JA 25.50) and washed twice with SET/P. The pellet was resuspended in 20 ml SET/P and the homogenate was centrifuged at 214,000 x g and 4°C for 25 min (Beckman Optima XL-80K; 90 Ti). The membranes were then solubilized in 400 ml TEM (16 mM Tris-HCl pH 8.1, 0.32 mM EDTA, 9.6 mM β-mercaptoethanol) containing 0.1% C<sub>12</sub>E<sub>10</sub>, followed by centrifugation at 142,000 x g and 4°C for 1 h (Beckman Optima XL-80K; 45Ti). The supernatant was cleared from lipids by filtration and concentrated to approximately 16 ml in a stirred ultrafiltration cell with a 10 kDa limit filtration membrane (Amicon). Two ml aliquots were distributed on discon-

tinuous sucrose density gradients (10%, 20%, 30% and 40% sucrose steps) and centrifugation was carried out at 342,000 x g and 4°C for 1.5 h (Beckman Optima XL-80K; VTi 65.1). The 30% sucrose fractions containing the V-ATPase holoenzyme were collected, diluted with three volumes of low salt buffer (20 mM Tris pH 8.1, 50 mM NaCl, 9.6 mM  $\beta$ -mercaptoethanol, 0.01% C<sub>12</sub>E<sub>10</sub>) and subjected to anion exchange chromatography on a 6 ml Resource Q column (GE Healthcare). Elution of the V-ATPase occurred with high salt buffer (20 mM Tris pH 8.1, 1 M NaCl, 9.6 mM  $\beta$ -mercaptoethanol, 0.01% C<sub>12</sub>E<sub>10</sub>) at 250-280 mM sodium chloride. The respective fractions were concentrated to 200  $\mu$ l in a Centricon-10 (Amicon) and applied on a Superdex 200 10/300 GL gel chromatography column (GE Healthcare). The elution occurred in 500  $\mu$ l fractions. To check for purity of the V-ATPase 10  $\mu$ l of each aliquot of interest were subjected to SDS-PAGE. The purest fractions were pooled and stored at 4°C.

For preparation of the *M. sexta* V<sub>O</sub> complex, midguts from starving larvae were collected and washed in SET, and resuspended in ET/P (5 mM Tris-HCl pH 8.1, 5 mM EDTA, 5 mM Pefabloc SC) before homogenization for 15 s as described above. Washing of the homogenate was carried out in ET/P as described above. The membrane pellet was then resuspended in ET/KI/P (5 mM Tris-HCl pH 8.1, 5 mM EDTA, 0.8 M KI, 5 mM Pefabloc SC) and incubated on ice for 30 min to allow stripping of the residual V<sub>1</sub> complex from the membrane. Then TEM was added to a final volume of 400 ml followed by centrifugation at 142,000 x g and 4°C for 1 h (Beckman Optima XL-80K; 45Ti). The membranes were again washed with 40 ml TEM and pelleted by centrifugation at 214,000 x g and 4°C for 25 min (Beckman Optima XL-80K; 90Ti). The pellet was then solubilized in 400 ml TEM containing 0.1% C<sub>12</sub>E<sub>10</sub> and membranes were removed by centrifugation at 142,000 x g and 4°C for 1 h (Beckman Optima XL-80K; 45Ti). The supernatant was filtrated, concentrated, and subjected to discontinuous sucrose density centrifugation as described above. The 20% sucrose fractions containing the V<sub>O</sub> complex were collected, four volumes of low salt buffer were added and the probe was subjected to anion exchange chromatography on a 6 ml Resource Q column (GE Healthcare) as described above. Elution of the V<sub>O</sub> complex occurred at 230-300 mM NaCl. The respective fractions were pooled and subsequently treated as described above.

### **2.3.3 Determination of protein concentration**

The protein concentration was determined with Amido Black as described in Wieczorek *et al.* (1990). For this purpose the probe and protein standards containing 2, 4 or 6  $\mu$ g of BSA, all in duplicate, were incubated with 300  $\mu$ l of Amido Black solution (26 mg in 100 ml acetic acid/methanol 1:10) for 5 min at 25°C. The proteins were then pelleted at 16,000 x g for 4 min and washed twice with 500  $\mu$ l acetic acid/methanol 1:10. The pellet was then resolved in 350  $\mu$ l 100 mM NaOH and the extinction was measured at 615 nm.

### **2.3.4 V-ATPase activity assay and determination of inorganic phosphate**

The activity of either the purified holoenzyme from *M. sexta* or the V-ATPase in yeast vacuoles was measured following the protocol of Wieczorek *et al.* (1990). All samples were prepared in triplicate, standards in duplicate.

Activity assays with *M. sexta* V-ATPase were carried out using 3 µg of protein in a final volume of 160 µl containing 50 mM Tris-MOPS (pH 8.1), 1 mM MgCl<sub>2</sub>, 20 mM KCl, 5 mM Tris-HCl, 3 mM β-mercaptoethanol, 1 mM ATP and 6.25% dimethyl sulfoxide, with or without V-ATPase inhibitor. The samples were preincubated for 10 min at 30°C and the reaction was started by the addition of ATP. After incubation for 2 min at 30°C the reaction was stopped by freezing the samples in liquid nitrogen. Standards containing 0, 10 or 25 nmol Pi were frozen immediately after preincubation and ATP was added afterwards. All samples were stored at -20°C.

To test the yeast V-ATPase activity, 3 µg of vacuolar protein were used in a final volume of 160 µl containing 50 mM Tris-MES pH 6.9, 3.75 mM MgCl<sub>2</sub>, 0.1 mM sodium orthovanadate, 20 mM KCl, 0.5 mM sodium azide, 5 mM Tris-HCl, 2 mM ATP and 6.25% dimethyl sulfoxide, with or without V-ATPase inhibitor. In general, the samples were treated as described above, but incubation in the presence of ATP was carried out for 20 min.

Determination of inorganic phosphate was also performed according to Wieczorek *et al.* (1990). This method is based on the generation of a complex of molybdate with free phosphate which itself then builds a complex with Malachite Green. The extinction of this complex was measured at 625 nm in a SpectraMax Plus (Molecular Devices) and the concentration of inorganic phosphate was calculated using the standard values.

### 2.3.5 Protein precipitation with trichloric acid

In order to apply larger amounts of protein on SDS gels, TCA precipitation was performed. One volume of 50% TCA was added to four volumes of the respective protein solution and the probe was incubated on ice for 15 min. The protein was then pelleted by centrifugation at 21,500 x g and 4°C for 10 min (Beckman Allegra 2IR) and washed twice with 500 µl ice cold acetone. Finally, the protein was resuspended in the appropriate volume of Laemmli buffer (125 mM Tris-HCl pH 6.8, 2% SDS, 5% sucrose, 0.005% bromophenol blue, 2% β-mercaptoethanol) and boiled for 45 s. The samples were either applied to SDS-PAGE immediately or stored at -20°C.

### 2.3.6 SDS-PAGE and Coomassie staining

Discontinuous polyacrylamide gel electrophoresis was performed according to Laemmli (1970). Separating gels with 17% acrylamide and 0.4% of cross linker in 330 mM Tris-HCl (pH 8.7), 0.1% SDS were covered with stacking gels containing 5.4% acrylamide with 2.3% of cross linker in 125 mM Tris-HCl (pH 6.8), 0.2% SDS. Prior to application on the gel the protein samples were boiled for 45 s in Laemmli buffer. Electrophoresis was carried out for 20 min at 15 mA and additional 30 min at 30 mA in SDS running buffer (100 mM Tris, 100 mM glycine, 0.1% SDS) using a Mini-PROTEAN II system (BioRad).

Separated proteins were either subjected to electroblotting or stained with Coomassie for 20 min (0.25% Coomassie Brilliant Blue R-250 in 50% methanol, 10% acetic acid). Destaining of the gel was achieved by boiling in H<sub>2</sub>O for 10-20 min at 600 W in a microwave.

### 2.3.7 Electroblothing and immunostaining

Transfer of proteins to nitrocellulose membranes (NC 2, SERVA) after SDS-PAGE was done by semi-dry electroblotting according to Towbin *et al.* (1979) using a Trans-Blot SD system (BioRad). Following the protocol of Kyhse-Andersen (1984) a three-part buffer system was used modified by the addition of 20% methanol. Protein transfer was carried out for 1 h with 1 mA per 1 cm<sup>2</sup> of SDS-gel and the transfer efficiency was checked by staining of the nitrocellulose membrane with 0.02% Ponceau S.

For immunostaining the nitrocellulose membrane was first incubated for 1 h at 25°C in blocking solution (5% milk powder in TTBSN (20 mM Tris-HCl pH 7.5, 0.5 M NaCl, 0.02% sodium azide, 0.05% Tween 20)) followed by the addition of the primary monoclonal antibody (Anti-Vma1p, mouse, Molecular Probes) diluted 1:3,000 with TTBSN containing 2.5% milk powder. After 1 h of incubation at 25°C the membrane was washed three times with TTBSN and then incubated for 1 h with alkaline phosphatase conjugated secondary antibody (Anti-mouse, Sigma) diluted 1:10,000 with TTBSN containing 2.5% milk powder. Subsequently the membrane was again washed as described above and finally the phosphatase reaction was started by the addition of 10 ml APP buffer (50 mM Tris-HCL pH 9.5, 100 mM NaCl, 50 mM MgCl<sub>2</sub>) containing 35 µl BCIP (50 mg/ml in 100% dimethylformamide) and 45 µl NBT solution (75 mg/ml in 70% dimethylformamide). The enzymatic reaction was stopped by intensive washing with H<sub>2</sub>O.

### 2.3.8 Vacuolar staining in *Saccharomyces cerevisiae*

Acidification of yeast vacuoles was checked *in vivo* using the fluorescent dye quinacrine according to Roberts *et al.* (1991). Cells were grown in YPDA pH 5.5 to the exponential phase, 1 ml of the culture was then cooled on ice for 5 min and the cells were pelleted by brief centrifugation in a microcentrifuge (PicoFuge, Stratagene). The pellet was resuspended in 100 µl YPDA pH 7.5 containing 200 µM quinacrine dihydrochloride (Sigma) followed by incubation in a Thermomixer comfort (Eppendorf) at 1400 rpm and 30°C for 1h. The suspension was then cooled on ice and the cells were pelleted and washed twice with a solution of 2% glucose in 50 mM MES/50 mM MOPS (pH 7.5). Finally, the cells were resuspended in 100 µl of 2% glucose (pH 7.5) and quinacrine staining was viewed within 15 min using the inverted microscope system IX70 (Olympus) with 100fold magnification (UPlanApo100x/1,35oil rios objective), and 430/24 excitation and 535/30 emission filters. Pictures were taken using a CoolSNAP-HQ2 kamera (Photometrics) and the MetaMorph Microscopy Automation & Image Analysis Software (Molecular Devices). When testing V-ATPase mutant strains, the fluorescence within the vacuoles was classified as positive (+) i.e. similar to the wild type strain or negative (-) i.e. like in the respective deletion strain (Fig. 2.1).

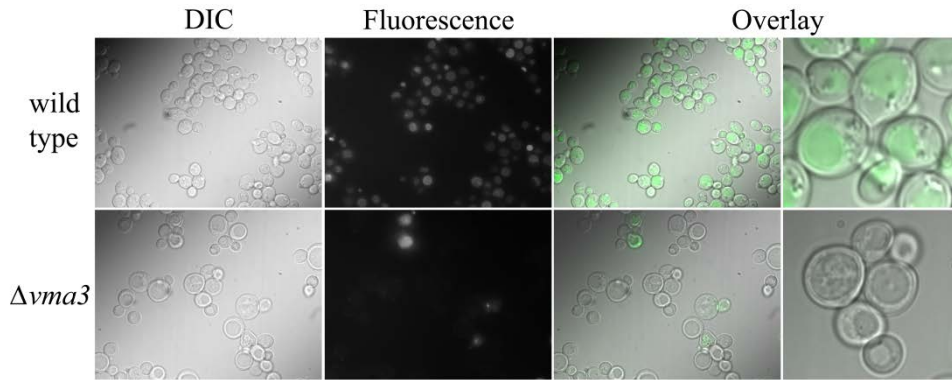


**Figure 2.1: Vacuolar staining with the fluorescent dye quinacrine.**

Pictures were taken at differential interference contrast (DIC) or fluorescence illumination and overlays were generated. At higher magnification, fluorescence within the vacuole of the wild type strain BMA64-1B is clearly visible while it is absent in the subunit c deletion strain ( $\Delta vma3$ ). Sporadic fluorescence visible in  $\Delta vma3$  can be assigned to dead cells as it engages not only the vacuole, but the whole cell. Fluorescence within the vacuoles of V-ATPase mutant strains was classified as positive (+) i.e. similar to the wild type strain or negative (-) i.e. like in the respective deletion strain.

### **2.3.9 Labeling of the *Manduca sexta* V-ATPase with NCD-4**

For NCD-4 labeling 100  $\mu\text{g}$  of the purified *M. sexta* V-ATPase or 20  $\mu\text{g}$  of the  $V_0$  complex were preincubated for 10 min at 25°C in 100  $\mu\text{l}$  solution containing 50  $\mu\text{M}$  archazolid A or 50  $\mu\text{M}$  bafilomycin A1 in 20 mM Tris-HCl pH 8.1, 50 mM NaCl, 9.6 mM  $\beta$ -mercaptoethanol and 0.01%  $C_{12}E_{10}$ . NCD-4 was then added to a final concentration of 0.1 mM, followed by incubation for 3 h at 25°C. Next, 20  $\mu\text{l}$  of each sample were subjected to SDS-PAGE and then the gels were fixed in 10% acetic acid, 40% ethanol for 30 min. The NCD-4 label was documented using the VersaDoc system (BioRad) with UV trans illumination and 520LP filter.

The correspondent competition assays were performed with 100  $\mu\text{g}$  of the purified *M. sexta* V-ATPase in 100  $\mu\text{l}$  buffer (see above). The protein was preincubated for 1 h at 25°C with 500  $\mu\text{M}$  of bafilomycin A1, concanamycin A, concanolid A or apicularen A, respectively, followed by the addition of 50  $\mu\text{M}$  archazolid A or dimethyl sulfoxide and further incubation as above. Then, NCD-4 was added to a final concentration of 0.1 mM and incubation was again carried out for 1 h at 25°C. Subsequently the samples were treated as described above.

### **2.3.10 Photo affinity labeling of the *Manduca sexta* V-ATPase**

Thirty  $\mu\text{g}$  of *M. sexta* V-ATPase in 20 mM Tris-HCl pH 8.1, 50 mM NaCl, 9.6 mM  $\beta$ -mercaptoethanol, 0.01%  $C_{12}E_{10}$  were incubated with 0.6 mM  $^{14}\text{C}$ -MD- or  $^{14}\text{C}$ -BD-archazolid or 1  $\mu\text{M}$   $^{14}\text{C}$ -concanolid A in a total volume of 40  $\mu\text{l}$  for 1 h at 25°C. Next, ATP was added to a final concentration of 1.5 mM and the samples were irradiated for 1 min with UV light (366 nm) on ice, followed by SDS-PAGE and phosphoscreen analysis as described in Huss *et al.* (2002). For competition assays the V-ATPase was incubated with 50  $\mu\text{M}$  concanamycin A for 1 h at 25°C before proceeding as described above. Computational analysis of gel images was done with the help of ImageQuant TL (GE



Healthcare) and Origin 8.1. In addition, the subunits of interest were cut out of the SDS-gel and subjected to scintillation counting (10,000 counts; LS 6500, Beckman Coulter).

## 2.4 Electron paramagnetic resonance (EPR) spectroscopy

EPR spectroscopy is currently emerging as a technique to elucidate the structure and dynamics of biomolecules, especially membrane proteins. For an overview on the different techniques and applications of spin labeling EPR spectroscopy see Klare and Steinhoff (2010; 2009). In brief, this method is based on the presence of one or more paramagnetic centers (i.e. unpaired electrons) in the structure of interest. For this purpose either naturally occurring paramagnetic centers (e.g. metal ions) can be used or paramagnetic centers can be introduced for example in proteins by site-directed spin labeling (SDLS). SDLS of proteins is commonly performed by cysteine substitution mutagenesis followed by the attachment of a nitroxide reagent (e.g. methanethiosulfonate) to the sulfhydryl group. Once a spin label is established in the sample, different EPR techniques are applicable. In continuous wave (*cw*) spectroscopy, a constant microwave frequency is generated to excite the paramagnetic center while the magnetic field is varied. The resulting EPR signal gives information about the mobility, local environment and solvent accessibility of the spin label. It also reflects dipolar interactions of different paramagnetic centers making the quantification of small inter spin distances (< 2 nm) possible. Furthermore, pulse EPR techniques, like for example four pulse DEER (Double Electron Electron Resonance), are used to determine inter spin distances of up to 8 nm, providing the possibility to follow long-range dynamics of protein structures. In this case, a certain series of microwave pulses is used to separately excite two different spin label fractions (observer and pump spins) (Fig. 2.2A). The dipolar interaction between the pump and the observer spins is reflected by the modulation of the observer spin signal amplitude. Since the frequency of the modulation ( $\nu$ ) is inversely proportional to the cube of the inter spin distance ( $r$ ),  $r$  can be derived from the following equation:  $\nu(r) = 52.04\text{MHz nm}^{-3}/r^3$  usually with the help of deconvolution or model-based methods (Böhme *et al.*, 2010). More details about DEER measurements are given in Fig. 2.2.

### 2.4.1 Protein preparation for EPR measurements

The *M. sexta* V-ATPase was purified as described in paragraph 2.3.2, except that  $\beta$ -mercaptoethanol was strictly omitted from the final gel filtration step, due to susceptibility of nitroxide groups to reductive agents. After purification the protein solution was concentrated to approximately 100  $\mu\text{M}$  in order to obtain good signal intensity during the measurements.

Vacuoles from *S. cerevisiae* were prepared as described in 2.3.1, but DTT was strictly omitted from the preparation. To further clean the purified vacuoles from reductive agents they were pelleted by centrifugation at 48,000 x g and 4°C for 20 min (Beckman Avanti J25, JA 25.50), washed with 1 ml buffer C and finally resuspended in the same buffer to a concentration of approximately 50  $\mu\text{M}$ .

### 2.4.2 Continuous wave (cw) EPR spectroscopy

To the protein sample, spin labeled inhibitor was added in a 10 to 12-fold molar excess from stock solutions in DMSO (SL-archazolid) or ethanol (NCCD). The concentration of the respective stock solution was adjusted not to exceed a final solvent concentration of 5% in the sample. 10-20  $\mu$ l of sample volume were filled in EPR glass capillaries (0.9 mm inner diameter). Room temperature cw EPR spectra were recorded using a Miniscope X-band bench top EPR spectrometer (MS200; Magnetech GmbH, Berlin, Germany) equipped with a rectangular TE102 resonator (microwave power: 10 mW; B-field modulation: 0.125 mT (= 1.25 Gauss)), or a home built X-band EPR spectrometer equipped with a Bruker dielectric resonator (microwave power: 0.4-0.6 mW; B-field modulation: 0.15 mT (= 1.5 Gauss)).

### 2.4.3 Distance measurements via four-pulse double electron electron resonance (DEER)

Unless denoted otherwise, spin labeled inhibitors were added as described in paragraph 2.4.2. Pulse EPR experiments were carried out at X-band frequencies (9.3-9.5 GHz) with a BrukerElexsys 580 spectrometer equipped with a BrukerFlexline split-ring resonator ER4118X-MS3 and a continuous flow helium cryostat (ESR900; Oxford Instruments) controlled by an Oxford Intelligent Temperature Controller ITC 503S.

All measurements were performed using the four-pulse DEER sequence:  $\pi/2$  ( $\nu_{\text{obs}}$ ) -  $\tau_1$ - $\pi$  ( $\nu_{\text{obs}}$ ) -  $t'$  -  $\pi$  ( $\nu_{\text{pump}}$ ) - ( $\tau_1 + \tau_2 - t'$ ) -  $\pi$  ( $\nu_{\text{obs}}$ ) -  $\tau_2$  - echo (Martin *et al.*, 1998; Pannier *et al.*, 2000). A two-step phase cycling (+  $\langle x \rangle$ , -  $\langle x \rangle$ ) was performed on  $\pi/2$  ( $\nu_{\text{obs}}$ ). Time  $t'$  is varied, whereas  $\tau_1$  and  $\tau_2$  are kept constant, the dipolar evolution time is given by  $t = t' - \tau_1$ . Data were analysed only for  $t > 0$ . The resonator was overcoupled to  $Q \sim 0$ -100; the pump frequency  $\nu_{\text{pump}}$  was set to the center of the resonator dip and coincided with the maximum of the nitroxide EPR spectrum, whereas the observer frequency  $\nu_{\text{obs}}$  was 65-67 MHz higher, coinciding with the low field local maximum of the spectrum. All measurements were performed at a temperature of 50 K with observer pulse lengths of 16 ns for  $\pi/2$  and 32 ns for  $\pi$  pulses and a pump pulse length of 12 ns. Deuterium modulation was averaged by adding traces at eight different  $\tau_1$  values, starting at  $\tau_{1,0} = 200$  ns and incrementing by  $\Delta\tau_1 = 8$  ns. Deuterated glycerol was added to a final concentration of 20% in all cases for its effect on the phase relaxation. Data points were collected in 8 ns time steps. The total measurement time for each sample was 8 - 32 h. Analysis of the data was performed with DeerAnalysis 2010 (Jeschke *et al.*, 2006).

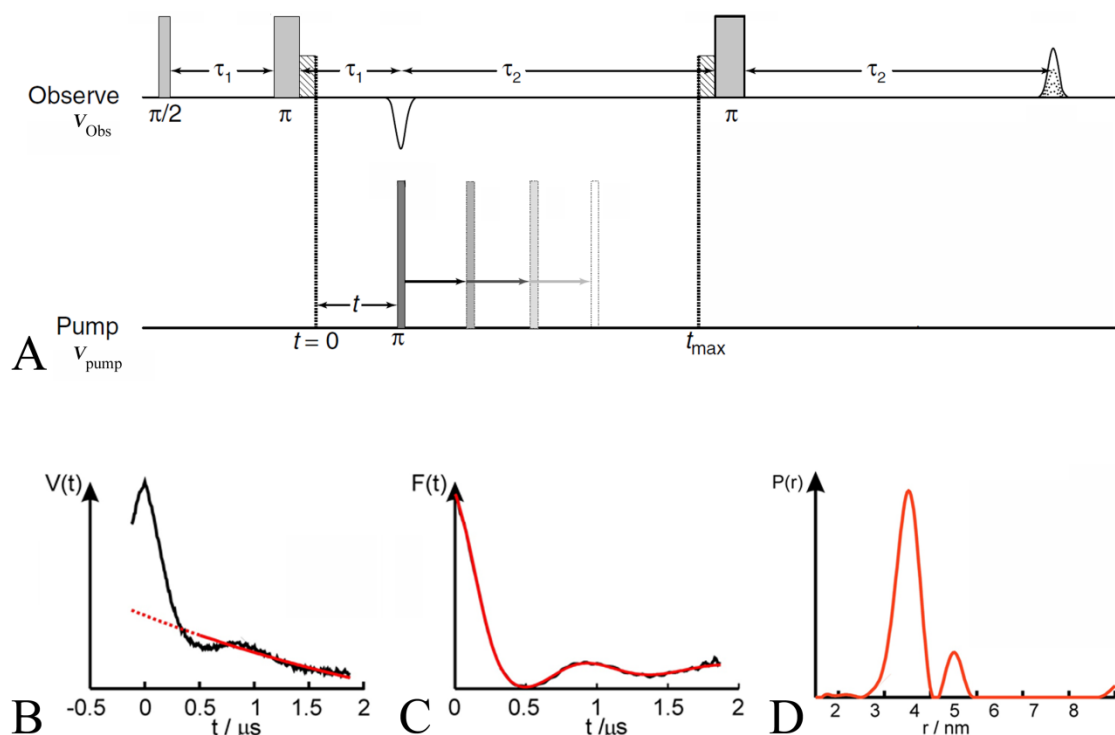


**Figure 2.2: Pulse sequence of a four-pulse DEER experiment.**

(A) In the first instance, one spin population (observer spins) is excited via a certain sequence of microwave pulses (Hahn-Echo sequence,  $\pi/2 - \tau_1 - \pi$ ) to generate a signal called Hahn-Echo. Once this echo is generated, a second spin fraction (pump spins) is excited via a pump pulse ( $\pi$ ) with increasing time ( $t$ ) after the echo. The resulting dipolar coupling between the pump and observer spins is reflected in the modulation of the Hahn-Echo amplitude which is visualized via the application of a third pulse ( $\pi$ ) on the observer spin fraction. Since the modulation frequency depends on the distance between the spin fractions, calculation of these distances is possible. Picture modified from Klare and Steinhoff (2010). (B) to (D) Processing of an EPR signal. The recorded signal  $v(t)$  (B) combines (1) the form factor component  $F(t)$  resulting from echo modulation by spins in the local environment ( $r < 8$  nm) and (2) the background factor  $B(t)$  caused by spins of neighboring objects in the sample. After subtraction of the background factor from the signal (C), the distance distribution  $P(r)$  (D) is obtained by deconvolution or model-based fitting of the form factor. Pictures kindly provided by J. P. Klare, University of Osnaabrück.

## 2.5 Computational methods

The 3D model of the *S. cerevisiae* c-ring was based on the crystal structure of the *E. hirae* K-ring, which shares 24% sequence identity and 68% similarity to the *S. cerevisiae* ring and as such is believed to share a very similar fold. The computational modeling was carried out as described in Bockelmann *et al.* (2010).

Curve fitting for the inhibition assays was performed with the help of Origin 8.1 using the hill1 equation. Amino acid sequence alignments were performed using the ClustalW program and further alignment tools provided by the Biology WorkBench 3.2. (<http://workbench.sdsc.edu>).

### 3. Results

#### 3.1 Site-directed mutagenesis of the *VMA3* gene in *Saccharomyces cerevisiae*

Archazolid was presumed to share at least part of its binding site with the plecomacrolide antibiotics concanamycin and bafilomycin as it prevented binding of a radioactive PAL derivative of concanamycin A ( $^{125}\text{I}$ -concanolid A) to subunit c of the V-ATPase in a competition assay (Huss *et al.*, 2005). The plecomacrolide binding site was identified in 2002 on the one hand via random mutagenesis in *N. crassa* (Bowman and Bowman, 2002) and on the other hand via PAL using  $^{125}\text{I}$ -concanolid A (Huss *et al.*, 2002). Further mutagenesis studies in *N. crassa* finally resulted in a model of the binding site which is proposed to be located at the interface of two adjacent c subunits at the  $V_O$  ring (Bowman *et al.*, 2006; Bowman *et al.*, 2004). The binding pocket is mainly formed by 11 amino acids located in helices 1 and 2 of one c subunit and in helix 4 of the adjacent c subunit (Bowman *et al.*, 2006; Fig 1.7). To investigate the contribution of these amino acids to the binding of archazolid in *S. cerevisiae*, those exchanges in Vma3p were chosen for site-directed mutagenesis that had increased the  $\text{IC}_{50}$  value for bafilomycin in *N. crassa* 10-fold or more.

##### 3.1.1 Site-directed mutagenesis of *VMA3*

In a spotting growth assay on medium with elevated calcium chloride (YPDA  $\text{CaCl}_2$ ) or alkaline pH (YPDA pH 7.5) the strain BMA64-1B $\Delta vma3$  ( $\Delta vma3$ ) exhibited a typical *vma<sup>-</sup>* phenotype (paragraph 1.3.2) proving the absence of assembled V-ATPase (Noumi *et al.*, 1991; Fig. 3.1). In addition, this strain was not capable of vacuolar acidification (Fig. 3.1). To test the ability of the plasmid-borne version of Vma3p to complement the deletion in BMA64-1B $\Delta vma3$ , the mutant strain was transformed with pRS415-*VMA3* and spotted on YPDA  $\text{CaCl}_2$  and YPDA pH 7.5. As can be seen in Fig. 3.1, the deletion was completely complemented by expression of Vma3p from the plasmid resulting in wild type growth of the transformed strain (Vma3) on all growth media. Acidification of the vacuole in Vma3 was verified by staining of the vacuolar lumen with quinacrine (Fig. 3.1). These results confirmed the suitability of the deletion strain and the plasmid pRS415-*VMA3* for subsequent mutagenesis studies.

Following successful mutagenesis (paragraph 2.2.10), the mutated plasmids were expressed in BMA64-1B $\Delta vma3$  and the resulting yeast strains were named according to the respective amino acid exchange in Vma3p. Amino acid exchanges selected as denoted in paragraph 3.1.1 were: T32I, I39F, I54F, G61S, F135L, Y142H and Y142N. These mutations are in the following referred to as “bafilomycin-mutations”. In addition to the known exchanges from *N. crassa* the respective amino acid residues in *S. cerevisiae* were also mutated to alanine (T32A, I39A, I54A, G61A, F135A and Y142A).

### 3.1.2 Influence of mutations on cell growth and vacuolar acidification

The ability of the mutant versions of Vma3p to substitute the wild type Vma3p in BMA64-1B $\Delta$ vma3 was tested with spotting growth assays and quinacrine staining (Fig. 3.1). In half of the strains, expression of the mutant Vma3p resulted in good complementation of the vma<sup>-</sup> phenotype on YPDA CaCl<sub>2</sub> and YPDA pH 7.5. The strains T32A, I39A, I54A and I54F exhibited wild type growth, and T32I, I39F and G61S grew only a bit more slowly at pH 7.5. Quinacrine staining was also positive in all of these strains, proving acidification of the vacuolar lumen. However, the strains G61A, F135A, F135L, Y142A, Y142H and Y142N showed strongly reduced growth in particular at pH 7.5 and vacuolar acidification was only observed in F135L. This suggests that especially mutations in helix 4 are less tolerable to the V-ATPase. Nevertheless, these results pointed to the assembly of an at least partially functional V-ATPase in all yeast strains bearing a mutation in Vma3p.

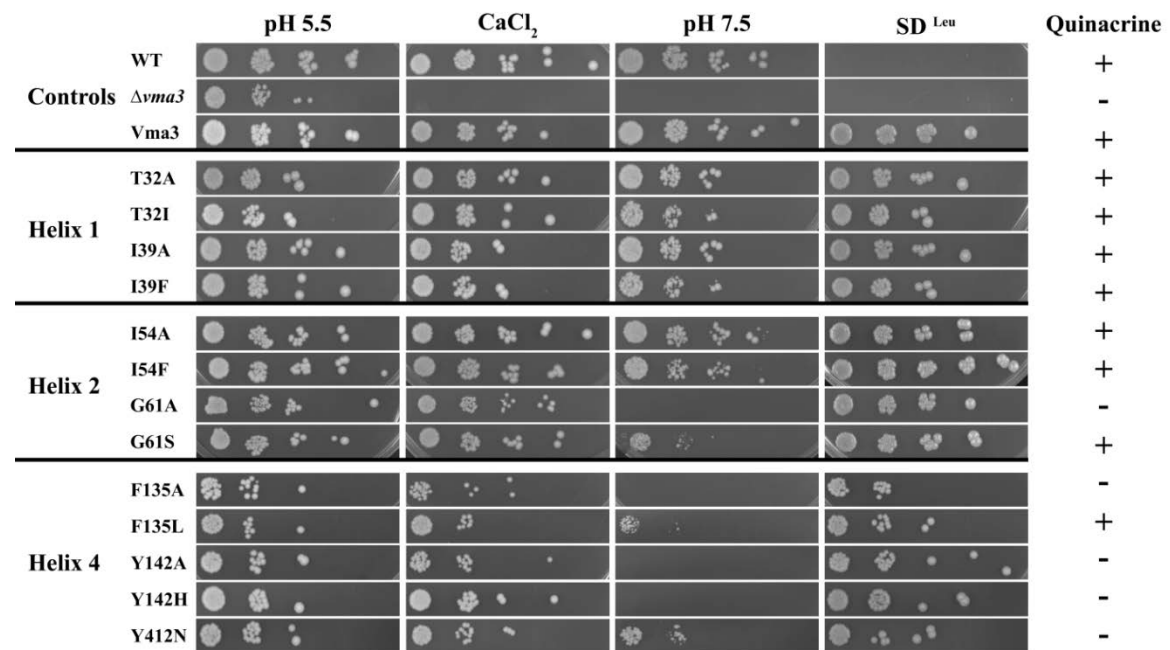


**Figure 3.1:** *In vivo* assays of yeast strains expressing mutated versions of the V-ATPase subunit Vma3p.

Cells were dropped on YPDA plates pH 5.5 with or without calcium chloride, on YPDA buffered to pH 7.5 and on selection medium without leucine (SD<sup>Leu</sup>). Quinacrine staining was used to visualize accumulation of protons in the vacuole of living yeast cells as indication for an intact V-ATPase as described in “Material and Methods”. The fluorescence within the vacuoles of V-ATPase mutant strains was classified as positive (+) i.e. similar to the wild type strain or negative (-) i.e. like in the respective deletion strain. WT, BMA64-1B;  $\Delta$ vma3, BMA64-1B $\Delta$ vma3; Vma3, BMA64-1B $\Delta$ vma3 expressing wild type Vma3p; strains expressing Vma3p with the indicated mutations.

### 3.1.3 Assembly and activity of the mutant V-ATPase

The results from the *in vivo* assays that indicated a functional V-ATPase were strengthened by Western Blot analysis of isolated vacuoles from the mutant strains. To proof the attachment of the V<sub>1</sub> complex to the V<sub>O</sub> complex at the vacuolar membrane an antibody against Vma1p was used (Noumi *et al.*, 1991). As can be seen in Fig. 3.2, a strong signal was visible in the wild type strain (WT), whereas Vma1p was not present in the *vma3* deletion strain ( $\Delta vma3$ ), indicating the absence of assembled V-ATPase at the vacuolar membrane. In contrast, in all mutant strains a clear signal of Vma1p was detected at the membrane confirming that none of the mutations impeded assembly of the V-ATPase.

Functionality of the mutant V-ATPases was also tested by measurement of the ATPase activity using isolated yeast vacuoles (Tab. 3.1). For all mutagenesis experiments the bafilomycin-, as well as the archazolid-sensitive, activities were calculated. As only negligible differences between these values became evident, the focus in the present study will be on the bafilomycin-sensitive activities in order to give the opportunity to compare the values with the recent literature. In case of the mutations presented in this paragraph, most of the Vma3p mutant strains showed bafilomycin-sensitive activity of approximately 50-100% of the wild type activity. The mutation Y142N led to a greater reduction of the V-ATPase activity with only 0.1  $\mu\text{mol}/\text{min}/\text{mg}$  which was however still 30% of the wild type activity. Only mutation Y142A resulted in an activity below 25% of the wild type activity and therefore, this strain was omitted from further experiments.

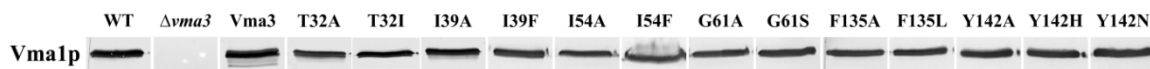


**Figure 3.2: Assembly of the V-ATPase in yeast strains expressing the mutant Vma3 proteins.**

The assembly of the mutant versions of Vma3p into V-ATPase complexes was verified by Western Blot analysis of isolated vacuolar membranes. Using an antibody against Vma1p, the attachment of the V<sub>1</sub> complex to the vacuolar membrane was interpreted as a proof for the correct assembly of the V<sub>1</sub>V<sub>O</sub> holoenzyme (Noumi *et al.*, 1991). WT, BMA64-1B;  $\Delta vma3$ , BMA64-1B $\Delta vma3$ ; Vma3, BMA64-1B $\Delta vma3$  expressing wild type Vma3p; Strains expressing Vma3p with the indicated mutations. For each strain 10  $\mu\text{g}$  of vacuolar protein were applied.

**Table 3.1: Bafilomycin A1 and archazolid A sensitive activity of vacuolar membranes isolated from yeast strains expressing either the wild type or a mutated version of Vma3p.**

Vacuolar membrane preparations and ATPase activity assays of the wild type (BMA64-1B) and the mutant strains were carried out as described under “Material and Methods”. The activities were corrected for the residual activity at the point of maximal inhibition by bafilomycin A1 and archazolid A, respectively. Values are the averages obtained from two or three independent vacuolar preparations with standard deviations as indicated.

Mutation in Vma3p	ATPase activity	
	sensitive to bafilomycin A1	sensitive to archazolid A
	$\mu\text{mol}/\text{min}/\text{mg}$	
<i>Control</i>		
BMA64-1B	0.30 ± 0.06	0.29 ± 0.11
<i>Helix 1</i>		
T32A	0.20 ± 0.04	0.22 ± 0.04
T32I	0.27 ± 0.08	0.25 ± 0.04
I39A	0.39 ± 0.04	0.46 ± 0.08
I39F	0.32 ± 0.11	0.36 ± 0.18
<i>Helix 2</i>		
I54A	0.20 ± 0.05	0.20 ± 0.07
I54F	0.18 ± 0.02	0.19 ± 0.01
G61A	0.15 ± 0.07	0.18 ± 0.03
G61S	0.18 ± 0.05	0.23 ± 0.02
<i>Helix 4</i>		
F135A	0.24 ± 0.08	0.31 ± 0.07
F135L	0.16 ± 0.03	0.15 ± 0.01
Y142A	0.05 ± 0.03	0.06 ± 0.02
Y142H	0.25 ± 0.13	0.26 ± 0.14
Y142N	0.10 ± 0.01	0.12 ± 0.02

### 3.1.4 Influence of mutations on inhibitor binding

The influence of the mutations in the Vma3p of *S. cerevisiae* on the binding of archazolid or bafilomycin was tested by activity assays on isolated yeast vacuoles at inhibitor concentrations ranging from 0.1 nM to 3.0  $\mu\text{M}$ . The  $\text{IC}_{50}$  value for the wild type strain BMA64-1B was 6.6 nM for archazolid A and 4.7 nM for bafilomycin A1 (Tab. 3.2). Regarding bafilomycin, our results in principle confirmed the data published for *N. crassa* (Bowman *et al.*, 2006). The most striking effect resulted from the G61S mutation that exhibited an approximately 70-fold higher  $\text{IC}_{50}$  value compared to the wild type *S. cerevisiae* strain (Tab. 3.2; Fig. 3.3A), being consistent with a 90-fold increase which had been reported for *N. crassa* (Bowman *et al.*, 2006). The mutations F135L, Y142H and Y142N had an approximately 10-fold higher  $\text{IC}_{50}$  value, which was also in the range of the published results (Bowman *et al.*, 2006). A notably lower increase of the  $\text{IC}_{50}$  value for the T32I mutation in *S. cerevisiae* as compared to *N. crassa* had already been observed before (Bowman *et al.*, 2004). In contrast to the results obtained for *N. crassa*, the mutation I39F had virtually no influence on the binding of bafilomycin in *S. cerevisiae* (Tab. 3.2.; Fig. 3.3A). Interestingly, the mutation I54F approximately halved the  $\text{IC}_{50}$  value for bafilomycin A1 in comparison to the wild type strain, suggesting a V-ATPase slightly more sensitive toward bafilomycin. However, the minor influence of the I54F mutation in contrast to the corresponding mutation in *N. crassa* is in line with previous

data for *S. cerevisiae* (Bowman *et al.*, 2006; Bowman *et al.*, 2004). The mutation of isoleucine 39, isoleucine 54 and glycine 61 to alanine in principle showed the same effect on the respective  $IC_{50}$  value as described above, while T32A had almost no influence (Tab. 3.2). In contrast, the mutation F135A resulted in an even 10-fold higher increase in the  $IC_{50}$  value for bafilomycin when compared to F135L, confirming the importance of phenylalanine 135 for inhibitor binding.

Regarding the binding of archazolid (Tab. 3.2; Fig. 3.3B), none of the mutations with a negative influence on the binding of bafilomycin showed a decrease of sensitivity. In contrast, most of the “bafilomycin-mutations” appeared to increase the sensitivity of the V-ATPase toward archazolid slightly, and the mutation Y142N even led to a strong increase of sensitivity, with an  $IC_{50}$  value approximately 10-fold lower when compared to the wild type strain. The finding that there was hardly any similarity regarding the effects of the mutations on bafilomycin and archazolid binding was quite surprising, because the results of previous competition experiments had implied that plecomacrolides and archazolid at least partially share a common binding site (Huss *et al.*, 2005).

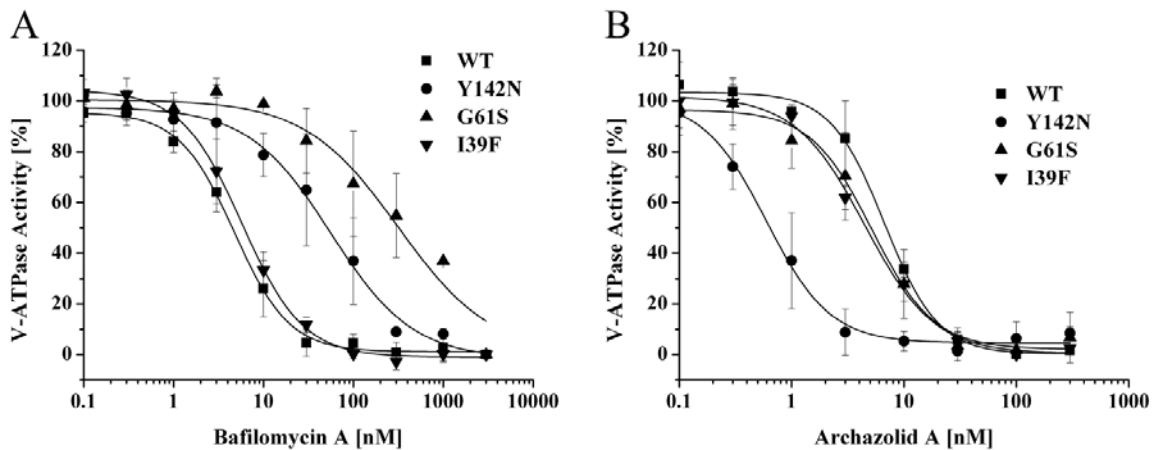


**Figure 3.3: Influence of “bafilomycin-mutations” in Vma3p of *Saccharomyces cerevisiae* on inhibitor binding.**

V-ATPase activities were measured on isolated yeast vacuoles of the wild type strain BMA64-1B (WT) and strains with mutations in Vma3p as indicated. Values are the average of three independent vacuolar preparations. Error bars are standard deviations. Absolute archazolid A and bafilomycin A1 sensitive activities are shown in Table 3.1,  $IC_{50}$  values in Table 3.2.



**Table 3.2: IC<sub>50</sub> values for the inhibition of the wild type and mutant strains by bafilomycin A1 and archazolid A.**

Vacuolar membrane preparations and ATPase activity assays were carried out as described under “Material and Methods”. The activities were corrected for the residual activity at the point of maximal inhibition by bafilomycin A1 and archazolid A, respectively. IC<sub>50</sub> values with the indicated standard errors result from plotting the average values obtained from two or three independent vacuolar preparations.

Mutation in Vma3p	Bafilomycin A1	Archazolid A	Bafilomycin A1	Archazolid A
	<i>IC<sub>50</sub> [nM]</i>		<i>Factor</i>	
<i>Control</i>				
BMA64-1B	4.7 ± 0.4	6.6 ± 0.5		
<i>Helix 1</i>				
T32A	3.3 ± 0.4	4.9 ± 1.1	0.7	0.4
T32I	38.4 ± 2.4	3.7 ± 0.9	8.0	0.6
I39A	6.4 ± 0.5	5.2 ± 0.7	1.4	0.8
I39F	5.8 ± 0.4	4.1 ± 0.4	1.2	0.6
<i>Helix 2</i>				
I54A	2.8 ± 0.5	2.0 ± 0.2	0.6	0.3
I54F	1.7 ± 0.1	3.4 ± 0.4	0.4	0.5
G61A	346.1 ± 64.8	6.3 ± 0.9	73.6	1.0
G61S	315.7 ± 72.7	4.7 ± 0.9	67.2	0.7
<i>Helix 4</i>				
F135A	489.2 ± 76.9	5.2 ± 0.7	104.1	0.8
F135L	35.7 ± 8.8	3.1 ± 0.4	7.6	0.5
Y142H	38.3 ± 6.4	4.1 ± 1.4	8.1	0.6
Y142N	56 ± 9.7	0.7 ± 0.1	12.0	0.1

## 3.2 Photo affinity labeling of the *Manduca sexta* V-ATPase

### 3.2.1 PAL derivatives of archazolid

To demonstrate the binding of archazolid to subunit c we performed cross-linking studies with radioactive photo-activatable analogues of the inhibitor. For this purpose derivatives with either one (MD-archazolid; Fig. 3.4A) or two (BD-archazolid; Fig. 3.4B) diazirinyl groups - with or without  $^{14}\text{C}$  - were synthesized based on prior structure function analysis (Menche *et al.*, 2007b; Menche *et al.*, 2007c). The non-radioactive derivatives were tested for inhibitory efficiency on the purified V-ATPase from *M. sexta* (Fig. 3.4C). The addition of one diazirinyl group had only a moderate effect, increasing the  $\text{IC}_{50}$  value, compared to that for archazolid, from  $0.016\ \mu\text{M}$  to  $0.15\ \mu\text{M}$ . The  $\text{IC}_{50}$  value of BD-archazolid was 40fold higher, but with  $0.6\ \mu\text{M}$  still in the low micromolar range. Therefore the  $^{14}\text{C}$ -labeled isotopologues of these derivatives were used for cross-linking experiments.

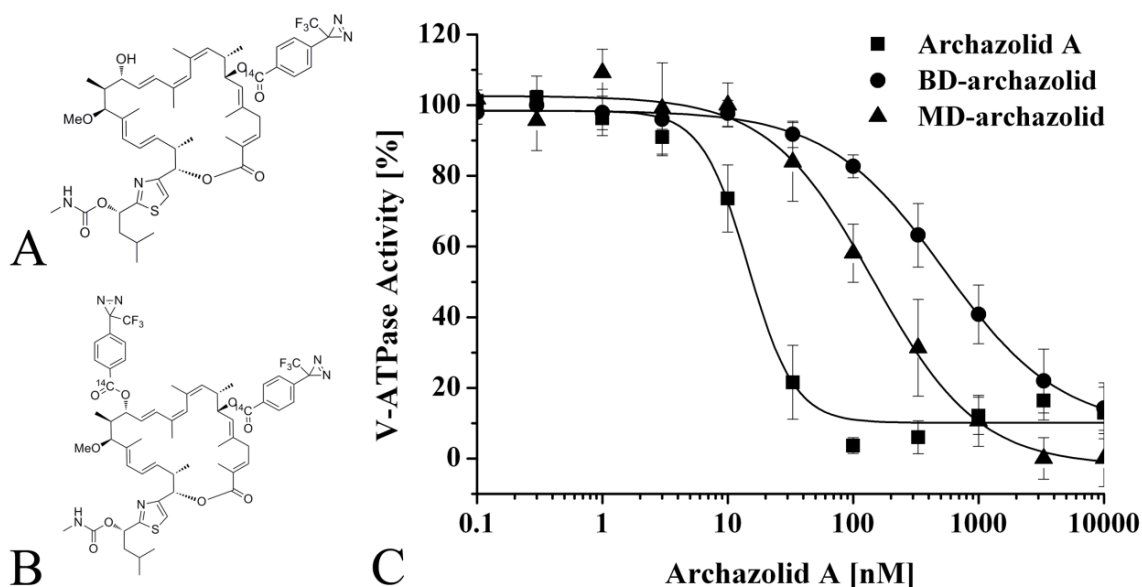


**Figure 3.4: Derivatives of archazolid A created for PAL studies.**

Based on structure function analysis (Menche *et al.*, 2007b; Menche *et al.*, 2007c) derivatives for cross-linking studies, MD- (A) and BD-archazolid (B), were created. (C) Inhibition of the V-ATPase by MD- and BD-archazolid. Purification of the *M. sexta*  $V_1V_0$  holoenzyme and following activity assays were carried out as described under “Material and Methods”. Values represent the average of three independent preparations, with error bars corresponding to standard deviations. V-ATPase activity sensitive to archazolid A was  $1.8 \pm 0.2\ \mu\text{mol}/\text{min}/\text{mg}$ . The  $\text{IC}_{50}$  values were  $0.016 \pm 0.002\ \mu\text{M}$  for the non-modified inhibitor,  $0.15 \pm 0.02\ \mu\text{M}$  for MD-archazolid and  $0.6 \pm 0.03\ \mu\text{M}$  for BD-archazolid.

### 3.2.2 Binding of PAL derivatives to subunit c of the V-ATPase

Autoradiograms of *M. sexta* V-ATPase labeled with  $^{14}\text{C}$ -MD- and  $^{14}\text{C}$ -BD-archazolid, respectively, are shown in Fig. 3.5. Due to the increased  $\text{IC}_{50}$  value of the compounds (Fig. 3.4C), a high concentration was needed for labeling, inevitably leading to a high overall background in the autoradiograms. Nevertheless, a prominent labeling of a band at the molecular mass of subunit c could be observed for both PAL inhibitors (Fig. 3.5A and B, black arrow). This labeling was drastically reduced after preincubation of the V-ATPase with 50  $\mu\text{M}$  concanamycin A (Fig. 3.5A and B). Because concanamycin A is known to bind to subunit c of the V-ATPase (Huss *et al.*, 2002), this result clearly points to the specific labeling of subunit c by  $^{14}\text{C}$ -MD and  $^{14}\text{C}$ -BD-archazolid. In addition, the identity of subunit c was confirmed by labeling with the PAL derivative of concanamycin,  $^{14}\text{C}$ -concanolid A (Bender *et al.*, 2007; Huss *et al.*, 2002) (Fig. 3.5C, black arrow). Labeling of additional subunits by  $^{14}\text{C}$ -concanolid A is currently investigated (Nardmann, C., Wieczorek, H. and Huss, M., manuscript in preparation). Excision of the bands of subunit c from the SDS-PAGE and subsequent evaluation of the radioactivity with a scintillation counter revealed a difference between the UV-treated and non-treated samples of  $25 \pm 0.25$  cpm for  $^{14}\text{C}$ -concanolid A and  $20 \pm 0.2$  cpm for  $^{14}\text{C}$ -MD-archazolid, both comprising one  $^{14}\text{C}$ -isotope, and  $37 \pm 0.37$  cpm for  $^{14}\text{C}$ -BD-archazolid which comprises two  $^{14}\text{C}$ -isotopes (means  $\pm$  standard deviations).

Upon incubation with  $^{14}\text{C}$ -BD-archazolid, a very slight difference between the UV-treated and non-treated samples became visible at the protein band with the highest molecular mass, representing the  $V_{\text{O}}$  subunit a (Fig. 3.5B; lane 1 and 2). However, the evaluation of these bands in a scintillation counter did not reveal a significant labeling of subunit a (data not shown) and furthermore, no difference was visible in the experiment presented in Fig. 3.5C (lane 3 and 4), indicating that the apparent labeling in Fig. 3.5B was an artifact. Due to limited amounts of  $^{14}\text{C}$ -BD-archazolid, these experiments could not be repeated.

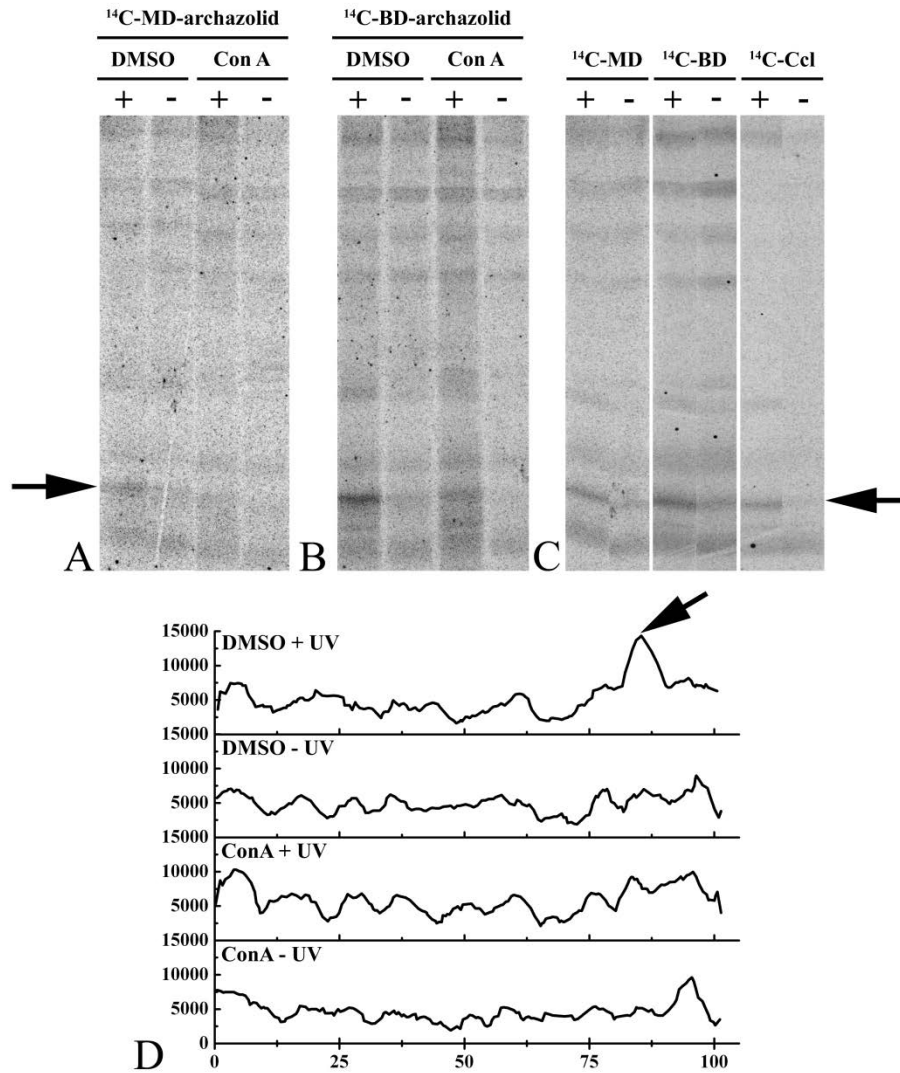


**Figure 3.5: Labeling of subunit c with radioactive derivatives of archazolid A.**

Purification of the *M. sexta* V-ATPase was carried out as described under “Material and Methods”. (A and B) The V-ATPase was preincubated with 50  $\mu$ M concanamycin A or with the solvent dimethyl sulfoxide. Next, <sup>14</sup>C-MD- (A) or <sup>14</sup>C-BD-archazolid (B) was added and the cross-linking reaction was induced by exposure to UV-light (366 nm) for 1 min (+). Controls without UV-exposure (-). Note that due to the lower affinity of the V-ATPase for MD- and BD-archazolid (Fig. 3.4C) the concentration of the <sup>14</sup>C-isotopologues for labeling has to be very high. This leads to an unavoidable high background in the gel. (C) The V-ATPase was incubated with the radioactive derivatives of either archazolid (<sup>14</sup>C-MD and <sup>14</sup>C-BD) or concanamycin A (<sup>14</sup>C-Ccl) and the cross-linking reaction was induced as described above (+). Controls without UV-exposure (-). (D) Line scan of the autoradiography shown in (B). Arrows indicating subunit c.

### 3.3 Fluorescent labeling of the *Manduca sexta* V-ATPase

#### 3.3.1 Binding competition of archazolid with NCD-4 at subunit c

The fluorescent carbodiimide NCD-4 (Chadwick and Thomas, 1983) specifically binds, like DCCD, to the essential glutamate within helix 4 of subunit c, leading to the inhibition of the V-ATPase (Finbow *et al.*, 1992). Labeling experiments with the *M. sexta* V-ATPase were used to find out, whether there is any interference between archazolid and NCD-4, which would indicate a binding of the macrolactone close to the essential glutamate.

The incubation of either the V-ATPase holoenzyme or the  $V_O$  complex with NCD-4 revealed a prominent band of appropriate size in the SDS-PAGE (Fig. 3.6; lane 1). In the holoenzyme this label was completely impeded by preincubation with archazolid A (lane 4), whereas bafilomycin A1 (lane 3) had no pronounced effect. Preincubation of the  $V_O$  complex with the inhibitors led to similar results, except that archazolid A did not completely prevent labeling of subunit c. This is probably due to a better accessibility of the c-ring in the free  $V_O$  complex or the higher abundance of subunit c in the  $V_O$  sample, resulting in labeling of some c subunits with NCD-4. The different effects of bafilomycin A1 and archazolid A were unexpected because previous data had shown that bafilomycin A1, B1 and archazolid A as well as concanamycin prevented labeling of subunit c with a radioactive derivative of concanamycin A ( $^{125}\text{I}$ -concanolide A) (Huss *et al.*, 2002; Huss *et al.*, 2005).  $\text{IC}_{50}$  values of all compounds are given in Fig. 3.7B.

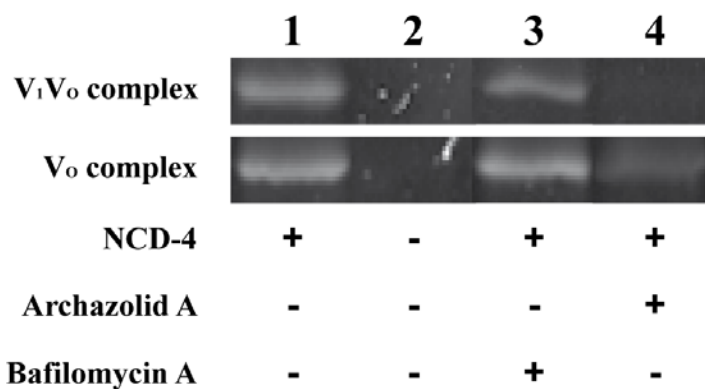


**Figure 3.6: NCD-4 labeling of the V-ATPase subunit c in the presence of archazolid and bafilomycin.**

Purification of the *M. sexta* V-ATPase and the NCD-4 labeling was carried out as described under “Material and Methods”. Either  $V_1V_O$  holoenzyme or the  $V_O$  complex was preincubated for 10 min at 25°C with 50  $\mu\text{M}$  bafilomycin A1 (lane 3) or archazolid A (lane 4), respectively. Then NCD-4 was added to a final concentration of 0.1 mM and the probe was incubated for 3 h at 25°C. Control reactions were performed using dimethyl sulfoxide for preincubation, followed by the addition of NCD-4 or pure ethanol (lanes 1 and 2). Of each sample approximately 20  $\mu\text{g}$  of protein was subjected to SDS-PAGE and the NCD-4 labeling of subunit c was documented under UV light (Versadoc, BioRad). The  $\text{IC}_{50}$  values were  $3.0 \pm 0.2 \mu\text{M}$  for NCD-4 (Fig. 3.7B),  $16 \pm 0.2 \text{ nM}$  for archazolid A (Fig. 3.4C) and  $9.0 \pm 0.8 \text{ nM}$  for bafilomycin A (Fig. 3.7B).

### **3.3.2 Suppression of archazolid binding monitored with NCD-4 labeling**

To find out the reason for the apparent discrepancy described in the preceding paragraph, we preincubated the V-ATPase of *M. sexta* with different inhibitors, followed in a first step by the incubation with archazolid A and in a second step by incubation with NCD-4 (Fig. 3.7A). After preincubation with an excess of the plecomacrolides, bafilomycin A1, concanamycin A and concanolide A, respectively, the addition of archazolid A no longer prevented the binding of NCD-4 to subunit c (Fig. 3.7A; lanes 3, 5 and 7; for IC<sub>50</sub> values see Fig. 3.7B). In contrast, preincubation with apicularen A, a member of the benzolactone enamides family of V-ATPase inhibitors, which is predicted to have a binding site totally different from that for archazolid and the plecomacrolides (Huss *et al.*, 2002; Huss *et al.*, 2005; Menche *et al.*, 2007c), did not impede the binding of archazolid A as indicated by a clear prevention of NCD-4 labeling (Fig. 3.7A; lane 9). Taken together, it is thus very likely that the binding sites for archazolid and the plecomacrolides overlap significantly, but to a smaller extent than expected before (Huss *et al.*, 2005).

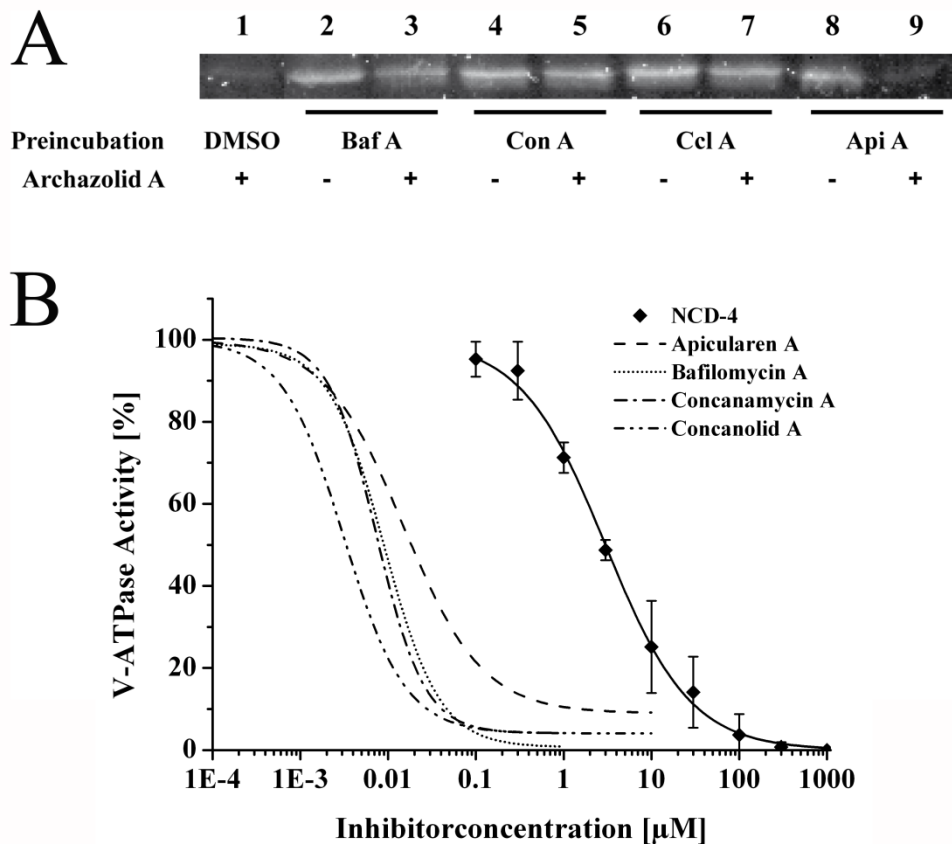


**Figure 3.7: Suppression of archazolid binding monitored with NCD-4 labeling of the V-ATPase subunit c.**

(A) Purification of the *M. sexta* V<sub>1</sub>V<sub>0</sub> holoenzyme and the NCD-4 labeling was carried out as described under “Material and Methods”. The V-ATPase was preincubated for 1 h at 25°C with an excess (0.5 mM) of either bafilomycin A1 (Baf A), concanamycin A (Con A), concanolide A (Ccl A), apicularen A (Api A) or with the solvent dimethyl sulfoxide. The samples were then incubated for 10 min at 25°C in the presence of 50 μM archazolid A (lanes 1, 3, 5, 7 and 9) or dimethyl sulfoxide (lanes 2, 4, 6 and 8). After that, all samples were additionally incubated for 1 h at 25°C with 0.1 mM NCD-4. Of each sample approximately 20 μg of protein was subjected to SDS-PAGE and the NCD-4 labeling of subunit c was documented under UV light (Versadoc, BioRad). (B) Inhibition curves of the inhibitors used in (A). Purification of the *M. sexta* V<sub>1</sub>V<sub>0</sub> holoenzyme and following activity assays were carried out as described under “Material and Methods”. The NCD-4 sensitive V-ATPase activity was  $2.2 \pm 0.4$  μmol/min/mg, the IC<sub>50</sub> value was  $3.0 \pm 0.2$  μM. Other IC<sub>50</sub> values were  $15 \pm 1.5$  nM for apicularen A (taken from Huss *et al.*, 2005),  $9.0 \pm 0.8$  nM for bafilomycin A,  $7.4 \pm 0.5$  nM for concanamycin A (taken from Huss *et al.*, 2002) and  $3.1 \pm 0.6$  nM for concanolide A (Nardmann *et al.*, manuscript in preparation). Values represent the average of at least two independent preparations, with error bars corresponding to the standard deviations.

### 3.4 Influence of further mutations within the proposed archazolid binding site

#### 3.4.1 Selection of amino acid residues for site-directed mutagenesis

As a consequence of the results described above we selected amino acids within Vma3p (Y66, I130, L131, I134, V138, L141, L144, I145) which we presumed to interact with archazolid for further mutagenesis studies. In the first instance amino acids I130, L131 or I134 were mutated to alanine and phenylalanine, respectively, in order to introduce either a small or a bulky side chain. During further studies, the amino acids were replaced by similar and structurally different amino acids, respectively, to strike a balance between the disturbance of protein structure on the one hand, and a significant influence of the mutation on inhibitor binding on the other hand.

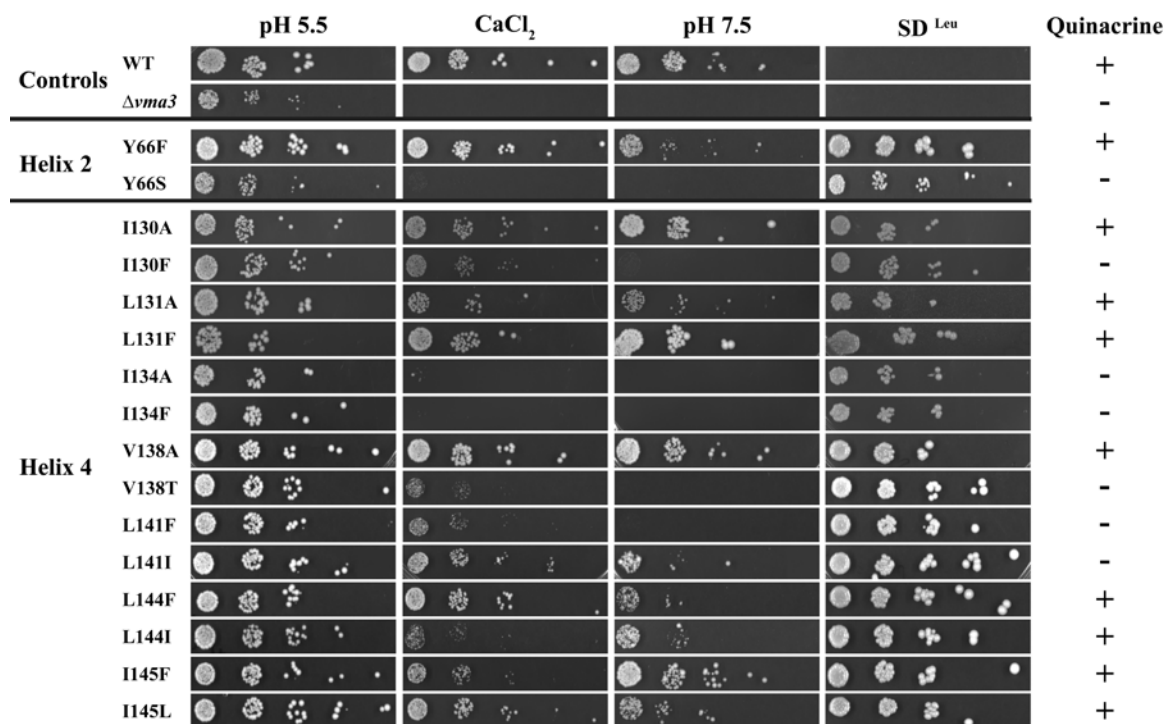


**Figure 3.8:** *In vivo* assays of yeast strains expressing Vma3p with selected mutations.

Cells were dropped on YPDA plates pH 5.5 with or without calcium chloride, on YPDA buffered to pH 7.5 and on selection medium without leucine (SD<sup>Leu</sup>). Quinacrine staining was used to visualize accumulation of protons in the vacuole of living yeast cells as indication for an intact V-ATPase as described in the “Material and Methods”. The fluorescence within the vacuoles of V-ATPase mutant strains was classified as positive (+) i.e. similar to the wild type strain or negative (-) i.e. like in the respective deletion strain. WT, BMA64-1B;  $\Delta vma3$ , BMA64-1B $\Delta vma3$ ; strains expressing Vma3p with the indicated mutations.

#### 3.4.2 Influence of mutations on cell growth and vacuolar acidification

The mutant strains were tested for growth on medium with pH 7.5 and on medium containing 0.1 M CaCl<sub>2</sub> at pH 5.5 (Fig. 3.8). Transformation of BMA64-1B $\Delta vma3$  with pRS415-VMA3 bearing the mutation I130A, L131F, V138A or I145F resulted in total complementation of the *vma*<sup>-</sup> phenotype on all media. The strains Y66F, L131A, L141I, L144F, L144I and I145L grew only slightly slower, while the mutations I130F, V138T



and L141F resulted in clearly reduced growth in particular at pH 7.5. Y66S, I134A and I134F exhibited a typical *vma<sup>-</sup>* phenotype. These results were supported by vacuolar staining of the strains with quinacrine (Fig. 3.8). Mutant strains with strongly reduced or impeded growth did not accumulate quinacrine in the vacuoles clearly pointing to a negative influence of these mutations on V-ATPase function. In contrast, the mutant strains which exhibited good cell growth also showed clear quinacrine staining (Y66F, I130A, L131A, L131F, V138A, L144F, L144I, I145F and I145L) proving acidification of the vacuole. Thus, most of the mutations performed in this set of experiments did not restrain the *in vivo* function of the V-ATPase too much.

### 3.4.3 Assembly and activity of the mutant V-ATPase

Assembly of the V-ATPase at the vacuolar membrane of the mutant strains was tested by Western blot analysis of isolated vacuoles. For this purpose, an antibody against the V<sub>1</sub> subunit Vma1p was used (Noumi *et al.*, 1991). As shown in Fig. 3.9, for all strains a clear signal of Vma1p could be detected, confirming that none of the mutations impeded the assembly of the V-ATPase at the membrane. For some mutations, in particular Y66S, L144F and L144I, the signal was clearly reduced indicating impaired assembly of the V-ATPase in these strains. Nevertheless, only mutation Y66S led to a *vma<sup>-</sup>* phenotype. In contrast, the strains I134A and I134L showed a strong signal for Vma1p but also exhibited a *vma<sup>-</sup>* phenotype in the *in vivo* assays (paragraph 3.4.2.). None of the strains exhibiting a *vma<sup>-</sup>* phenotype was used for further experiments.

Functionality of the mutant V-ATPases in all other strains was additionally tested by measurement of the ATPase activity using isolated yeast vacuoles (Tab. 3.3). Again, most of the mutant strains showed bafilomycin-sensitive activity of more than 50% up to 100% of the wild type activity. Only two strains (L131A and L141F) showed higher reduction in the activity which was, however, approximately 40% of that of the wild type. Mutation I145L even led to an increase in V-ATPase activity of 80% suggesting that this mutation enhances V-ATPase function.

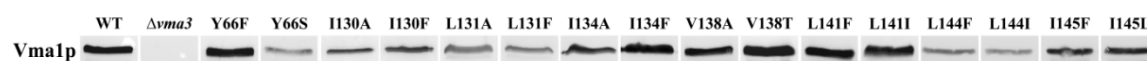


**Figure 3.9: Assembly of the V-ATPase in yeast strains expressing Vma3p with selected mutations.**

The assembly of the mutated versions of Vma3p into V-ATPase complexes was verified by Western Blot analysis of isolated vacuolar membranes, using an antibody against Vma1p. WT, BMA64-1B;  $\Delta vma3$ , BMA64-1B $\Delta vma3$ ; Strains expressing the Vma3p with the indicated mutations. For each strain 10  $\mu$ g of vacuolar protein were applied.

**Table 3.3: Bafilomycin A1 and archazolid A sensitive activity of vacuolar membranes isolated from yeast strains expressing either the wild type or a mutated version of the Vma3p.**

Vacuolar membrane preparations and ATPase activity assays of the wild type (BMA64-1B) and the mutant strains were carried out as described under “Material and Methods”. The activities were corrected for the residual activity at the point of maximal inhibition by bafilomycin A1 and archazolid A, respectively. Values are the averages obtained from two or three independent vacuolar preparations with standard deviations as indicated.

Mutation in Vma3p	ATPase activity	ATPase activity
	sensitive to bafilomycin A1	sensitive to archazolid A
	<i>μmol/min/mg</i>	
<i>Control</i>		
BMA64-1B	0.30 ± 0.06	0.29 ± 0.11
<i>Helix 2</i>		
Y66F	0.31 ± 0.05	0.34 ± 0.06
<i>Helix 4</i>		
I130A	0.20 ± 0.06	0.17 ± 0.03
L131A	0.11 ± 0.05	0.13 ± 0.04
L131F	0.18 ± 0.03	0.20 ± 0.02
V138A	0.28 ± 0.02	0.27 ± 0.06
V138T	0.25 ± 0.10	0.26 ± 0.10
L141F	0.14 ± 0.01	0.10 ± 0.01
L141I	0.28 ± 0.11	0.26 ± 0.13
L144F	0.40 ± 0.08	0.33 ± 0.03
L144I	0.23 ± 0.01	0.22 ± 0.03
I145F	0.18 ± 0.07	0.25 ± 0.09
I145L	0.54 ± 0.01	0.48 ± 0.08

### 3.4.4 Influence of mutations on inhibitor binding

Regarding bafilomycin, most of the established mutations rendered the V-ATPase only slightly more resistant (V138A, L141F and I145L) or slightly more sensitive (Y66F, L141I, L144F and I145F) to the inhibitor (Tab. 3.4). Thus, it is not likely that these amino acids interact directly with bafilomycin. In contrast, the mutation L131A and especially V138T exhibited a more striking effect with an approximately 10-fold increase of the IC<sub>50</sub> value for bafilomycin (Tab. 3.4; Fig. 3.10A). On the other hand, the mutations I130A, L131F and L144I notably reduced the IC<sub>50</sub> value approximately 5-fold indicating a V-ATPase more sensitive toward the inhibitor.

Concerning archazolid, the additional mutations in general also only led to slight changes of the IC<sub>50</sub> value and in most cases made the V-ATPase more sensitive toward the inhibitor (Tab. 3.4). Remarkably, the mutation L144I revealed the strongest effect with an IC<sub>50</sub> value 10-fold lower than in the wild type strain, clearly pointing to a V-ATPase more sensitive toward archazolid (Tab. 3.4; Fig. 3.10B).

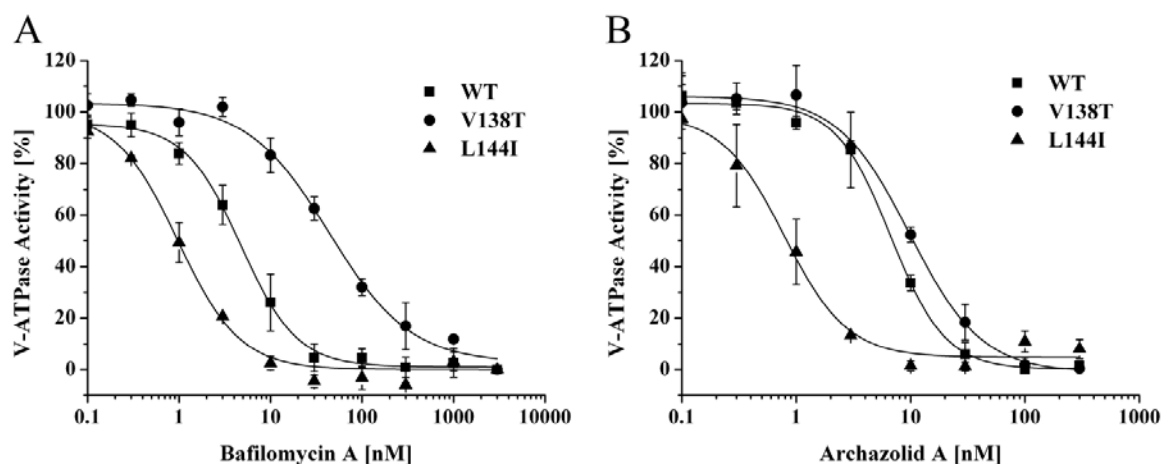


**Figure 3.10: Influence of selected mutations in Vma3p of *Saccharomyces cerevisiae* on inhibitor binding.**

V-ATPase activities were measured on isolated yeast vacuoles of the wild type strain BMA64-1B (WT) and strains with mutations in Vma3p as indicated. Values are the average of three independent vacuolar preparations. Error bars are standard deviations. Absolute archazolid A and bafilomycin A1 sensitive activities are shown in Table 3.3,  $IC_{50}$  values in Table 3.4.

**Table 3.4:  $IC_{50}$  values for the inhibition of the wild type and mutant strains by bafilomycin A1 and archazolid A.**

Vacuolar membrane preparations and ATPase activity assays were carried out as described under “Material and Methods”. The activities were corrected for the residual activity at the point of maximal inhibition by bafilomycin A1 and archazolid A, respectively.  $IC_{50}$  values with the indicated standard errors result from plotting the average values obtained from two or three independent vacuolar preparations.

Mutation in Vma3p	Bafilomycin A1	Archazolid A	Bafilomycin A1	Archazolid A
	$IC_{50}$ [nM]		Factor	
<i>Control</i>				
BMA64-1B	$4.7 \pm 0.4$	$6.6 \pm 0.5$		
<i>Helix 2</i>				
Y66F	$2.9 \pm 0.4$	$5.6 \pm 0.3$	0.6	1
<i>Helix 4</i>				
I130A	$0.9 \pm 0.1$	$3.3 \pm 0.6$	0.2	0.5
L131A	$29.1 \pm 3.5$	$3.1 \pm 0.7$	6.2	0.5
L131F	$1.0 \pm 0.2$	$7.8 \pm 0.8$	0.2	1.2
V138A	$8.1 \pm 1.0$	$4.6 \pm 0.9$	1.7	0.7
V138T	$43.8 \pm 7.1$	$8.6 \pm 1.2$	9.3	1.3
L141F	$11.3 \pm 1.0$	$4.2 \pm 1.0$	2.4	0.6
L141I	$1.6 \pm 0.2$	$3.7 \pm 0.5$	0.3	0.6
L144F	$2.5 \pm 0.4$	$4.5 \pm 0.6$	0.5	0.7
L144I	$1.0 \pm 0.1$	$0.8 \pm 0.1$	0.2	0.1
I145F	$1.8 \pm 0.2$	$4.4 \pm 1.2$	0.4	0.7
I145L	$11.9 \pm 1.5$	$8.8 \pm 1.7$	2.5	1.4

### 3.5 Double mutation in *VMA3* and mutagenesis of *VMA11*

#### 3.5.1 Selection of amino acid residues for site-directed mutagenesis

The mutagenesis of *VMA3* revealed that amino acid exchanges Y142N and L144I strongly influence the binding of archazolid, as indicated by the 10-fold reduction of the  $IC_{50}$  value for this inhibitor. To test whether the combination of the two exchanges would enforce the effect on archazolid binding, a Y142N-L144I double mutant was generated in *Vma3p*.

To elucidate whether *Vma11p* also comprises an archazolid binding site, single amino acid exchanges were generated in *Vma11p* at sites corresponding to tyrosine 142 and leucine 144 in *Vma3p* (i.e. tyrosine 150 and methionine 152). For this purpose the deletion mutant BY4742- $\Delta vma11$  (Euroscarf, Germany) and the plasmid pRS415-*VMA11* containing *VMA11* and its native promoter were used (paragraph 2.2.10). Complementation of the *vma<sup>-</sup>* phenotype of BY4742- $\Delta vma11$  by transformation with pRS415-*VMA11* had been shown before (Voss, F., Diploma thesis, University of Osnabrück, 2010). In addition to tyrosine 150 and methionine 152, glycine 67 in *Vma11p* was also mutated, because the exchange of the corresponding glycine 61 in *Vma3p* to serine exhibited the strongest effect on binding of bafilomycin. As shown for *Vma3p* (paragraph 3.1.1), glycine 67 in *Vma11p* was substituted for serine and tyrosine 150 for asparagine. Methionine 152 was exchanged to alanine and phenylalanine, respectively.

#### 3.5.2 Influence of mutations on cell growth and vacuolar acidification

As can be seen in Fig. 3.11, the transformation of BMA64-1B $\Delta vma3$  with pRS415-*VMA3* bearing the double mutation Y142N-L144I in *Vma3p* only resulted in a partial complementation of the *vma<sup>-</sup>* phenotype. Cell growth in this strain was strongly reduced on  $CaCl_2$  and completely prevented at pH 7.5. Because vacuolar acidification was already disturbed in the Y142N single mutant (paragraph 3.1.1), quinacrine staining was not performed with the Y142N-L144I strain.

In contrast, the mutations performed in *Vma11p* did not exhibit a striking influence on cell growth (Fig. 3.12). All strains grew well on elevated  $CaCl_2$  concentrations and on pH 7.5, cell growth was only slightly reduced when compared to the wild type strain. Even the strain bearing the mutation Y150N, which corresponds to mutation Y142N in *Vma3p*, nearly exhibited wild type growth. All strains mutated in *Vma11p* showed quinacrine accumulation in the vacuole, indicating V-ATPase mediated proton translocation (Fig. 3.12). The good tolerance of the V-ATPase for these mutations is likely due to the fact that *Vma11p* is only present in a single copy in the  $V_O$  ring.

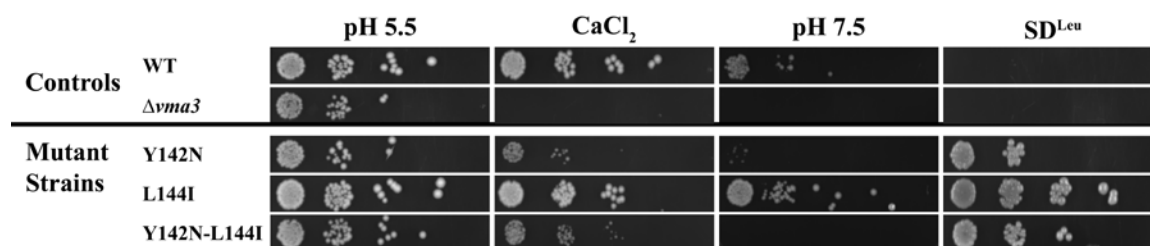


**Figure 3.11: *In vivo* assay of yeast strains expressing Vma3p with double mutation.**

Cells were dropped on YPDA plates pH 5.5 with or without calcium chloride, on YPDA buffered to pH 7.5 and on selection medium without leucine ( $SD^{Leu}$ ). WT, BMA64-1B;  $\Delta vma3$ , BMA64-1B $\Delta vma3$ ; Strains expressing Vma3p with the indicated mutations.

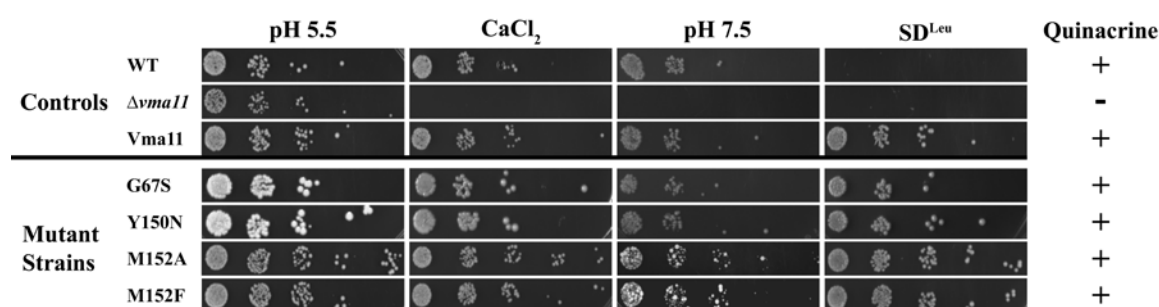


**Figure 3.12: *In vivo* assays of yeast strains expressing mutated versions of Vma11p.**

Cells were dropped on YPDA plates pH 5.5 with or without calcium chloride, on YPDA buffered to pH 7.5 and on selection medium without leucine ( $SD^{Leu}$ ). Quinacrine staining was used to visualize accumulation of protons in the vacuole of living yeast cells as indication for an intact V-ATPase as described in “Material and Methods”. The fluorescence within the vacuoles of V-ATPase mutant strains was classified as positive (+) i.e. similar to the wild type strain or negative (-) i.e. like in the respective deletion strain. WT, BY4742;  $\Delta vma11$ , BY4742- $\Delta vma11$ ; Strains expressing Vma11p with the indicated mutations.

### 3.5.3 Assembly and activity of the mutant V-ATPase

Assembly of the V-ATPase was tested by Western blot analysis of isolated vacuoles using an antibody against Vma1p (Fig. 3.13). For the Vma3p double mutant Y142N-L144I, although the threefold amount of protein was applied, only a very low signal when compared to the wild type strain (WT1, BMA64-1B) could be detected. This result clearly showed that V-ATPase assembly was almost completely prevented in Y142N-L144I as it was already indicated by strongly reduced growth of this strain on selective media (paragraph 3.5.2.). In line with these results, only negligible V-ATPase activity was detected in vacuoles isolated from this strain (data not shown). Accordingly, since the single mutant Y142N already had a negative influence on V-ATPase function, the double mutation even worsened this effect. For this reason Y142N-L144I was not used for further experiments.

Regarding the mutations in Vma11p, Western blot analysis also supported the results of the growth assay, revealing almost no difference in the signal intensity for Vma1p in most of the strains compared to the wild type (Fig. 3.13, WT2, BY4742). Additionally, most of the strains exhibited 100% of wild type activity (Tab. 3.5). For the mutant strains M152A and M152F the signal intensity for Vma1p was slightly reduced which is in line

with a reduction of the V-ATPase activity to approximately 80% of the wild type activity in these strains.

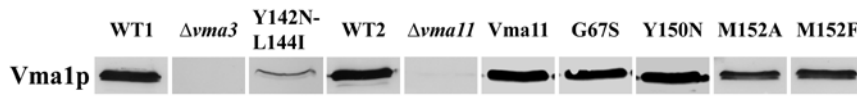


**Figure 3.13: Assembly of the V-ATPase in the Vma3p double mutant and in yeast strains expressing mutant versions of Vma11p.**

The assembly of the V-ATPase complexes in the Vma3p double mutant and in yeast strains bearing a mutation in Vma11p was verified by Western Blot analysis of isolated vacuolar membranes. Using an antibody against Vma1p, the attachment of the  $V_1$  complex to the vacuolar membrane was interpreted as a proof for the correct assembly of the  $V_1V_0$  holoenzyme (Noumi *et al.*, 1991). WT1, BMA64-1B;  $\Delta vma3$ , BMA64-1B $\Delta vma3$ ; Y142N-L144I, Vma3p bearing the indicated double mutation; WT2, BY4742;  $\Delta vma11$ , BY4742- $\Delta vma11$ ; Vma11, BY4742- $\Delta vma11$  expressing wild type Vma11p; Strains expressing Vma11p with the indicated mutations. For each strain 10  $\mu$ g of vacuolar protein were applied, for Y142N-L144I 30  $\mu$ g were used.

**Table 3.5: Bafilomycin A1 and archazolid A sensitive activity of vacuolar membranes isolated from yeast strains expressing either the wild type or a mutated version of Vma11p.**

Vacuolar membrane preparations and ATPase activity assays of the wild type (BY4742) and the mutant strains with indicated mutations were carried out as described under “Material and Methods”. The activities were corrected for the residual activity at the point of maximal inhibition by bafilomycin A1 and archazolid A, respectively. Values are the averages obtained from two independent vacuolar preparations with standard deviations as indicated.

Mutation in Vma11p	ATPase activity	ATPase activity
	sensitive to bafilomycin A1	sensitive to archazolid A
	<i>μmol/min/mg</i>	
<i>Control</i>		
BY4742	0.27 ± 0.13	0.25 ± 0.01
<i>Mutant strains</i>		
G67S	0.19 ± 0.06	0.19 ± 0.00
Y150N	0.45 ± 0.11	0.37 ± 0.06
M152A	0.22 ± 0.02	0.20 ± 0.00
M152F	0.22 ± 0.01	0.20 ± 0.01

### 3.5.4 Influence of mutations on inhibitor binding

Inhibition assays with either bafilomycin or archazolid revealed no striking effect of the mutations in Vma11p on inhibitor binding (Tab. 3.6). The mutation G67S showed the strongest influence on binding of bafilomycin but nevertheless, the  $IC_{50}$  value was only reduced approximately 3-fold when compared to the wild type strain (BY4742). Concerning archazolid, none of the mutant strains clearly changed the  $IC_{50}$  value with regard to the wild type, indicating that they do not influence inhibitor binding. One may thus assume that Vma11p does not contain binding sites for these inhibitors or, that a mutation in a single proteolipid subunit is not sufficient to change the affinity for these compounds.

**Table 3.6: IC<sub>50</sub> values for the inhibition of the yeast V-ATPase bearing a mutation in Vma11p by bafilomycin A1 and archazolid A.**

Vacuolar membrane preparations and ATPase activity assays of the wild type (BY4742) and the mutant strains with indicated mutations were carried out as described under “Material and Methods”. The activities were corrected for the residual activity at the point of maximal inhibition by bafilomycin A1 and archazolid A, respectively. IC<sub>50</sub> values with the indicated standard errors result from plotting the average values obtained from two independent vacuolar preparations.

Mutation in Vma11p	Bafilomycin A1	Archazolid A	Bafilomycin A1	Archazolid A
	<i>IC<sub>50</sub> [nM]</i>		<i>Factor</i>	
<i>Control</i>				
BY4742	2.6 ± 0.6	5.7 ± 0.8		
<i>Mutant strains</i>				
G67S	1.0 ± 0.1	5.4 ± 0.5	0.4	0.9
Y150N	2.0 ± 0.1	3.9 ± 0.3	0.8	0.7
M152A	3.2 ± 0.4	5.7 ± 1.2	1.2	1.0
M152F	1.7 ± 0.3	4.2 ± 0.5	0.7	0.7

### 3.6 Inhibition of mutant V-ATPases by derivatives of archazolid

#### 3.6.1 Selection of archazolid derivatives

In the preceding paragraphs the influence of the V-ATPase structure on inhibitor binding examined by site-directed mutagenesis and biochemical approaches has been described. To further elucidate the structure function relationship between archazolid and the V-ATPase, the influence of the structure of the inhibitor on this interaction was investigated. For this purpose, three different derivatives of archazolid A exhibiting modified features at different parts of the structure were selected (archazolid C, descarb-archazolid and oxo-archazolid; Fig. 3.14). These compounds were tested on yeast vacuoles on the one hand purified from the wild type strain BMA64-1B and, on the other hand, from the mutant strains Y142N and L144I because these two mutations had resulted in a 10-fold decrease of the  $IC_{50}$  value for archazolid A (paragraph 3.1.4 and 3.4.4). A different effect of these mutations on the binding of the archazolid derivatives would give indications for the structural features of the inhibitor that interact with the specific amino acid side chains.

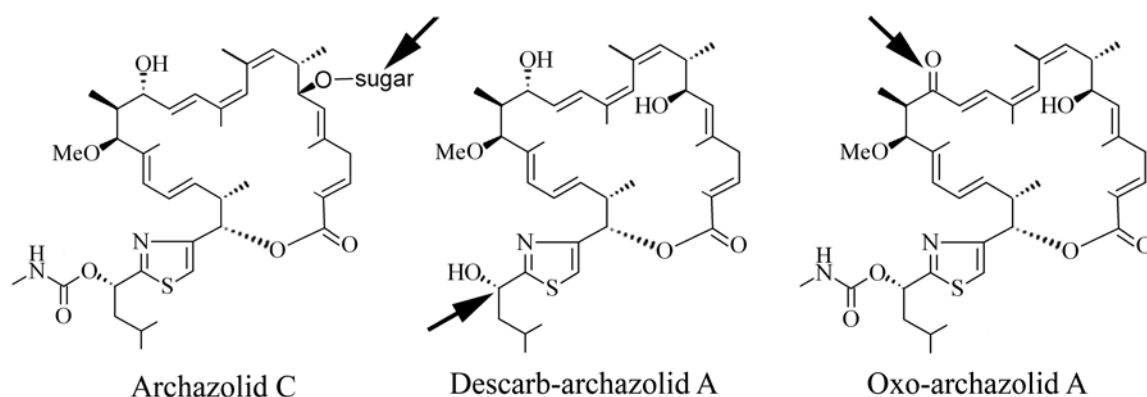


**Figure 3.14: Structures of derivatives of archazolid A.**

Depicted are three derivatives of archazolid A exhibiting modified features at different positions (black arrows). Archazolid C with a sugar group at C-7, 1'-descarbamoyl-archazolid A (descarb-archazolid) lacking the C-1' carboxamide group and 15-dehydro-archazolid A (oxo-archazolid) bearing a carbonyl instead of a hydroxyl group at position C-15.

#### 3.6.2 Influence of structural differences on inhibition of the yeast V-ATPase

Presented in Fig. 3.15A are the curves obtained for the inhibition of the V-ATPase from the three yeast strains by archazolid A, clearly showing the 10-fold decreased  $IC_{50}$  value in Y142N and L144I (paragraph 3.1.4 and 3.4.4). In contrast to archazolid A, archazolid C which comprises a sugar group at C-7, did not show an inhibition of the wild type V-ATPase at the concentrations used in this assay (Fig. 3.15B). Nevertheless, an inhibition of both mutant V-ATPases by archazolid C was visible at micromolar concentrations, confirming the influence of the mutations Y142N and L144I on inhibitor binding (Fig. 3.15B, Tab. 3.7). Additionally, descarb-archazolid which inhibited the wild type ATPase with an  $IC_{50}$  value of 13 nM, also showed a 10-fold decrease of the  $IC_{50}$  value for Y142N (2 nM) and a threefold decrease for L144I (4 nM) (Fig. 3.15C, Tab. 3.7). In sum-



mary, the decrease of the  $IC_{50}$  value for archazolid C and descarb-archazolid in both mutant V-ATPases supports the assumption that the amino acid residues tyrosine 142 and leucine 144 are involved in inhibitor binding.

In contrast, oxo-archazolid showed no striking difference in the inhibition of the wild type and the mutant V-ATPase, exhibiting  $IC_{50}$  values in the range of 200 to 300 nM for all three strains (Fig. 3.15D, Tab. 3.7). The missing influence of mutations Y142N and L144I on oxo-archazolid might be an indication for the importance of the hydroxyl group at C-15 for the enzyme-inhibitor interaction.

With regard to archazolid A and descarb-archazolid a difference between the overall shapes of the inhibition curves became obvious (Fig. 3.15A and C). Despite the fact that both compounds inhibit the V-ATPase in almost the same concentration range, the slope of the curves was decreased in the case of descarb-archazolid, pointing to a decrease in the cooperativity of inhibitor binding when compared to archazolid A. In line with this assumption, the Hill coefficients of the inhibition curves for descarb-archazolid were all approximately 1 (WT:  $1.0 \pm 0.1$ ; Y142N:  $0.9 \pm 0.1$ , L144I:  $1.0 \pm 0.1$ ), while the values for archazolid A were approximately 1.7 (WT:  $1.8 \pm 0.2$ ; Y142N:  $1.5 \pm 0.2$ , L144I:  $1.7 \pm 0.2$ ). This indicates that the C-1' carboxamide group of archazolid permits cooperative binding of the inhibitor.

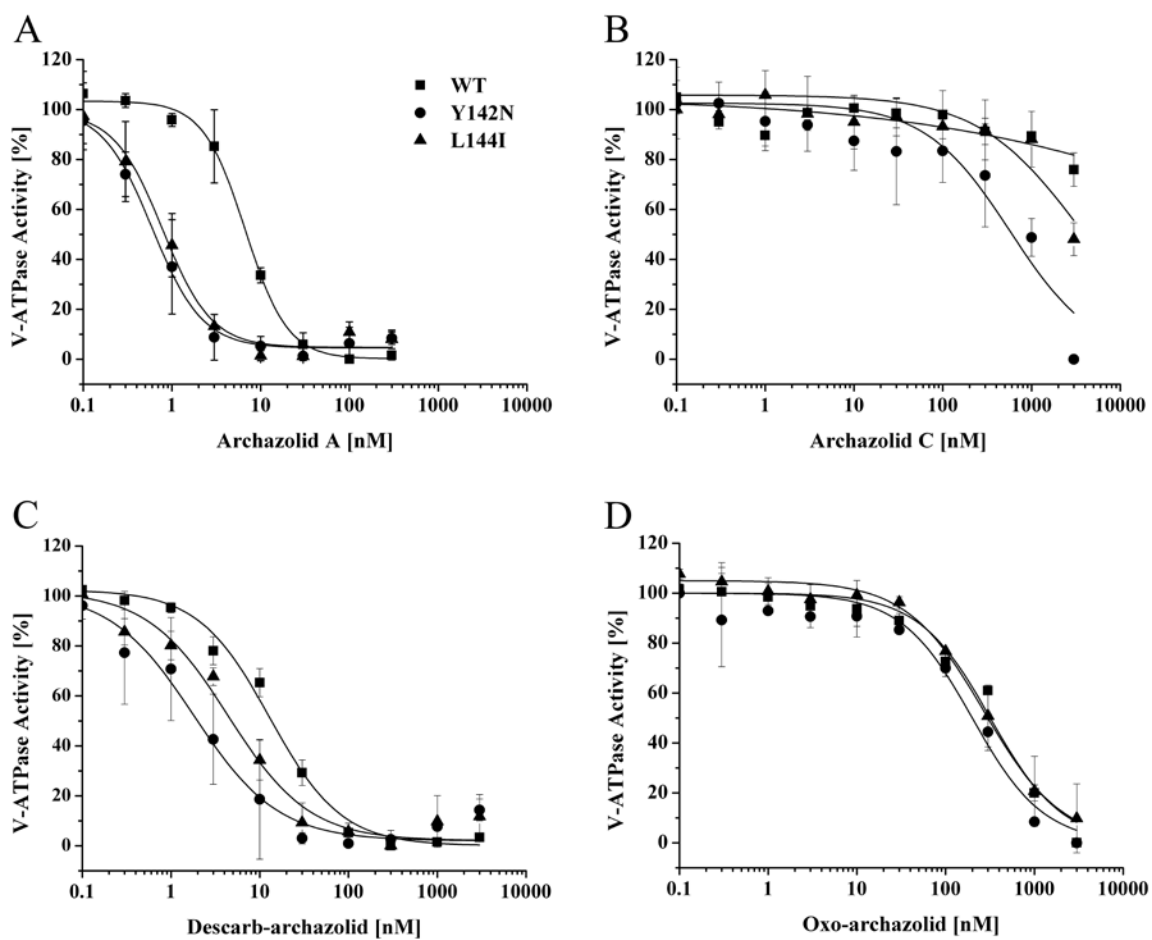


**Figure 3.15: Inhibition of wild type and mutant yeast V-ATPase by derivatives of archazolid A.**

V-ATPase activities were measured on isolated yeast vacuoles of the wild type strain BMA64-1B (WT) and the mutant strains Y142N and L144I, respectively (A). Values are the average of two independent vacuolar preparations. Error bars are standard deviations.  $IC_{50}$  values for all inhibitors are given in Table 3.7. The inhibition curves for archazolid A (A) were compared with the curves obtained for three archazolid derivatives archazolid C (B), descarb-archazolid (C) and oxo-archazolid (D).

**Table 3.7:  $IC_{50}$  values for the inhibition of wild type and mutant yeast V-ATPase by derivatives of archazolid A.**

Vacuolar membrane preparations and ATPase activity assays were carried out as described in the “Material and Methods”. The activities were corrected for the residual activity at the point of maximal inhibition by the respective inhibitor.  $IC_{50}$  values with the indicated standard error result from plotting the average values obtained from two independent vacuolar preparations; n.m., not measurable.  $IC_{50}$  values of the respective inhibitor obtained for each mutant strain were compared to the  $IC_{50}$  value for the wild type strain BMA64-1B.

Strain	Archazolid A	Archazolid C	Descarb-archazolid	Oxo-archazolid
<i>IC<sub>50</sub> [nM] (Factor compared to wild type)</i>				
<i>Wild type</i>				
BMA64-1B	6.6 ± 0.5	n. m.	13.0 ± 0.5	320.0 ± 40.0
<i>Mutant strains</i>				
Y142N	0.6 ± 0.1 (0.1)	570.0 ± 160.0	1.8 ± 0.3 (0.1)	200.0 ± 30.0 (0.6)
L144I	0.8 ± 0.1 (0.1)	3400.0 ± 1300.0	4.4 ± 0.7 (0.3)	270.0 ± 20.0 (0.8)

### 3.7 Biological activity of novel archazolid derivatives.

To gain more insights into the structural features of archazolid that determine its biological function, novel derivatives of the inhibitor were evaluated for their inhibitory efficiency against the *M. sexta* V-ATPase (Fig. 3.16).

One aim of the synthetic derivatization of archazolid was to reduce its hydrophobicity in order to enable NMR studies on the biologically active conformation of the inhibitor which were till then impeded by solubility problems (T. Carlomagno, EMBL Heidelberg (Germany), personal communication). For this purpose, allyl-phosphate groups were attached to C-7 and C-15 of the macrolactone ring of archazolid, yielding the polar bisphospho-archazolid (BP-archazolid, Fig. 3.16A). However, the biological activity of this compound was totally abolished, as reflected by the unaffected high V-ATPase activity in the presence of micromolar concentrations of BP-archazolid (Fig. 3.16C). Since archazolid interacts with the membrane embedded part of the V-ATPase, the polar modifications probably prevent the access of the inhibitor to its target site.

Archazolid F (Fig. 3.16B) is a natural derivative of archazolid isolated from *A. gephyra* that bears an unusual 3,4-, instead of a 2,3-double bond (Horstmann *et al.*, 2011). The inhibition assays (Fig. 3.16C) clearly showed that archazolid F ( $IC_{50} = 14.0$  nM) exhibits almost the same efficiency when compared to archazolid A ( $IC_{50} = 9.0$  nM). Thus, the shift of the double bond does not seem to influence the structural features that are necessary for the binding of archazolid to the *M. sexta* V-ATPase.

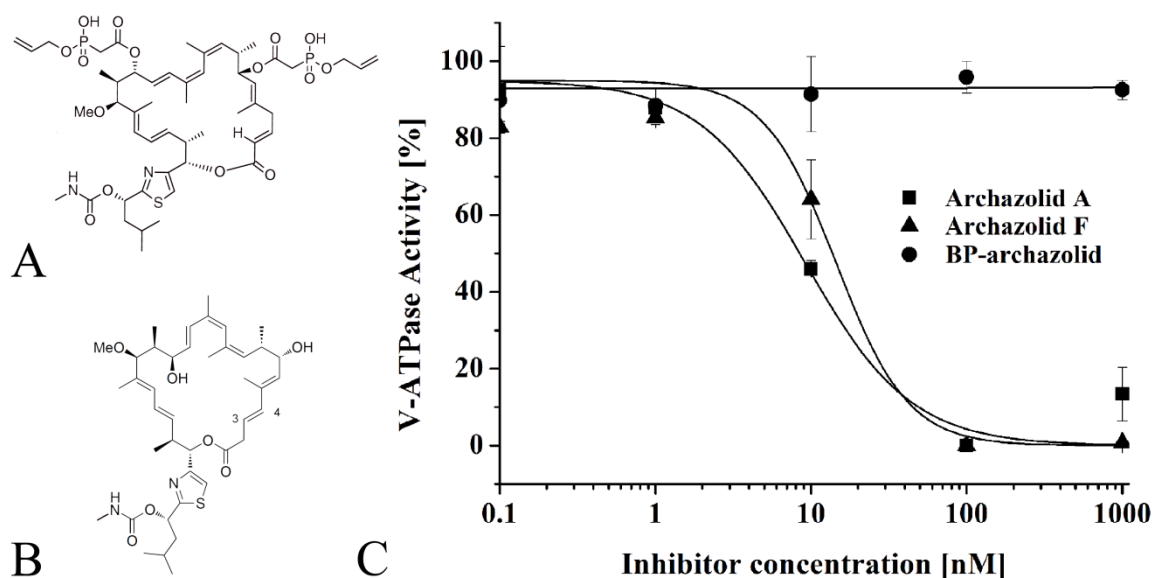


**Figure 3.16: Inhibition of the *Manduca sexta* V-ATPase by bisphospho-archazolid and archazolid F.**

To decrease the hydrophobicity of archazolid, monoallyl-phosphate groups were attached to C-7 and C-15 of the macrolactone ring, yielding bisphospho-archazolid (BP-archazolid, A). Archazolid F (B), isolated from *A. gephyra*, is a natural isomer of archazolid B in which the 2,3-double bond is shifted to the 3,4-position (Horstmann *et al.*, 2011). The biological activity of both compounds was evaluated via activity assays on isolated V-ATPase from the *M. sexta* midgut (C). Values are the average of two independent preparations with indicated standard deviations.  $IC_{50}$  values were  $9.0 \pm 3.0$  nM for archazolid A and  $14.0 \pm 5.0$  nM for archazolid F.

### 3.8 EPR spectroscopy as a tool for the study of inhibitor binding to the V-ATPase

To enable the investigation of the V-ATPase-inhibitor interaction via EPR spectroscopy, spin-labeled (SL) derivatives of archazolid A and DCCD were synthesized by the group of D. Menche (University of Heidelberg, Germany). In this process a nitroxide spin-label was attached to the C-7 hydroxyl group of archazolid A (SL-archazolid) and to one nitrogen atom of the carbodiimide group within DCCD (NCCD), respectively (Fig. 3.17).

All EPR measurements and data analysis were carried out in collaboration with J. P. Klare (Department of Physics, University of Osnabrück, Germany). In the first instance, *cw* spectroscopy of SL-archazolid and purified yeast vacuoles from subunit *c* mutant strains was used to visualize the influence of selected amino acid exchanges on binding of the inhibitor. Another major approach of the EPR studies was to perform distance measurements via DEER with SL-inhibitors bound to the V-ATPase in order to resolve the number of *c* subunits in the  $V_O$  ring. This approach is based on the assumption that a single inhibitor binding site exists in each proteolipid subunit and thus enables distance determination between bound SL-inhibitors and by that provides the opportunity to calculate the amount of subunits in the ring based on geometrical considerations.

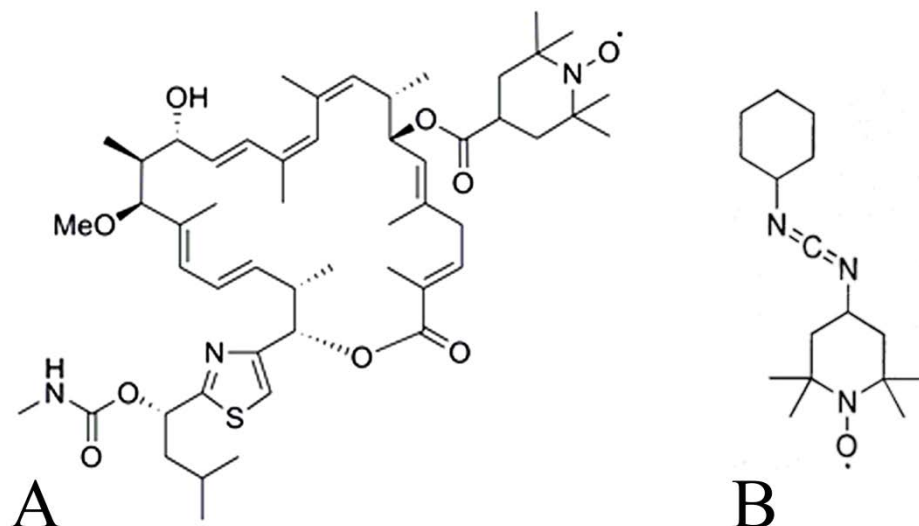


**Figure 3.17: Structures of spin-labeled V-ATPase inhibitors.**

To enable the investigation of enzyme-inhibitor interaction via EPR spectroscopy, a nitroxide spin-label was attached to C-7 of archazolid (SL-archazolid, A) and to one nitrogen of DCCD (NCCD, B), respectively. It was shown previously that modifications at C-7 of archazolid A only moderately affect the inhibition properties of the compound (see paragraph 1.6.3).

#### 3.8.1 Binding properties of spin-labeled V-ATPase inhibitors

Tab. 3.8 summarizes the inhibition properties of the SL-inhibitors and clearly shows that the  $IC_{50}$  values of NCCD for either the *M. sexta* or the *S. cerevisiae* enzyme were almost identical with the values of the non-modified inhibitor. In contrast, the efficiency of SL-archazolid was evidently reduced as reflected in the approximately 100-fold elevated  $IC_{50}$  values, but however, this compound still efficiently inhibited the V-ATPase from *M. sexta* and *S. cerevisiae*.

As shown in Fig. 3.18A, a three-peak pattern was visible in the *cw* spectrum for NCCD in  $H_2O$  (black). This pattern arises from the interaction of the free electron with

the nuclear spin ( $I$ ) of the nitrogen atom ( $I = 1$ ), called hyperfine interaction. The three resonance lines were very sharp and exhibited almost equal amplitude, what is characteristic for unrestricted mobility of a nitroxide spin-label. In the presence of the *M. sexta* V-ATPase (blue), binding of the inhibitor was evident as displayed by the strongly increased width of the central resonance line and broadening of the whole spectrum, which reflects the decreased spin-label mobility in the protein environment.

Different characteristics were visible in the spectra obtained for SL-archazolid in H<sub>2</sub>O or bound to the *M. sexta* V-ATPase (Fig. 3.18B). Strong exchange coupling, represented by a broad line over the whole spectrum, was visible for SL-archazolid in H<sub>2</sub>O with 10% DMSO (black). Exchange coupling originates from spin-labels being in very close proximity (< 1 nm) to each other and indicated, in this case, the formation of inhibitor dimers or multimers. This phenomenon most probably reflects the low solubility of SL-archazolid in H<sub>2</sub>O that is commonly observed for the archazolid inhibitors. Some exchange coupling was still visible when the inhibitor was mixed with detergent-solubilized V-ATPase (blue). The remaining inhibitor complexes in this case might be an artifact resulting from the very high protein (~ 100 μM) and inhibitor concentrations (~ 1.5 mM) used in the experiment which presumably led to the accumulation of inhibitor complexes. In line with this assumption, no exchange coupling was observed in samples with lower protein content (~ 30 μM) (Fig. 3.18C). This leads to the conclusion that under normal conditions archazolid monomers interact with the target site. However, further experiments are needed to clarify the occurrence of inhibitor dimers in these samples and to prevent perturbation of the spectra in following experiments.

Nevertheless, in summary, the addition of the nitroxide spin-label to either archazolid or DCCD did not dramatically change the inhibition properties of the compounds and binding of the SL-inhibitors to the V-ATPase was clearly visualized in the *cw* EPR spectra.

**Table 3.8: Inhibition properties of spin-labeled V-ATPase inhibitors.**

The inhibition properties of SL-archazolid and NCCD were tested on purified V-ATPase from *M. sexta* as well as on isolated vacuoles from *S. cerevisiae*. Protein purification and activity assays were performed as described under “Material and Methods”, except that β-mercaptoethanol and DTT were omitted from the preparation. Preincubation of the protein with DCCD and NCCD was carried out for 1 h at 30°C. IC<sub>50</sub> values with the indicated standard error result from plotting the average values obtained from two independent preparations.

	Archazolid A	SL-archazolid	DCCD	NCCD
	<i>IC50 [nM] (Factor compared to non-labeled inhibitor)</i>			
<i>M. sexta</i>				
V-ATPase	10.0 ± 0.9	610.0 ± 60.0 (60)	18.0 ± 6.0	22.0 ± 3.3 (1)
<i>S. cerevisiae</i>				
V-ATPase	7.0 ± 0.3	750.0 ± 90.0 (107)	180.0 ± 70	110.0 ± 30.0 (1)

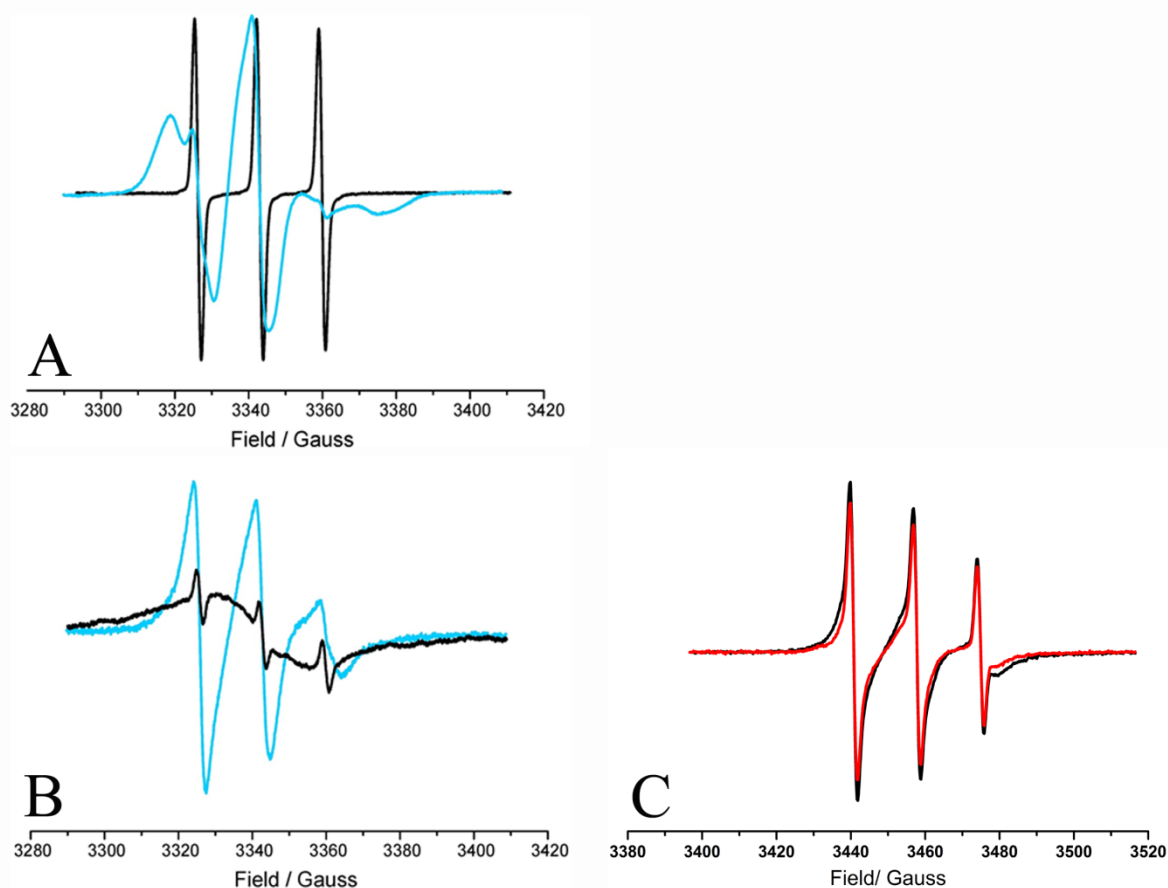


**Figure 3.18: CW spectra of spin-labeled inhibitors bound to the *Manduca sexta* V-ATPase.**

Room temperature X band cw EPR spectra of NCCD (100  $\mu$ M) in H<sub>2</sub>O (A; black spectrum) and SL-archazolid (1 mM) in H<sub>2</sub>O with 10% DMSO (B; black spectrum), respectively, and of SL-inhibitors bound to the *M. sexta* V-ATPase (blue spectra). Spectra with bound inhibitors were obtained after 1 h of incubation at room temperature with a protein concentration of approximately 85  $\mu$ M and an at least 12-fold excess of inhibitor, and spectra of free inhibitors (black) were subtracted. Binding of SL-inhibitors to the protein led to a strong decrease of the spin-label mobility, as can be seen by noticeable line broadening in the blue spectra. Both spectra of SL-archazolid showed strong exchange coupling which resulted from inhibitor dimers in the sample. (C) Room temperature X band cw EPR spectra of the *M. sexta* V-ATPase (32  $\mu$ M) incubated with SL-archazolid (400  $\mu$ M) for either 20 min (black) or 5h (red). In both spectra, no exchange coupling was visible, indicating that inhibitor dimers were not present in this sample.

### 3.8.2 Binding of spin-labeled inhibitors to the *Saccharomyces cerevisiae* V-ATPase

As for the *M. sexta* V-ATPase, binding of SL-archazolid to the V-ATPase from the *S. cerevisiae* wild type strain BMA64-1B resulted in broadening of the EPR spectrum indicating restriction of the spin-label side chain mobility and thus binding of the inhibitor (Fig. 3.19, black). To elucidate whether the effects of amino acid exchanges in subunit c of the V<sub>O</sub> complex directly influence the cw EPR spectrum of SL-archazolid, measurements were also performed with vacuoles isolated from the subunit c mutant strains Y142N and L144I, as both these strains exhibited a 10-fold increased sensitivity to archazolid A (paragraph 3.1.4 and 3.4.4).

As can be seen in Fig. 3.19, the spectra obtained for both mutant strains (blue and orange spectra) were explicitly different compared to the wild type spectrum and indicat-

ed increased restriction of the spin label mobility in both cases. In addition, exchange coupling was visible in these spectra, being strongest for Y142N (blue) and reflecting the presence of inhibitor dimers in these samples. It is very likely that the high concentration of vacuoles and inhibitor in the sample favored the dimerization of the inhibitor and hence led to the observed exchange coupling as it was discussed in the preceding paragraph. Since the protein content within the vacuolar membranes may be variable in different yeast strains and preparations, the amount of inhibitor dimers in the sample may have varied in the respective experiments. This probably led to the different extent of exchange coupling observed in the spectra of the contemplated strains.

The broadening of the central resonance line observed in the spectra of both mutant strains was pronounced especially for Y142N (blue), indicating that the mobility restriction of the spin-label was strongest in this mutant V-ATPase. For L144I (orange), line broadening was also evident yet the effect was not as pronounced as for Y142N. Besides the line broadening, sharp tips of the EPR lines were striking in the L144I spectrum, reflecting the presence of a notable fraction of unbound inhibitors in this sample. This distinctive feature most probably resulted from the reduced incubation time (30 min compared to > 180 min) in this experiment. The shortened incubation time was necessary due to highly reducing conditions in the vacuolar membranes of L144I that caused very fast fading of the EPR signal and thus impeded long-time incubation with SL-archazolid. Nevertheless, in summary, the spectra of both mutant strains clearly indicated that tyrosine 142 and leucine 144 are either directly involved in binding of the inhibitor or that the mutations led to structural changes within the c subunits which affected inhibitor binding. These data are in line with the results from the inhibition assays presented in paragraph 3.1.4 and 3.4.4 and add to the conclusion that archazolid interacts with these respective amino acid residues.

Unfortunately, the reducing conditions described above seem to be an intrinsic feature of most of the vacuolar membranes used in this study for which no appropriate experimental solution could yet be found. Problems with the reducing conditions became explicitly obstructive in the case of NCCD which was used to examine the interaction of archazolid and the essential glutamate residue e.g. via competition assays monitored with *cw* spectroscopy. This inhibitor was even more susceptible to the reducing conditions, which is probably due to the slower binding mode of this compound that presumably led to the reduction of the nitroxide spin label prior to inhibitor binding. Therefore, it was to date not possible to obtain a suitable EPR signal of NCCD bound to the *S. cerevisiae* V-ATPase. Nevertheless, first attempts were made to wash vacuolar membranes with 10 mM KNO<sub>3</sub> which evidently improved the signal intensity (J. P. Klare, personal communication) and thus provides the possibility to optimize the experimental setting and finally produce reliable spectra.

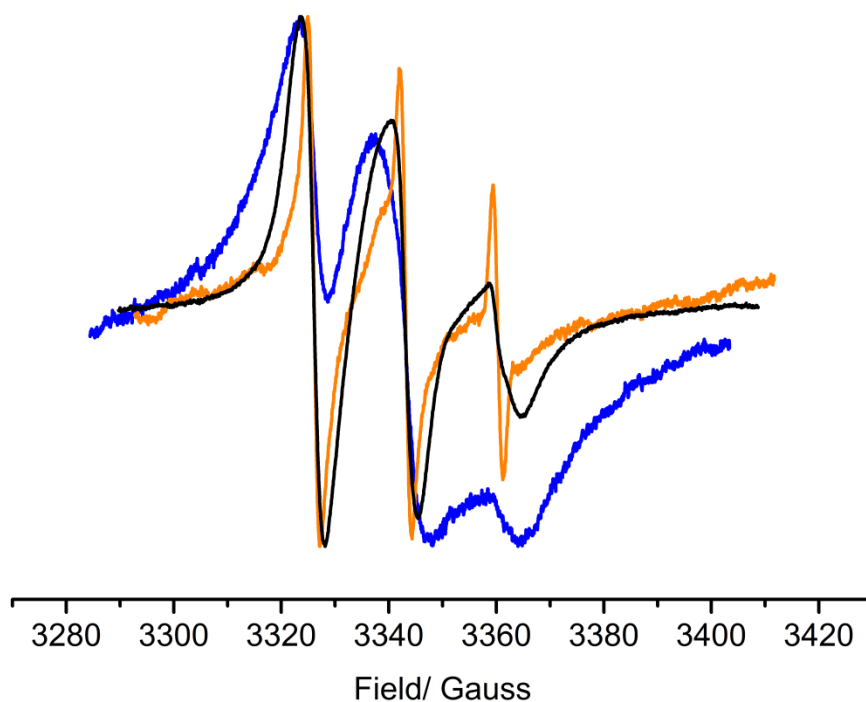


**Figure 3.19:** *Cw* spectra of SL-archazolid bound to the *Saccharomyces cerevisiae* V-ATPase.

Room temperature X band *cw* EPR spectra of SL-archazolid bound to the V-ATPase in *S. cerevisiae* vacuoles isolated from either the wild type strain BMA64-1B (black) or the subunit *c* mutant strains Y142N (blue) and L144I (orange), respectively. Incubation with SL-archazolid was performed for at least 3h for BMA64-1B and Y142N. Due to highly reducing conditions in the vacuolar membranes of L144I, the incubation time had to be reduced to only 30 min in this case. This led to a large amount of unbound inhibitor in the sample as visible in the sharp tips of the three peaks. Nevertheless, explicit changes were visible in the spectra of both mutant strains when compared to the wild type spectrum, clearly indicating a notable influence of the mutations on inhibitor binding.

### 3.9 Distance measurements on the *c* ring of the V-ATPase

Due to the high protein concentrations ( $\sim 100 \mu\text{M}$ ) needed for the DEER measurements, the *M. sexta* V-ATPase was used to elucidate the stoichiometry of the *c* ring with either NCCD or SL-archazolid. Fig. 3.20A shows the DEER form factor with the respective fit obtained by Tikhonov regularization (see paragraph 2.4, Fig. 2.2) and the resulting distance distribution for NCCD bound to the *M. sexta* V-ATPase. Unexpectedly, these experiments revealed a distance distribution of the nitroxide groups with several peaks at distances between approximately 2 and 5 nm (Fig. 3.20B). With respect to the size of the single *c* subunits, the comparatively high amount of distances in this narrow range can only be explained, if NCCD can bind in two alternative orientations to the protein. Binding of DCCD (and thus its derivatives) occurs via the formation of a covalent bond from an acidic amino acid residue to one nitrogen atom of the inhibitor (Azzi *et al.*, 1984; Chadwick and Thomas, 1985). Because of the symmetric structure of the carbodiimide group, this bond can be formed at two sites of the inhibitor; hence the inhibitor can bind in two different orientations to the protein. This special feature of carbodiimides provides



an explanation for the occurrence of diverse peaks in the DEER experiments with NCCD and consequently, because the proper analysis of these data is very difficult, the use of this compound for distance measurements seems to be limited. On the other hand, the great advantage of DCCD analogues for such studies is the clearly defined binding site within the protein which largely facilitates interpretation of the data.

Due to the very complex distance distribution obtained with NCCD, SL-archazolid was used for further DEER measurements as this inhibitor is expected to bind in one distinct orientation. For these experiments SL-archazolid was diluted approximately 5-fold with non-labeled archazolid to prevent dipolar interactions originating from the formation of inhibitor dimers (paragraph 3.8.1) that would lead to perturbation of the DEER signal. Despite the comparatively high signal-to-noise ratio of this experiment, as shown in Fig. 3.20C, analysis of the data was possible and yielded three peaks with maxima at distances of 1.9 nm, 3.4 nm and 4.5 nm, respectively (Fig. 3.20D). First attempts to compare these data with c ring crystal structures revealed a good fit for inter c subunit distances in the decameric ring of *E. hirae* (Murata *et al.*, 2005) (J. P. Klare, personal communication), thus suggesting that the *M. sexta* V<sub>O</sub> ring might also contain ten c subunits. However, since the exact binding position of archazolid at the c subunit is not yet known, the position of the spin label within the protein is also not clear, leading to a quite high uncertainty of the fitting result. Therefore, a detailed knowledge of the orientation of the inhibitor within its binding site is a prerequisite to finally assign the number of c subunits with SL-archazolid.

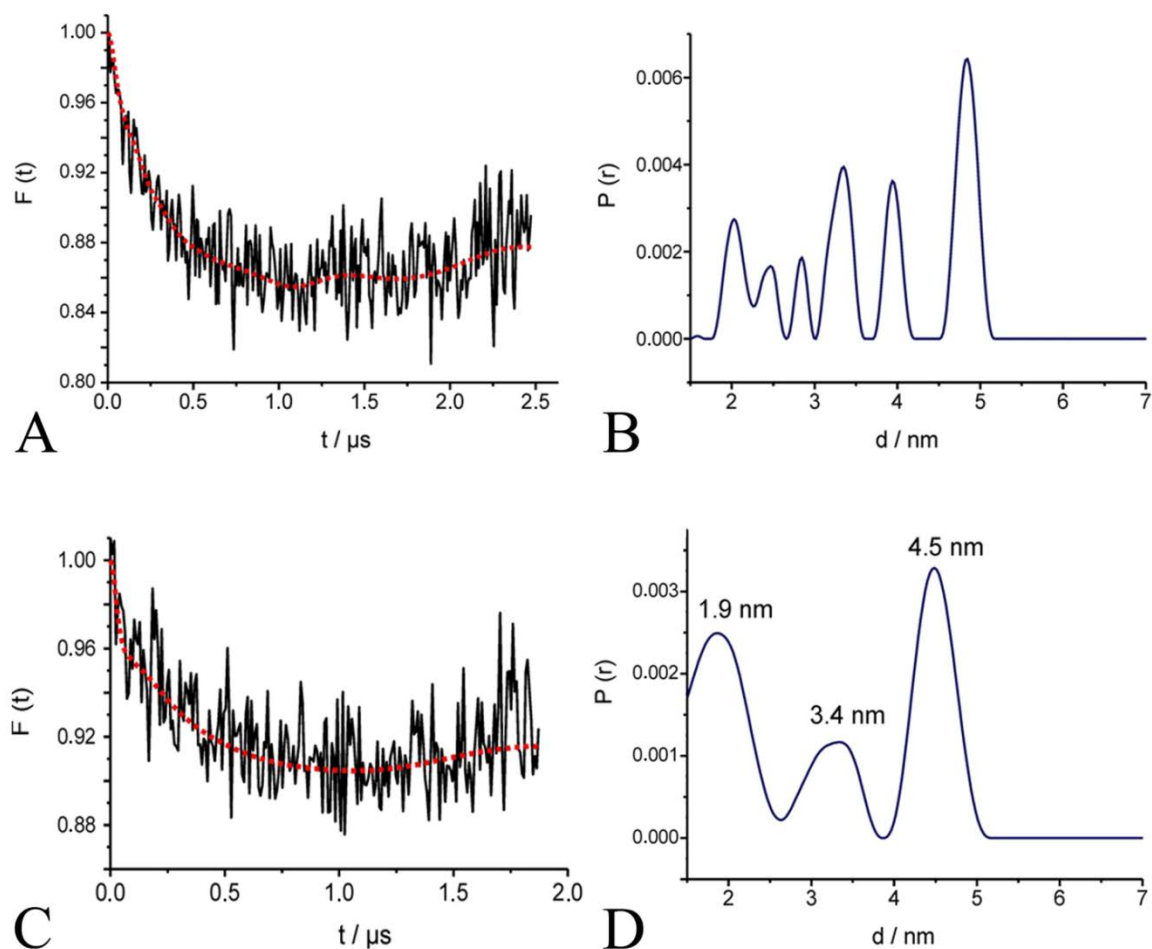


**Figure 3.20: DEER measurements with NCCD and SL-archazolid bound to the *Manduca sexta* V-ATPase.**

DEER form factors  $F(t)$  with fits (red) obtained by Tikhonov regularization and corresponding distance distributions  $P(r)$  for NCCD (A and B) and SL-archazolid (C and D), respectively. The distance distribution for NCCD bound to the V-ATPase revealed several peaks at distances between approximately 2 and 5 nm (B). In contrast, for SL-archazolid a distance distribution with three major peaks centered at distances of 1.9, 3.4 and 4.5 nm was obtained (D). Inhibitor:protein concentrations (stoichiometries) were: 640  $\mu\text{M}$ :80  $\mu\text{M}$  (12:1) for NCCD and 500  $\mu\text{M}$ :50  $\mu\text{M}$  (10:1) for SL-archazolid which was spin-diluted with archazolid A to eliminate dipolar interactions resulting from the formation of SL-archazolid dimers (see paragraph 3.8.1) that would otherwise perturb the DEER signal. The final spin concentration of SL-archazolid was approximately 70  $\mu\text{M}$ .

## 4. Discussion

### 4.1 Inhibitor binding to the V-ATPase V<sub>O</sub> complex

Up to now it was proposed for representatives of all three major classes of V-ATPase inhibitors that they interact with the V<sub>O</sub> complex of the V-ATPase. Firstly, two independent approaches, (1) PAL studies on the *M. sexta* V-ATPase with a radioactive concanamycin derivative (<sup>125</sup>I-concanolid A) (Huss *et al.*, 2002), and (2) mutagenesis studies in *N. crassa* (Bowman and Bowman, 2002), identified subunit c as a binding partner of the plecomacrolide inhibitors. Further mutagenesis studies in *N. crassa* finally resulted in a model of the plecomacrolide binding site located at the interface of two adjacent c subunits within the V<sub>O</sub> ring (Bowman *et al.*, 2006; Bowman *et al.*, 2004; paragraph 1.6.1, Fig. 1.7). Secondly, the benzolactone enamide salicylhalamide was shown to prevent proton transport of the isolated V<sub>O</sub> complex from bovine clathrin coated vesicles (Xie *et al.*, 2004), and labeling of the *M. sexta* V-ATPase with a radioactive PAL derivative of apicularen identified both subunit c and a as binding partners of the compound (Nardmann, C., Wieczorek, H. and Huss, M., manuscript in preparation). Thirdly, archazolid was shown to prevent binding of <sup>125</sup>I-concanolid A to subunit c, and hence it was proposed that the inhibitor shares at least part of its binding site with the plecomacrolide antibiotics (Huss *et al.*, 2005). Taking all these results together, it is obvious that the V<sub>O</sub> complex provides a major point of attack for V-ATPase inhibitors.

All the inhibitory compounds mentioned herein are secondary metabolites mainly produced by bacteria (paragraph 1.6). Secondary metabolites are proposed to function as chemical defense mechanism which increases the potential of organisms to fight competitors and predators (Demain and Fang, 2000). In this regard, targeting a substantial protein molecule like the V-ATPase with an inhibitory chemical substance appears especially efficient. Since the V<sub>O</sub> complex fulfills the main function of the enzyme, the proton translocation, it obviously offers a proper destination for inhibitory attack. Therefore, it is not surprising that most of the V-ATPase inhibitors, known so far, seem to interact with the highly conserved c subunit of the V<sub>O</sub> ring.

Since the amino acid sequence of c subunits from various organisms from yeast to mammals shows sequence identities of 55 to 80% (Fig. 4.1), V-ATPase inhibitors isolated from microbial organisms are highly efficient against V-ATPases from a broad range of organisms. Likewise, they are also evaluated as lead compounds to develop drugs against V-ATPase associated human diseases (reviewed in Keeling *et al.*, 1997 and Niikura, 2006). In this regard, the high sequence conservation of the inhibitor target evidently complicates the development of selective compounds inhibiting single tissue specific isoforms of the V-ATPase. For this reason, a detailed knowledge of the crucial structural features that determine the inhibitor-target interaction is necessary to optimize the binding properties of the compounds, and ultimately to develop isoform specific inhibitors valuable for disease treatment.

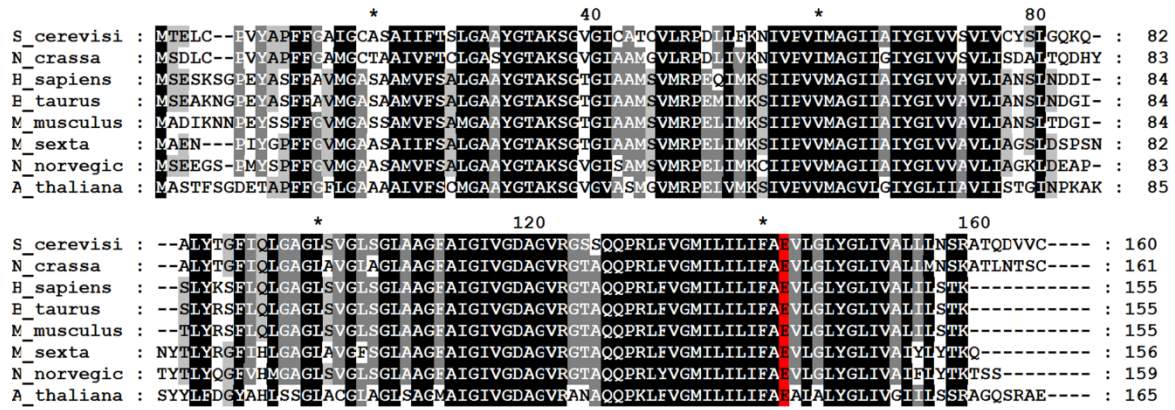


**Figure 4.1: Amino acid alignment of V-ATPase c subunits from different organisms.**

The alignment was performed using ClustalW and c subunit sequences as follows: *Saccharomyces cerevisiae* (Swiss-Prot: P25515.1), *Neurospora crassa* (Swiss-Prot: P31413.1), *Homo sapiens* (Swiss-Prot: P27449.1), *Bos taurus* (Swiss-Prot: P23956.1), *Mus musculus* (Swiss-Prot: P63082.1), *Manduca sexta* (Swiss-Prot: P31403.1), *Nephrops norvegicus* (Swiss-Prot: Q26250.1), *Arabidopsis thaliana* (Swiss-Prot: P59227.1). Highly conserved, conserved and less conserved residues are colored in black, gray and light-gray, respectively. The essential glutamate within helix 4 is highlighted in red. Sequence identities with respect to the *S. cerevisiae* protein are: *N. crassa*: 80%, *H. sapiens*: 67%, *B. taurus*: 67%, *M. musculus*: 67%, *M. sexta*: 69%, *N. norvegicus*: 67%, *A. thaliana*: 55%.

#### 4.2 The plecomacrolide binding site in *Saccharomyces cerevisiae*

The binding site of the plecomacrolides within the V-ATPase of *N. crassa* was described in detail by the Bowman group which identified a set of 23 amino acid positions, at which the exchange of the side chain conferred resistance primarily to bafilomycin (Bowman and Bowman, 2002; Bowman *et al.*, 2006; Bowman *et al.*, 2004). Nevertheless, due to impeded growth of most of the mutant yeast strains, only two of these mutations (T32I and I54F) could be repeated in *S. cerevisiae* (Bowman *et al.*, 2004). However, the results presented in this thesis clearly show that these mutations can also be established in *S. cerevisiae*, as confirmed by the assembly of a functional V-ATPase with at least 30% of wild type enzyme activity in nearly all mutant strains (paragraph 3.1 and 3.4). This result might be explained by the usage of a non-tagged version of subunit c expressed by its native promoter that probably leads to an optimal expression of the mutant proteins. In addition, the yeast strain used in this study might be more tolerant to low V-ATPase activity and can thus cope with more severe mutations in subunit c. In line with this assumption, Pali *et al.* (2004b) successfully established the mutations F135L and Y142H in *S. cerevisiae* by using the same strain background.

For the “bafilomycin-mutations” in *N. crassa* it was shown that most of them only exhibit a minor effect on the sensitivity for concanamycin (Bowman *et al.*, 2006). Thus, it was presumed that, despite the fact that the binding sites of both compounds overlap, they are not completely identical. In this regard, the influence of the mutations presented in this thesis on the binding of concanamycin was not examined, and likewise, the present paragraph will focus on the binding site of bafilomycin as a general example for the plecomacrolide inhibitors.

Concerning the binding of bafilomycin in *S. cerevisiae*, a similar effect as published for *N. crassa* could be expected because of the high sequence identity (80%, Fig. 4.1) of the c subunits between these two species. In general, this expectation was confirmed as all mutations known so far except I39F also showed an influence on bafilomycin binding in *S. cerevisiae* (paragraph 3.1.4; Tab. 3.2). The different contribution of the single amino acid residues to the inhibitor binding in either *N. crassa* or *S. cerevisiae* can be explained by slight disparities in the proteolipid structure which result in modest variations of the inhibitor binding site. These variations might also be the reason for small differences in the sensitivity of V-ATPases from different species to the inhibitor. For example, Bowman *et al.* (2004) reported an IC<sub>50</sub> value for bafilomycin of 8.9 nM for the *N. crassa* and 3.8 nM for the *S. cerevisiae* wild type strain, respectively. Nevertheless, because of the high overall sequence conservation of the c subunits, the IC<sub>50</sub> values of bafilomycin in various organisms all reside in the low nanomolar range (Dröse and Altendorf, 1997).

Apart from the amino acid residues which were confirmed to be part of the plecomacrolide binding site in *S. cerevisiae*, valine 138 was found to also participate in the binding of bafilomycin, as its mutation to threonine increased the IC<sub>50</sub> value for the inhibitor about 10-fold (paragraph 3.4.4; Fig. 3.10A and Tab. 3.4). In regard to the model of the *S. cerevisiae* c ring (Fig. 4.2), it is obvious that valine 138 (highlighted in olive) is the “missing link” between tyrosine 142 (highlighted in blue) and the other amino acids forming the bafilomycin binding site (all in cyan). The 5-fold decrease of the IC<sub>50</sub> value exhibited by the L144I mutation points to a V-ATPase more sensitive to bafilomycin. This effect is quite surprising, because leucine 144 does not reside within the proposed bafilomycin binding site (Bowman *et al.*, 2006; paragraph 1.6.1; Fig. 1.7). However, since the side chain of amino acid 144 is located in close proximity to tyrosine 66 in helix 2, the L144I mutation might have an indirect effect on the arrangement of the “bafilomycin amino acids” in helix 2 (Fig. 4.2B and C).

Taking into account that the yeast V<sub>O</sub> ring apart from subunit c also comprises c' and c'', it is of interest, whether these additional proteolipids provide inhibitor binding sites as well. In the present study, the amino acids corresponding to glycine 61, tyrosine 142 and leucine 144 in subunit c were mutated in c' (glycine 67, tyrosine 150 and methionine 152), to address this issue (paragraph 3.5). Two of these amino acids, glycine and tyrosine, were shown to be directly involved in binding of bafilomycin to subunit c (paragraph 3.1.4), but for c' no striking influence of amino acid exchanges on inhibitor binding was detected. Bowman *et al.* (2004) already established mutations in subunit c' (T38I, F143L, Y150N) and c'' (F106L, Y113N) of *S. cerevisiae*, corresponding to the mutations conducted in the *N. crassa* c subunit before, but in these subunits they did not reveal any influence on the binding of bafilomycin. In this regard, it was suggested that, if subunits c' and c'' contribute to inhibitor binding, the presence of non-mutated high affinity c subunits probably superposes the effect of mutations in the former subunits (Bowman *et al.*, 2006). To elucidate the influence of mutations in c' and c'' on plecomacrolide binding it will therefore be necessary to perform concomitant mutations in subunit c.

Concerning the inhibition mechanism of the plecomacrolide antibiotics, it was proposed that they either prevent rotation of the c ring relative to subunit a, and/or block

the internal torsion of helix 4 (Bowman *et al.*, 2004). This helical swiveling was proposed to be necessary to allow proton access to the essential acidic residue, according to an NMR-based model of the F-ATPase c subunit (Fillingame and Dmitriev, 2002). However, in regard to more recently obtained c ring crystal structures, it became evident that helical swiveling is not required for proton transport (Junge and Nelson, 2005; Meier *et al.*, 2005). Meier *et al.* (2005) already mentioned that specific labeling of the essential acidic residue by DCCD could not be reconciled with a torsion of helix 4 that would hide this residue within the interior of subunit c (see also Fig. 4.2). The competition assays presented in paragraph 3.3.1 (Fig. 3.6) of this thesis clearly show that preincubation of the *M. sexta* V-ATPase with bafilomycin does not prevent binding of the DCCD analogue NCD-4 to the essential glutamate. Thus, it is evident that the binding of bafilomycin does not change the proteolipid structure to such an extent that the glutamate residue is no more accessible from the membrane bilayer. Therefore, it is most likely that the plecomacrolide inhibitors do not explicitly block the proton translocation site, but rather inhibit V-ATPase function by disturbance of the V<sub>O</sub> ring rotation.

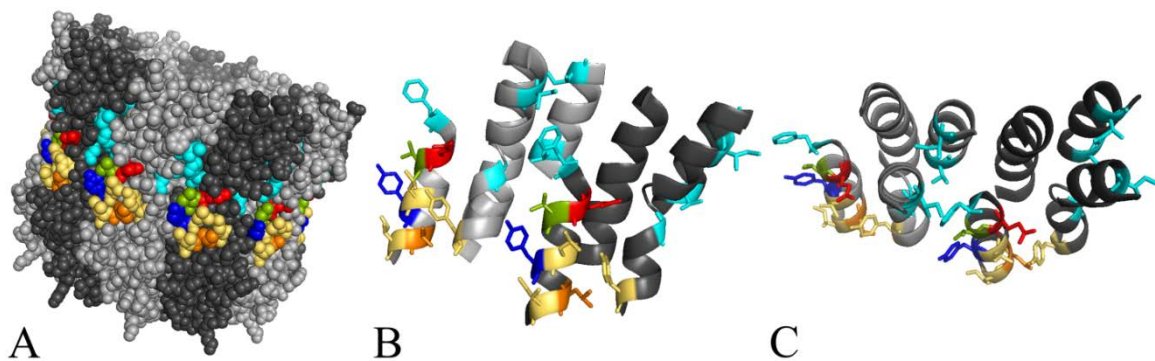


**Figure 4.2:** Model of the inhibitor binding sites in subunit c of the V-ATPase from *Saccharomyces cerevisiae*.

The *S. cerevisiae* c subunit amino acid sequence was fitted onto the *E. hirae* K ring structure (Murata *et al.*, 2005). Presented here are a side (B) and a top view (C) of the region of interest between two adjacent c subunits and the full, putatively decameric c ring structure (A). The alternating c subunits are colored in light or dark gray. Threonine 32, isoleucine 39, isoleucine 54, glycine 61, phenylalanine 135 (all cyan), and valine 138 (olive) participate in binding of bafilomycin, tyrosine 142 (blue) is involved in binding of both inhibitors, whereas glutamate 137 (red) is only part of the archazolid binding site. Further mutations in the putative binding site of archazolid revealed that amino acid leucine 144 (orange) is also involved in inhibitor binding, whereas tyrosine 66, leucine 141, and isoleucine 145 (all beige) are not.

### 4.3 The binding site of archazolid

#### 4.3.1 Location of the binding site within the V<sub>O</sub> ring

In view of the assumption that archazolid and the plecomacrolides partially share the same binding site within the V-ATPase subunit c (Huss *et al.*, 2005), it was surprising that most of the “bafilomycin-mutations” had only very little influence on archazolid binding (paragraph 3.1.4). In contrast, the mutations Y142N and L144I notably changed the IC<sub>50</sub> value resulting in a V-ATPase, which was 10-fold more sensitive to archazolid (paragraph 3.1.4 and 3.4.4). Since both, tyrosine 142 and leucine 144, are located in the middle of the membrane, with the leucine slightly oriented to the extra-cytoplasmic side (Fig. 4.2A), it seems reasonable to assume that archazolid interacts with the equatorial region of the c ring.

The findings from the mutagenesis studies, which mark a striking difference in the binding sites of archazolid and bafilomycin, were additionally supported by the results obtained from the labeling experiments with NCD-4. Labeling of subunit c was prevented by preincubation with archazolid but not with bafilomycin (paragraph 3.3, Fig. 3.6) or concanamycin (Fig. 3.7A). Altogether, these results clearly show that the binding site of archazolid is more distinct from the plecomacrolide binding site than expected before (Huss *et al.*, 2005). The archazolid binding site obviously comprises the essential glutamate in helix 4, whereas the plecomacrolides do not interfere with this region of the V-ATPase.

As can be seen in the model of a ring of c subunits of *S. cerevisiae* (Fig. 4.2), the amino acids that contribute to bafilomycin binding (highlighted in cyan) are located on the opposite side of the essential glutamate 137 (highlighted in red) at the interface between two adjacent c subunits. The only exception is tyrosine 142 (highlighted in blue), which is oriented toward the membrane facing side of helix 4. In addition, leucine 144 (highlighted in orange) is also oriented in this direction. Based on this model, binding of archazolid possibly occurs within one single c subunit and not at the interface of two c subunits. Fig. 4.2A also indicates that the plecomacrolide binding site mainly resides in the cytosolic half of the membrane bilayer as it had been shown in the three-dimensional model for the c ring from *N. crassa* before (Bowman *et al.*, 2006). In contrast, tyrosine 142, leucine 144, and the essential glutamate 137, are located in the middle of the membrane. Combining these factors, it is very likely that the binding site of archazolid is located within the triangle of tyrosine 142, leucine 144, and the essential glutamate at the equatorial region of a single c subunit.

By modeling the proposed inhibitor binding sites for bafilomycin and archazolid at the crystal structure of the K ring of the V-ATPase from *E. hirae* with bound DCCD (PDB code 2DB4; Fig. 4.3A and B), it becomes obvious that the bulky molecule archazolid (green) covers the binding site of DCCD (red) as well as the amino acids tyrosine 142 and leucine 144 at the membrane facing side. In contrast, bafilomycin (yellow) is restricted to the interface of two adjacent subunits and may not interfere with DCCD. Despite the fact that most of the “bafilomycin-mutations” have only negligible influence on archazolid, the prevention of archazolid binding by preincubation with different

plecomacrolide antibiotics (Fig. 3.5; Fig. 3.7A and B) points to the interference of both inhibitor classes. As the amino acid tyrosine 142 contributes to the binding of bafilomycin and archazolid (paragraph 3.1.4), it is most probable that the binding sites overlap in this region of the V-ATPase (Fig. 4.2). Taken together, this model of the archazolid binding site helps to explain the apparent discrepancy between the previous finding that archazolid prevents labeling of subunit c with [<sup>125</sup>I]-concanolide A (Huss *et al.*, 2005), and the results from the mutagenesis studies described in the present study. Taking into account that the effect of the mutations in subunit c of *N. crassa* on the related molecules bafilomycin and concanamycin is already different (Bowman *et al.*, 2006), the disparity between the effects of archazolid and bafilomycin is not surprising. Archazolid is a bulkier molecule than bafilomycin or concanamycin and thus may not fit into the interface between two c subunits (Fig. 4.3C).

Concerning archazolid, again the question arises if subunits c' and c'' in yeast are also targeted by the inhibitor. To address this issue, the effect of amino acid exchanges of tyrosine 150 and methionine 152 in c' (corresponding to tyrosine 142 and leucine 144 in subunit c) on the binding of archazolid was tested (paragraph 3.5.4). Since mutation of the corresponding positions in subunit c led to a strong decrease in the IC<sub>50</sub> value for the compound, it was assumed that the mutation of a single inhibitor binding site might be sufficient to increase the affinity of the whole c ring. Hence, mutation of c' alone might already lead to a lower IC<sub>50</sub> value for archazolid. In contrast to this expectation, for none of the performed mutations a significant change of the IC<sub>50</sub> value was detected (paragraph 3.5.4, Tab. 3.6). This leads to two feasible explanations. On the one hand, due to heterogeneity of the binding site in c', the effect of these mutations might be too small to produce a striking change in the IC<sub>50</sub> value. On the other hand, it is possible that at least subunit c' does not contain a binding site for archazolid. Since the inhibitor binding site probably resides within one single c subunit, c' and c'' do not necessarily have to provide additional contact sites with the inhibitor. In contrast, as the binding site of bafilomycin is built up of two parts by two neighboring subunits (Bowman *et al.*, 2006, paragraph 4.2), the contribution of all three types of proteolipids seems to be more likely in case of this inhibitor.



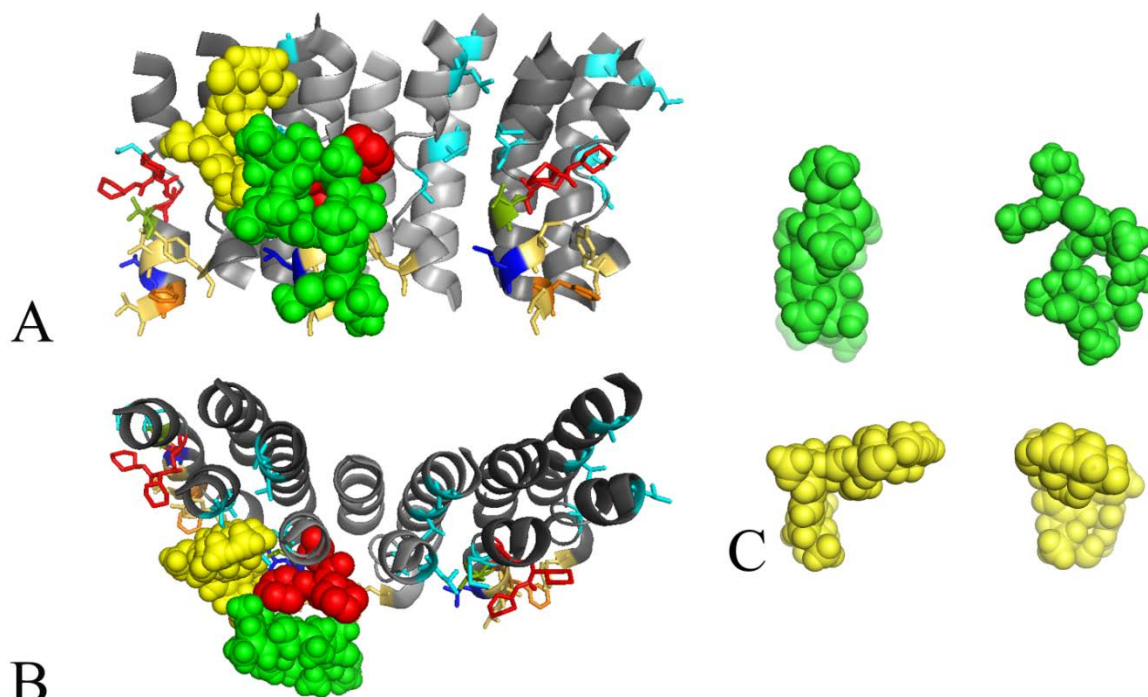


**Figure 4.3: Inhibitor binding sites with respect to the binding site of DCCD at the K ring of *E. hirae* (PDB code 2DB4).**

Shown here are a side (A) and a top view (B) of the region of interest in the K ring with the three-dimensional space fill structures of archazolid (green), bafilomycin (yellow) and DCCD at glutamate 139 (red). The alternating K subunits are colored in light or dark gray. Colored amino acid residues correspond to the sites mutated in *S. cerevisiae*. Valine 34, alanine 41, leucine 56, glycine 63, and methionine 137 (all cyan), tyrosine 68, isoleucine 143, and valine 147 (all beige), threonine 140 (olive), leucine 144 (blue), and phenylalanine 146 (orange).

#### 4.3.2 Contribution of single amino acid residues

Regarding the influence of amino acid exchanges on inhibitor binding in general, a striking difference between bafilomycin and archazolid became evident. For bafilomycin, the respective side chains are closely clustered and almost all mutations within the binding site revealed a strong influence on the inhibitor-protein interaction (paragraph 3.1.4 and 4.2). In contrast, mutagenesis within the proposed archazolid binding site in most cases did not show a clear effect (paragraph 3.4.4). This might lead to the conclusion that these residues are not involved in binding. However, because the macrolactone ring of archazolid is a highly hydrophobic structure, it is also possible that the inhibitor-protein contact in this region is mainly caused by hydrophobic interactions. Therefore, it may be possible that the amino acid exchanges performed throughout this study did not influence the binding of archazolid because they did not change the hydrophobicity of the binding site. In this regard, more radical substitutions, for example the exchange to a polar residue, may lead to a stronger effect. Nevertheless, amino acid exchanges in such a highly conserved region of the protein have to be evaluated carefully because they can easily disturb the function of the protein.

The notable increase in sensitivity for archazolid achieved by mutations Y142N and L144I has to be explained by an alteration of the inhibitor binding site that leads to a

higher affinity for the inhibitor. However, the interpretation of the contribution of single amino acid residues to the interaction with the inhibitor is difficult because the exact structure of the protein and the orientation of the inhibitor are not yet known. Nevertheless, in some cases different amino acid exchanges at the same position give hints about the structural features that might determine the binding specificity.

Since for example the Y142H mutation has a smaller influence than the mutation Y142N (paragraph 3.1.4; Tab. 3.2), it is likely that the binding of archazolid is facilitated in the absence of a ring structure at position 142 (Fig. 4.4B). In addition, the fact that the Y142N mutation does not decrease the  $IC_{50}$  value of oxo-archazolid (paragraph 3.6.2; Fig. 3.15 and Tab. 3.7), points to an interaction of the amino acid at position 142 with the C-15 region of the inhibitor. It might thus be possible that the hydroxyl group at C-15 of the non-modified compound forms an additional hydrogen bond with the carboxyl side chain when tyrosine 142 is exchanged for asparagine. This would lead to a stronger interaction of the inhibitor with its target site and hence decrease the  $IC_{50}$  value. In contrast, for oxo-archazolid, which lacks the C-15 hydroxyl group, no additional hydrogen bond can be built and hence, the  $IC_{50}$  value is not decreased in Y142N. This assumption is supported by docking studies of archazolid and the c subunit performed by S. Dreisigacker (University of Heidelberg, Germany) and T. Carlomagno (EMBL Heidelberg, Germany). In these studies the inhibitor in the conformation determined by Fares *et al.* (2008) was docked at the *S. cerevisiae* c ring model presented in this study using the docking programs Autodock and Drugscore. In the resulting model the formation of a hydrogen bond between the C-15 hydroxyl group and the mutant asparagine 142 was observed (S. Dreisigacker and T. Carlomagno, personal communication).

An additional hydrogen bond formation could also explain the decrease of the  $IC_{50}$  value observed for the L144I mutation, as the isomerization of the side chain might produce a new enzyme-inhibitor contact site. Despite the fact that the decrease of the  $IC_{50}$  is again not observed for oxo-archazolid, the C-15 hydroxyl group of archazolid is no likely candidate for the interaction with isoleucine, because this does not provide a hydrogen acceptor group. Hence, other structural features presumably determine the interaction of the inhibitor with leucine 144.

As reflected in the increased  $IC_{50}$  values for oxo-archazolid in all yeast strains tested so far, the dehydrogenation of the C-15 hydroxyl strikingly reduces the inhibitor-target interaction (paragraph 3.6.2; Fig. 3.15 and Tab. 3.7). This result is in line with previous tests of this derivative which revealed a 20-fold higher  $IC_{50}$  value for the purified *M. sexta* V-ATPase, and virtually no inhibition of mammalian cell line growth (Menche *et al.*, 2007b). It was presumed that this effect originates from an overall change in the 3D structure of the compound, leading to partial perturbation of its biological activity. It might thus be possible that the effect of the L144I mutation is destroyed by this global conversion of the inhibitor, and not just by the absence of a specific side chain interaction. In line with this assumption, the influence of the mutation L144I on binding of all the archazolid derivatives tested in this study is less pronounced when compared to the original compound (paragraph 3.6.2; Fig. 3.15 and Tab. 3.7). The docking results mentioned above, predict a hydrophobic binding pocket either between leucine 144, isoleucine 145 and leucine 149, or in the region of phenylalanine 135, isoleucine 58 and threo-

nine 32, where the isobutyl group of the thiazol side chain fits in. The second orientation of the binding pocket cannot be reconciled with the mutagenesis studies performed so far because neither the mutation of phenylalanine 135, nor of threonine 32, clearly influenced the binding efficiency of archazolid (paragraph 3.1.4; Tab. 3.2). In contrast, the first model evidently provides an explanation for the influence of the amino acid exchange at position 144, as the exchange of leucine to isoleucine might induce a structural change in this binding pocket that facilitates hydrophobic interactions, without the explicit formation of an additional hydrogen bond (Fig. 4.4B). The exchange of isoleucine 145 to either leucine or phenylalanine, on the other hand, did not result in a pronounced effect on the IC<sub>50</sub> value for archazolid (paragraph 3.4.4; Tab. 3.4). In this case, the structural change of the side chain does not seem to influence the hydrophobic interactions. Regarding the docking results, ongoing calculations will presently reveal the exact orientation of archazolid bound to its target site and thus facilitate interpretation of the mutagenesis data.

The influence of the mutations Y142N and L144I on the binding of archazolid was further supported by the results obtained from *cw* EPR spectroscopy with SL-archazolid and isolated yeast vacuoles. For both mutant V-ATPases a definite reduction of the spin label mobility of SL-archazolid bound to the protein was visible when compared to the non-mutated enzyme (paragraph 3.8.2; Fig. 3.19). Therefore, the respective amino acids are either directly involved in inhibitor binding as discussed before, or the amino acid exchanges induce general structural changes in the archazolid binding site which facilitate binding of the compound. In this regard, *cw* EPR spectroscopy in combination with site-directed spin labeling of the protein (paragraph 2.4) could be used to reveal small distance interactions of archazolid with these residues. However, for this purpose it will be necessary to introduce a spin label like methanethiosulfonate (MTSSL) at the respective amino acid positions (Klare and Steinhoff, 2009) and examine dipolar coupling of the intrinsic spin label with SL-archazolid. Because MTSSL binds to the reactive sulfhydryl group of cysteine side chains, such residues have to be engineered at the side of interest within the protein, and existing cysteine residues have to be eliminated to avoid unwanted spin label interactions (Klare and Steinhoff, 2009). Since the *S. cerevisiae* c subunit contains six native cysteine residues distributed over the whole sequence (Fig. 4.1), it does obviously not provide the best prerequisites to apply this method. In contrast, the *N. norvegicus* subunit c which can fully substitute the yeast protein (Harrison *et al.*, 1994), contains only one native cysteine (Fig. 4.1). This protein was already successfully used for EPR studies with the V-ATPase inhibitors concanamycin and INDOL (Páli *et al.*, 2004b) and could thus also be used to further characterize the archazolid binding pocket.

Irrespective of the fact that no definite conclusion can be drawn about the nature of distinct interactions of archazolid with single amino acid residues so far, the results discussed herein provide sufficient evidence to propose a more elaborate model of the position of the inhibitor within its target site (Fig. 4.4A). In this model, the C-15 hydroxyl group is located in close proximity to tyrosine 142, while the isobutyl side chain resides near leucine 144, and in addition, covering of the essential glutamate 137 by archazolid gets obvious.

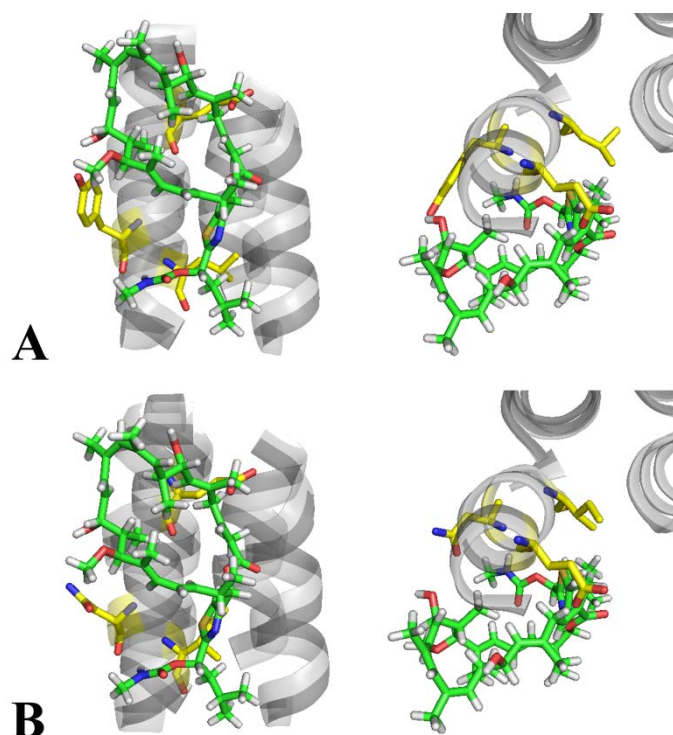


**Figure 4.4: Proposed position of archazolid within its target site.**

The 3D structure of archazolid was manually docked at the proposed binding site within the c subunit of *S. cerevisiae* using the PyMOL program. Displayed are a side (left panel) and a top view from the cytoplasmic side of the membrane (right panel) of either the wild type binding site (A) or the binding site with amino acid exchanges Y142N and L144I (B). The carbon backbone of the crucial amino acid side chains at positions 137, 142 and 144 is displayed as yellow sticks, the backbone of archazolid as green sticks. Further atoms are colored as follows: red, oxygen; blue, nitrogen; orange, sulfur; white, hydrogen. Please note that hydrogen atoms are not displayed in the protein structure. Differences in the inter-molecule distances visible in A and B originate only from the manual exchange of the amino acid residues and do not reflect any calculated values.

### 4.3.3 Involvement of the essential glutamate

The competition assays of different V-ATPase inhibitors with the fluorescent DCCD derivative NCD-4 presented in this study univocally showed that the archazolid binding site comprises the essential glutamate residue within the c subunit (paragraph 3.3; Fig. 3.6). This result offers three different interpretations of how the inhibitor binding affects the glutamate residue and thus prevents binding of NCD-4. Firstly, it is possible that archazolid directly interacts with the acidic side chain most likely via the formation of a hydrogen bond. Secondly, binding of the inhibitor to its target site may shield the glutamate residue from access of NCD-4 from the membrane side. Thirdly, inhibitor binding may induce conformational changes within the c ring and therefore indirectly prevent access of NCD-4.

Regarding the location of the amino acid residues tyrosine 142 and leucine 144 with respect to the essential glutamate, the latter possibility does not seem very likely. The direct interaction of archazolid with the former two amino acid residues will, due to the dimensions of the compound, automatically lead to shielding of the glutamate (Fig. 4.4). Hence, the question arises, whether the glutamate side chain is directly or indi-

rectly affected by the inhibitor. For oligomycin, a macrolactone which binds to the F-ATPase membrane complex, it was proposed that it builds a hydrogen bond with the essential aspartate residue within the *E. coli* c subunit (Green *et al.*, 2009). However, in this case, a hydroxyl group of the spiroketal side chain of the inhibitor functions as proton donor and the macrolactone ring is proposed to interact with subunit a. In contrast, labeling of the *M. sexta* V-ATPase with radioactive PAL derivatives of archazolid identified only subunit c as binding partner (paragraph 3.2.2; Fig. 3.5). In both PAL derivatives used for these experiments the diazirinyl side chain was attached to the macrolactone ring, thus confirming that the ring structure interacts with subunit c in the case of archazolid. Due to the carboxyl side chain of the essential glutamate residue, the formation of a hydrogen bond with hydrogen atoms of the macrolidic ring seems to be logical. However, the glutamate residues that are accessible from the lipid phase of the membrane, from where the hydrophobic inhibitor molecules most likely will attack, are in their protonated state (paragraph 1.2.3). Thus, these residues would function as proton donor and the macrolactone ring would have to provide an acceptor e.g. a carbonyl group. The only native carbonyl group present in the macrolidic ring of archazolid is located at C-1 close to the thiazol side chain (paragraph 1.6.3; Fig. 1.6D). In view of the proposed orientation of the inhibitor at the V-ATPase (Figure 4.4), this carbonyl group is not in close proximity to the glutamate side chain, indicating that it does not interact with this residue. Yet, such a preliminary model cannot lead to clear statements about the contributing structural features.

Preliminary data from *cw* EPR measurements of a mutant yeast V-ATPase, with all essential glutamate residues exchanged for glutamine, revealed only minor changes of the spectrum when compared to the one obtained with wild type vacuoles (data not shown). These results indicate that the loss of the carboxyl side chain has some influence on archazolid binding and probably reduces the enzyme-inhibitor interaction to a small extent. But, due to very low protein content in these vacuoles, and a therefore low signal-to-noise ratio of the spectra, these conclusions remain speculative in the first instance. However, it is feasible to presume that the essential glutamate does not have a strong impact on the binding of archazolid. In line with this assumption, the computational docking of the inhibitor did not reveal a hydrogen bond formation with the essential glutamate, but archazolid occluded this side chain in both of the possible binding modes (S. Dreisigacker and T. Carlomagno, personal communication). In summarizing all these considerations, one can thus suppose that the essential glutamate is not directly involved, but obstructed upon, the binding of archazolid.

#### 4.3.4 Contribution of the inhibitor structure

Regarding the protein structure, the contribution of the amino acid residues tyrosine 142 and leucine 144 to the binding of archazolid is evident. Concerning the structure of the inhibitor, radioactive labeling studies revealed that the macrolactone ring interacts with the  $V_O$  c subunit (paragraph 3.2.2; Fig. 3.5). In addition, it became clear that the C-15 hydroxyl group of archazolid is a major pharmacophoric part of the structure (paragraph 3.4.2 and 4.3.2), as it was already proposed by Menche *et al.* (2007b). In this arti-

cle, it was also stated that the C-7 hydroxyl group most likely contributes to inhibitor binding, since its modification drastically increased the  $IC_{50}$  values of the respective derivatives. Archazolid C, a natural derivative of archazolid which contains a sugar group at C-7, exhibited a drastically elevated  $IC_{50}$  value for mammalian cells and the purified *M. sexta* V-ATPase (Menche *et al.*, 2007d). Moreover, the wild type V-ATPase from *S. cerevisiae* was virtually not affected by this inhibitor (paragraph 3.6.2; Tab. 3.7). In contrast, the removal of the carboxamide group at C-1' had almost no influence on the efficiency of the V-ATPase inhibition (Menche *et al.*, 2007b; paragraph 3.6.2; Tab. 3.7). However, the C-1 carboxamide group seems to be responsible for cooperative binding of archazolid, as indicated by a decreased Hill coefficient of approximately 1 for descarchazolid when compared to archazolid A (paragraph 3.6.2).

In line with the previous findings, most recent studies on novel natural derivatives of archazolid, archazolid E and F, revealed that glycosylation at C-15 (archazolid E) has a smaller effect on the inhibition properties of the compound than the modification of C-7 (Horstmann *et al.*, 2011). Taking all these results together, it is obvious that the “northern part” of the macrolactone ring of archazolid is the main structural feature that provides the pharmacophoric properties of the compound and thus it is likely that this part of the inhibitor interacts with the binding site in the V-ATPase. In this regard, it would be interesting to investigate whether the C-7 hydroxyl group is also directly involved in binding of archazolid.

Archazolid F, an isomer of archazolid B where the 2, 3-double bond is shifted to the 3, 4-position, exhibited approximately 10-fold higher efficacy against mammalian cell lines with respect to its relatives archazolid A and B (Horstmann *et al.*, 2011). Moreover, slight preferences of archazolid F for some of the cell lines could be observed, emphasizing the impact of the macrolactone ring structure on the biological activity of the inhibitor. In structure-function studies of bafilomycin it was shown that, beside the impact of the single hydroxyl group within the macrolactone ring, the dienic system is also an important feature for the binding properties of the compound (Gagliardi *et al.*, 1998a). In addition, it was proposed that the higher efficiency of concanamycin when compared to bafilomycin is due to a higher flexibility of the 18-membered versus the 16-membered macrolactone ring that might allow an induced fit of the inhibitor to its protein target (Bindseil and Zeeck, 1994). Thus, a certain degree of flexibility in the macrolactone structure might provide an improved and more specific inhibitor-protein interaction. The 24-membered ring of archazolid might in this regard offer broad possibilities to modify and optimize its binding properties.

## 4.4 A proposed binding mechanism

### 4.4.1 Archazolid interferes with the proton translocation mechanism

Since the binding site of archazolid comprises the conserved glutamate residue that is essential for proton translocation, it is likely that this inhibitor directly prevents the transport of protons. Unfortunately, no crystal structure of the  $V_O$  ring is available yet which would allow identification of all residues involved in proton transport, and thus provide the opportunity to study their interaction with archazolid. In contrast, for different F-ATPase  $F_O$  rings as well as for the *E. hirae*  $A_O$  ring crystal structures are available (Meier *et al.*, 2006; Meier *et al.*, 2005; Murata *et al.*, 2005; Pogoryelov *et al.*, 2009; Vollmar *et al.*, 2009). These structures revealed a set of amino acid residues within the c subunits that are involved in proton and sodium ion translocation, respectively. Because of the close relation of proteolipid subunits of all rotary ATPases (reviewed in Müller and Grüber, 2003), these data were used to get knowledge about the residues critical for proton transport in the V-ATPases (Fig. 4.5). For this purpose, the amino acid sequences of the *S. cerevisiae* and the *E. hirae* c subunit were split between the second and third transmembrane helix and both parts were separately aligned to the respective F-ATPase proteolipid sequences (Fig. 4.5A and B). The highly conserved critical residues were then transferred to the *S. cerevisiae* sequence. As can be seen in Fig. 4.5A, a tyrosine within the second helix of the F-ATPase proteolipids, which is involved in ion transport, can be found in *E. hirae* as well as in *S. cerevisiae* (tyrosine 66). Hence, one can assume that this residue also contributes to proton transport in yeast. In line with this presumption, the exchange of tyrosine 66 to serine performed in the course of this study totally disturbed protein function and also drastically reduced protein assembly (paragraph 3.4). However, consistent with previous results (Noumi *et al.*, 1991), the mutation to phenylalanine had no effect on either assembly or activity of the enzyme. This suggests that the ring structure at position 66 has an important impact on the whole structure and function of the V-ATPase. In addition to the critical tyrosine residue, the amino acid located seven positions downstream of the highly conserved tyrosine (methionine 59 in *S. cerevisiae*), was shown to be crucial for ion transport (Fig. 4.5A). Since the backbone carbonyl group is the contributing feature in this case, it is likely that the methionine 59 of *S. cerevisiae* also participates in proton translocation. Hence, the proposed proton translocation system within the *S. cerevisiae* c subunit consists of at least three amino acids, tyrosine 66, methionine 59 and glutamate 137 (Fig. 4.5C).

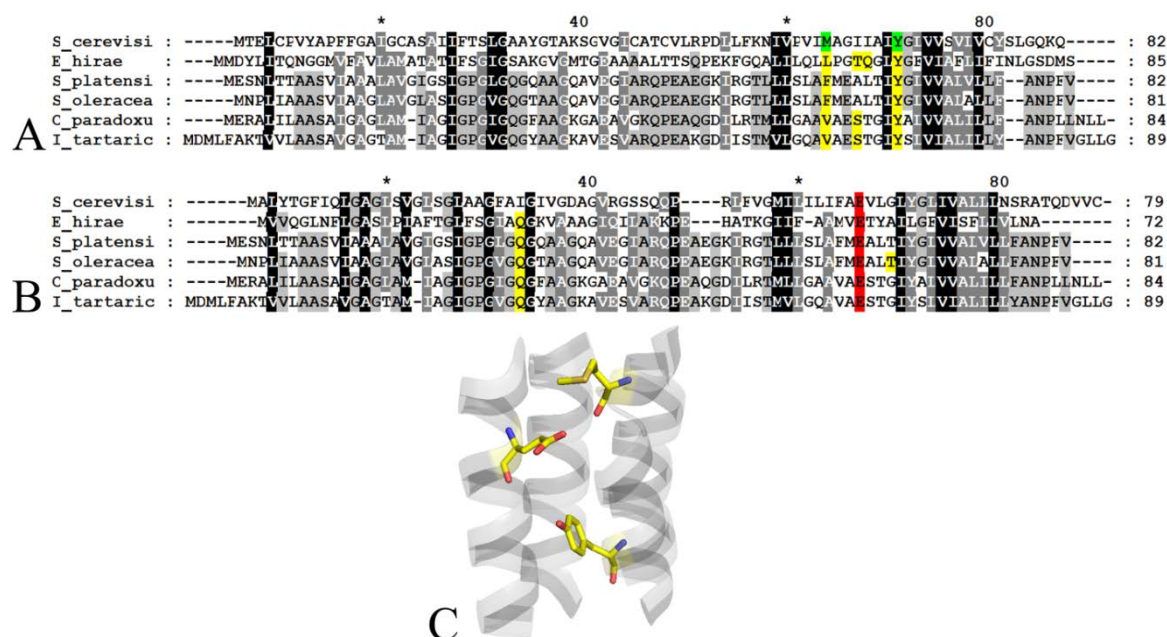


**Figure 4.5: Proposed proton translocation site of the *Saccharomyces cerevisiae* c subunit.**

(A) and (B) ClustalW alignment of c subunit amino acid sequences as follows: *Saccharomyces cerevisiae* (Swiss-Prot: P25515.1), *Enterococcus hirae* (Swiss-Prot: P43457.1), *Spirulina platensis* (PDB: 2WIE), *Spinacia oleracea* (Swiss-Prot: P69447.1), *Clostridium paradoxum* (Swiss-Prot: Q0ZS24.1), *Ilyobacter tartaricus* (Swiss-Prot: Q8KRV3.1). Either the C-terminal (A) or the N-terminal half (B) of the protein sequence of *S. cerevisiae* and *E. hirae* was aligned to the F-ATPase c subunits of the organisms mentioned above. Highly conserved, conserved and less conserved residues are colored in black, gray and light-gray, respectively. The essential glutamate within helix 4 is highlighted in red. The amino acid residues that contribute to proton or sodium transport in the F-ATPase subunits (Meier *et al.*, 2006; Meier *et al.*, 2005; Pogoryelov *et al.*, 2009; Vollmar *et al.*, 2009) and the *E. hirae* protein (Murata *et al.*, 2005) are highlighted in yellow. Critical and highly conserved amino acid positions were transferred to the *S. cerevisiae* protein (green). (C) Structure of the proposed proton translocation site within subunit c of *S. cerevisiae*. Side chains of glutamate 137, tyrosine 66 and methionine 59 are represented as yellow sticks with atoms colored as follows: red, oxygen; blue, nitrogen; orange, sulfur. Please note that hydrogen atoms are not displayed in the protein structure.

In regard to the location of this amino acid triad, it is obvious that archazolid might affect all of them and accordingly disturb the proton translocation mechanism of the c ring. However, for the mutation Y66F, no striking influence on archazolid binding was observed (paragraph 3.4.4; Fig. 3.10; Tab. 3.4). Based on previous considerations (paragraph 4.3.2), it seems likely that the interference with this residue results from hydrophobic interactions that will probably not be changed by the substitution of tyrosine with phenylalanine. Likewise, it is also possible that this side chain is simply occluded by archazolid as it was discussed for the essential glutamate before (paragraph 4.3.3). More severe exchanges of tyrosine 66 will probably lead to disruption of the protein function as shown for the mutation Y66S, and thus seem to be inapplicable to clarify the involvement of this amino acid in archazolid binding. In contrast, methionine 59 provides a more promising target for prospective mutagenesis studies because, in this case, the protein backbone, and not the side chain, is involved in proton coordination. Hence, the exchange of the side chain will probably not change the primary function of this amino acid, but might reveal an influence on archazolid binding.



Concerning the mode of inhibition, one can assume that archazolid might shield the glutamate from proton access. However, since archazolid most probably binds to the protonated form of subunit c (paragraph 4.3.3), it will strictly speaking not shield the glutamate from proton access, but rather prevent proton release from the c subunits to the extra-cytoplasmic space, hence freeze the glutamate in its protonated state. Anyway, in consequence, archazolid most likely directly prevents proton exchange across the membrane, and therefore, it disturbs the most important functional feature of the V-ATPases, namely the proton translocation mechanism. In this regard, it is not surprising that this compound represents such a highly efficient inhibitor of this enzyme class.

This proposed inhibition mechanism may likewise provide further explanation for the striking difference in the amount of amino acid residues that were shown to contribute to the binding of archazolid and bafilomycin, respectively (paragraph 3.1.4 and 3.4.4). One may assume that if archazolid directly blocks the proton binding site, only a few stronger contacts to the protein (like e.g. hydrogen bonds) are needed to provide sufficient inhibition efficiency. In contrast, if bafilomycin really functions like a “stick in a wheel”, tight binding to its target site will be a prerequisite to block rotation of the c ring with respect to subunit a. Furthermore, for archazolid, which binds to the membrane facing side of subunit c, the number of contact sites with the protein may be comparatively small with respect to bafilomycin, which intercalates between two c subunits.

#### 4.4.2 Does archazolid prevent rotation of the c ring?

Archazolid is docked at the membrane facing surface of the c ring (paragraph 4.3.1; Fig. 4.2 and 4.3). In this regard, one could presume that archazolid, despite its interference with the proton translocation mechanism, also blocks the rotation of the c ring relative to subunit a, as it was proposed for bafilomycin before (Bowman *et al.*, 2004). Radioactive labeling of the V-ATPase with PAL derivatives of archazolid, however, definitely only identified subunit c as binding partner of the inhibitor (paragraph 3.2.2; Fig. 3.5). The diazirinyl groups of both PAL derivatives used in this study are attached to the macrolactone ring which probably provides the main contact site with subunit c (paragraph 4.3.4). Hence, it may be possible that the interaction with subunit a occurs at a different site of the inhibitor. The attachment of a diazirinyl group to another part of the inhibitor, for example the thiazol side chain, may therefore also lead to labeling of this subunit. Different positions of the diazirinyl in concanamycin also led to labeling of, on the one hand, subunit c alone (Huss *et al.*, 2002) and, on the other hand, subunit c and a, highlighting the importance of both subunits for the enzyme-inhibitor interaction in this case (Nardmann, C., Wieczorek, H. and Huss, M., manuscript in preparation).

However, because archazolid is a flatter molecule than plecomacrolide inhibitors like bafilomycin (Fig. 4.3C), it perhaps does not get into contact with subunit a. Furthermore, the crystal structure of the *E. hirae* membrane rotor revealed a concave overall shape, with the essential glutamate residues located in the center of the dip (Murata *et al.*, 2005), which is in line with the structures found for F-ATPase membrane rings (Meier *et al.*, 2005; Pogoryelov *et al.*, 2009). Assuming that the concave shape also occurs in V-ATPases, as implemented in the *S. cerevisiae* c ring model presented herein (Fig. 4.2), the

binding site of archazolid accurately covers the dip within the c ring (picture not shown). In this regard, it seems even more reasonable that archazolid does not interfere with subunit a and therefore does not block the rotation of the c ring. Nevertheless, cryo-electron microscopic images of the A-ATPase from *T. thermophilus* revealed a small, nose-like structure within the a subunit that directly interacts with the equatorial region of the c ring and has thus been discussed to contribute to proton translocation (Lau and Rubinstein, 2010). An equivalent structure in V-ATPases would evidently interfere with archazolid bound to the proton translocating site of subunit c, and consequently, archazolid would block rotation of the ring. However, despite the increased resolution of current electron microscopic images (Lau and Rubinstein, 2010; Muench *et al.*, 2009), it is not yet possible to definitely assign distances at the a/c interface. Thus, the question whether archazolid also interferes with subunit a remains unsolved at this point.

### 4.5 Design of more specific derivatives

The main objective of the present study was to gain more knowledge about the binding and inhibition mechanism of the novel V-ATPase inhibitor archazolid, and the outcome should contribute to the design of more specific derivatives of this compound. The results presented herein provide convincing evidence that archazolid blocks the proton translocating site within subunit c. In this regard, the inhibitor seems to be already highly efficient. As both amino acid exchanges that influenced inhibitor binding rendered the V-ATPase more sensitive toward archazolid (paragraph 3.1.4 and 3.4.4) it is obvious that the efficiency of the inhibitor-target interaction could still be increased. Further investigation of amino acid exchanges in combination with chemical derivatization of the inhibitor will gradually extend the information about crucial components for inhibitor binding. Nevertheless, due to the extremely high sequence conservation the V-ATPase c subunits (Fig. 4.1), it is unlikely that such information will lead to the discovery of highly sensitive natural isoforms that, furthermore, represent valuable drug targets. Thus, chemical engineering of archazolid seems to be the only feasible way to achieve isoform specific V-ATPase inhibition.

To design an isoform specific derivative of archazolid the exact knowledge of the biological active conformation of the inhibitor will be utmost helpful. In course of the collaborative project “Conformation activity relationship of the archazolids: Development of a novel class of highly potent V-ATPase inhibitors” (VolkswagenStiftung) efforts were made by the group of Teresa Carlomagno (EMBL, Heidelberg, Germany) to elucidate the biologically active conformation of archazolid in the presence of the purified *M. sexta* V-ATPase by means of NMR spectroscopy. However, due to solubility problems, it was not possible to examine the inhibitor structure under such conditions (T. Carlomagno, personal communication). Furthermore, the attachment of polar groups to the inhibitor, that was performed to circumvent these solubility problems, destroyed its biological function (paragraph 3.7). To reveal the functional conformation of the inhibitor by NMR spectroscopy, it will thus be necessary to carefully evaluate polar modification of the inhibitor.

The importance of the macrolactone ring of archazolid for its binding properties became evident in a variety of different approaches (paragraph 4.3.4). In this regard, it

will be interesting to investigate whether the macrolactone ring itself or even more simplified structures also inhibit V-ATPase function. The synthesis of highly simplified structural analogues of bafilomycin, the indoles, revealed a compound (SB242784) with almost the same inhibition efficiency when compared to its precursor (Nadler *et al.*, 1998). Remarkably, this compound exhibited a clear preference for the osteoclast versus the kidney and adrenal V-ATPase, *in vitro* and *in vivo*, raising the possibility of pharmacological application of this compound (Gagliardi *et al.*, 1998b; Nadler *et al.*, 1998; Visentin *et al.*, 2000). Also in this case, the importance of the dienic system for the inhibition properties of SB242784 was highlighted (Nadler *et al.*, 1998; see also paragraph 4.3.4). In this regard, the recently discovered archazolid F, an isomer of archazolid B (Horstmann *et al.*, 2011; paragraph 3.7 and 4.3.4), provides important information about the crucial features of the dienic system of archazolid. Ultimately, the macrolactone ring structure of this natural derivative, in combination with the information about other critical structural features, may help to develop an improved and more specific synthetic derivative of archazolid useful as a lead compound in drug research.

## 4.6 Toward the structure of the c ring

### 4.6.1 Using V-ATPase inhibitors to elucidate the c ring stoichiometry

Due to the lack of high resolution structures of the proteolipid ring, spin labeled (SL) V-ATPase inhibitors have emerged as a valuable tool to study the enzyme-inhibitor interaction and thus provide insights into the inhibition mechanism of the compounds (Dixon *et al.*, 2003). SL derivatives were for example used to elucidate the interaction of concanamycin and indol inhibitors with the V-ATPase c subunit (Dixon *et al.*, 2008; Páli *et al.*, 2004b). In addition, EPR spectroscopy was also applied to study the structure and assembly of the *N. norvegicus* c ring revealing e.g. information about the localization of the essential glutamate residue (Páli *et al.*, 1995; Páli *et al.*, 1999). The examination of the *M. sexta* V<sub>O</sub> ring stoichiometry with spin labeled V-ATPase inhibitors nicely adds to the successful application of such compounds for the elucidation of structural and functional components of the enzyme.

While the number of crystal structures of F- and A-ATPase c rings is continuously increasing, the information about V-ATPase membrane rotors is still limited to the comparatively low resolution of electron microscopic images. Electron microscopy of the bovine V<sub>O</sub> ring suggested a hexameric arrangement of the proteolipid subunits (Gregorini *et al.*, 2007). Nevertheless, the currently most detailed 3D model of a V<sub>O</sub> complex, obtained by cryo-electron microscopy of the *M. sexta* V-ATPase, favors a number of ten c subunits in the ring like it was shown for *E. hirae* (Muench *et al.*, 2009; Murata *et al.*, 2005). The results from DEER experiments performed with SL-archazolid bound to the *M. sexta* V-ATPase presented in paragraph 3.9 (Fig. 3.20C and D) of this thesis can also be reconciled with a decameric structure of the c ring. However, since the exact orientation of the bound archazolid is not yet known, the position of the spin label cannot clearly be assigned. Due to this inaccuracy, the number of c subunits can only be narrowed down to nine to eleven subunits, but however, a hexameric arrangement can most likely be ex-

cluded (J. P. Klare, personal communication). To get more precise information about the correct number of *c* subunits, the measurements have yet to be repeated, ideally with a lower signal-to-noise ratio, and the distances have to be recalculated with respect to the final docking model of archazolid.

Due to its location within the protein, NCCD, the SL derivative of DCCD, would represent a highly valuable tool for DEER measurements, as its binding site is clearly defined. Unfortunately, because of the symmetry of the reactive carbodiimide group, the inhibitor can bind in two different orientations to the protein, leading to a mixed distance distribution in the DEER measurements (paragraph 3.9; Fig. 3.20A and B). Thus, no conclusion about the number of *c* subunits could be drawn in the case of NCCD, so far. Currently, the group of Dirk Menche (University of Heidelberg, Germany) is designing a new spin labeled analogue of DCCD that preferentially binds in one distinct orientation and should thus overcome the disadvantage of the inhibitor while conserving its benefits. Since DCCD binds to proteolipid subunits of all types of rotary ATPases, such a compound would be of general use for the assignment of subunit compositions in membrane rings by means of EPR spectroscopy.

### 4.6.2 Considerations about the physiological impact of the *c* ring stoichiometry

In combining the DEER results presented herein with the cryo-electron microscopic data obtained by Muench *et al.* (2009), growing evidence is provided that the *M. sexta* V-ATPase might contain a decameric membrane rotor. Thus, the model of a hexameric membrane rotor in V-ATPases that is believed to be valid e.g. for the bovine enzyme (Gregorini *et al.*, 2007), may not be realized in the *M. sexta* enzyme. With regard to the crystal structure of the decameric *E. hirae* membrane ring, Murata *et al.* (2005) already discussed the hexameric ring model, thereby proposing that it will be proven wrong by high resolution methods. In this regard, the current picture of the *M. sexta* *c* ring structure provides first hints that either V-ATPases in general might contain a decameric membrane rotor, or that the stoichiometry of  $V_O$  rotors might not be fixed for all organisms.

In view of the diverse functions of V-ATPases from different organisms or cell types (reviewed in paragraph 1.5), it seems reasonable to assume that the number of *c* subunits within the  $V_O$  ring may vary with regard to the duties of the enzyme like it is currently discussed for F-ATPase rotor rings (von Ballmoos *et al.*, 2008). The relevance of these variations is not yet understood, but it is proposed that the ring size represents an adaptation to the physiological requirements of the respective organism. Hence, under equal energetic conditions, a large *c* rotor, like the *S. platensis* ring containing 15 *c* subunits (Pogoryelov *et al.*, 2009), would represent a low efficiency system, because of the high  $H^+/ATP$  ratio, while a small ring size would increase the efficiency of the enzyme. In transferring this concept to V-ATPases, which consume ATP to drive ion translocation, the *in vivo* situation would be vice versa. Thus, a large rotor would represent the more efficient system, as it would transfer a higher amount of protons per ATP molecule. Nevertheless, in this case, the transport efficiency is limited by the energy provided by ATP hydrolysis. The proton electrochemical gradient generated by the V-ATPases is thus reflected in the equation:  $\Delta G_{ATP/n} = RT2.3\log([H^+]_i/[H^+]_o) + F\Delta\Psi$ , where  $\Delta G_{ATP/n}$  is the

energy of ATP hydrolysis per mol divided by the amount of transported protons (according to the number of *c* subunits in the ring),  $R = 8.3 \text{ kJmol}^{-1}\text{K}^{-1}$ ,  $T = 300\text{K}$  and  $F = 96.5 \text{ kJv}^{-1}\text{mol}^{-1}$  (Harvey and Wieczorek, 1997).

Concerning the V-ATPase in the *M. sexta* midgut, the potential difference  $\Delta\Psi$  across the GCAM is approximately 240 mV while there is almost no difference in the proton concentration ( $[\text{H}^+]_i/[\text{H}^+]_o$ ) (Harvey and Wieczorek, 1997). Thus, provided that ATP hydrolysis supplies  $\sim 50 \text{ kJmol}^{-1}$ , the maximum amount of protons transported per ATP can be estimated by:

$$n = 50 \text{ kJmol}^{-1} / 96.5 \text{ kJv}^{-1}\text{mol}^{-1} \times 0.24 \text{ V} \approx 2$$

Hence, from a thermodynamic point of view, the number of protons transported per ATP is limited to 2 and a decameric *c* ring in the *M. sexta* V-ATPase seems to be improbable as it suggests, from simple stoichiometric calculations (*c* ring size/ three ATP cleavage sites) (Junge *et al.*, 2009; Muench *et al.*, 2011), a  $\text{H}^+/\text{ATP}$  ratio of 3.3. Evidently, a hexameric arrangement of *c* subunits in the ring would nicely fit to the thermodynamics calculations. Nevertheless, puzzling inconsistency between  $\text{H}^+/\text{ATP}$  ratios specified by ring sizes and proton translocation rates found *in vivo* was also described for F-ATPases, and is still a matter of debate (discussed in von Ballmoos *et al.*, 2008; Junge *et al.*, 2009). In this regard, one may suppose that a decameric V-ATPase *c* ring can be realized in nature, despite the fact that it does not match the thermodynamic restraint.

It was proposed that intrinsic uncoupling, termed “slipping”, of rotary ATPases might be an explanation for the difference of expected and experimentally determined coupling ratios (Tomashek and Brusilow, 2000). Slipping of the enzymes occurs if either a proton translocation, or an ATP hydrolyzing, step is skipped during the reaction cycle. This is proposed to increase the dynamic control of the enzyme over varying energetic conditions (Tomashek and Brusilow, 2000). Based on this assumption, one can hypothesize that a decameric *c* ring in the *M. sexta* V-ATPase might serve to accommodate changes in the energy status of the midgut membrane system. For V-ATPases in lemon fruit it was proposed that the  $\text{H}^+/\text{ATP}$  stoichiometry may decrease from 2 to 1, on the one hand, in response to an increasing  $\Delta\text{pH}$  (fruit isoform), and on the other hand, with respect to an increasing membrane potential (epicotyl isoform) (Müller and Taiz, 2002). It was presumed that this variability may arise from the ability of these V-ATPases to induce a conformational change within some *c* subunits such that they do no longer contribute to proton translocation.

With regard to the *M. sexta* V-ATPase it might be possible that the  $\text{H}^+/\text{ATP}$  ratio at normal physiological conditions is 2, while a higher coupling ratio is used to counteract or recover a drop in the membrane potential which occurs for example during molting when the V-ATPase dissociates (Sumner *et al.*, 1995). Nevertheless, this would mean that most of the time four *c* subunits are physiologically dispensable which seems to be rather inefficient, and would explicitly contradict tight coupling of the two rotary complexes that is proposed to be realized at least for F-ATPases (Junge *et al.*, 2009). A reliable regulation of the membrane potential, with regard to its importance for the whole midgut transport system, might yet be worth the coupling inefficiency. However, this assumption remains highly speculative and, to draw reliable conclusions, the model of a decameric *c* ring in the *M. sexta* V-ATPase evidently needs further experimental verification. An im-

proved EPR method for distance measurements with spin labeled inhibitors should provide the required accuracy to determine ring sizes, and furthermore, will have the advantage of a non-static system when compared to crystal structures. However, validation of the decameric c ring model would obviously challenge the present concept about the structure-function relationship of the V-ATPases.

## 5. Summary

Archazolid is a novel and highly efficient inhibitor of the V-ATPase, an enzyme currently emerging as a potential therapeutic target to treat severe diseases like cancer or osteoporosis. The intention of the present thesis was to characterize the archazolid binding site within the V-ATPase on the molecular level in order to facilitate archazolid-based drug design in the future.

V-ATPases are ubiquitous membrane energizing protein complexes consisting of a cytosolic ATP-hydrolyzing  $V_1$  domain and a  $V_O$  domain which mediates proton translocation via a membrane embedded ring of c subunits. Each of the c subunits contains a conserved glutamate residue essential for proton transport within the center of its fourth transmembrane helix. Initial labeling experiments with  $^{14}\text{C}$ -derivatives of archazolid and the *M. sexta* V-ATPase clearly identified the c subunit as binding partner for the inhibitor as it had already been presumed from previous studies. Concurrently performed site-directed mutagenesis studies in *S. cerevisiae* revealed that the amino acids tyrosine 142 and leucine 144, located within the fourth transmembrane helix of subunit c, contribute to archazolid binding. Strikingly, mutation of these amino acids to either asparagine or isoleucine resulted in a V-ATPase approximately 10-fold more sensitive to the inhibitor, indicating increased inhibitor-target interaction in both cases. These results were strengthened by cw EPR studies with a spin labeled derivative of archazolid bound to the *S. cerevisiae* V-ATPase which also revealed stronger inhibitor-target interaction in the respective mutant enzymes. Furthermore, the removal of the C-15 hydroxyl group of archazolid impeded the increase in sensitivity upon exchange of tyrosine 142, definitely suggesting close proximity of C-15 and this amino acid.

NCD-4, a fluorescent derivative of DCCD, a covalently binding inhibitor which specifically targets the conserved glutamate, was used to examine the supposed interaction of archazolid with this amino acid residue. In competition assays with NCD-4, archazolid clearly prevented binding of the compound to the *M. sexta* V-ATPase while the established plecomacrolide inhibitors did not. This result inevitably showed that the archazolid binding site comprises the essential glutamate residue. Since the three amino acids tyrosine 142, leucine 144 and glutamate 137 (positions according to the *S. cerevisiae* c subunit) form a triangle within the central part of subunit c, the archazolid binding site most likely resides within a single c subunit. Thus, the archazolid binding site proposed herein is explicitly different from the binding site described for the plecomacrolide V-ATPase inhibitors which intercalate between two c subunits and do not directly interfere with the proton translocation site. In conclusion, this suggests also a different inhibition mechanism of the two inhibitor classes and in this regard, one may presume that only archazolid directly prevents proton translocation by the c ring.

The spin labeled derivative of archazolid was also used to enlighten the stoichiometry of c subunits within the  $V_O$  ring which is, due to a lack of high-resolution structures, still an unsolved secret in V-ATPase research. Provided that each c subunit contains a single inhibitor binding site, distance measurements between the inhibitor molecules enable the calculation of subunit numbers. The measurements, performed via DEER spectroscopy on spin labeled archazolid bound to the *M. sexta* V-ATPase, revealed a clear

distance distribution that suggested, based on the supposed binding site of archazolid, a number between 9 and 11 subunits in the ring. This number is in line with a previously suggested decameric arrangement of the *M. sexta* ring and excludes a hexameric structure which is frequently assumed to be valid for V-ATPases. Current docking studies with archazolid will hopefully reveal a more detailed model for the inhibitor orientation within its target site and thus enable a definite assignment of the *M. sexta* V<sub>O</sub> ring stoichiometry. Due to the highly conserved structure of V-ATPase c subunits and thus conservation of the archazolid binding site, this technique may subsequently be used to enlighten the c ring stoichiometry in other V-ATPases of interest.



## 6. References

- Abrahams, J. P., Leslie, A. G., Lutter, R. and Walker, J. E.** (1994). Structure at 2.8 Å resolution of F<sub>1</sub>-ATPase from bovine heart mitochondria. *Nature* **370**, 621-8.
- Azuma, M., Harvey, W. R. and Wieczorek, H.** (1995). Stoichiometry of K<sup>+</sup>/H<sup>+</sup> antiport helps to explain extracellular pH 11 in a model epithelium. *FEBS Lett* **361**, 153-6.
- Azzi, A., Bragadin, M. A., Neri, G., Farnia, G. and Tamburro, A. M.** (1973). A spin-label carbodiimide as a probe for mitochondrial ATPase. *FEBS Lett* **30**, 249-252.
- Azzi, A., Casey, R. P. and Nalecz, M. J.** (1984). The effect of *N,N*-dicyclohexylcarbodiimide on enzymes of bioenergetic relevance. *Biochim. Biophys. Acta* **768**, 209-26.
- Baldwin, K. M. and Hakim, R. S.** (1991). Growth and differentiation of the larval midgut epithelium during molting in the moth, *Manduca sexta*. *Tissue Cell* **23**, 411-22.
- Bauerle, C., Ho, M. N., Lindorfer, M. A. and Stevens, T. H.** (1993). The *Saccharomyces cerevisiae* VMA6 gene encodes the 36-kDa subunit of the vacuolar H<sup>+</sup>-ATPase membrane sector. *J. Biol. Chem.* **268**, 12749-57.
- Beltran, C. and Nelson, N.** (1992). The membrane sector of vacuolar H<sup>+</sup>-ATPase by itself is impermeable to protons. *Acta. Physiol. Scand. Suppl.* **607**, 41-7.
- Bender, T., Huss, M., Wieczorek, H., Grond, S. and Zezschwitz, P. v.** (2007). Convenient Synthesis of a [1-<sup>14</sup>C]Diazirinybenzoic Acid as a Photoaffinity Label for Binding Studies of V-ATPase Inhibitors. *Eur. J. Org. Chem.* **2007**, 3870-3878.
- Beutler, J. A. and McKee, T. C.** (2003). Novel marine and microbial natural product inhibitors of vacuolar ATPase. *Curr. Med. Chem.* **10**, 787-96.
- Beyenbach, K. W. and Wieczorek, H.** (2006). The V-type H<sup>+</sup> ATPase: molecular structure and function, physiological roles and regulation. *J. Exp. Biol.* **209**, 577-89.
- Bindseil, K. U. and Zeeck, A.** (1994). The chemistry of unusual macrolides, 2. Spectroscopic and biosynthetic investigations of the V-type ATPase inhibitor concanamycin A. *Liebigs Ann. Chem.* **1994**, 305-312.
- Bockelmann, S., Menche, D., Rudolph, S., Bender, T., Grond, S., von Zezschwitz, P., Muench, S. P., Wieczorek, H. and Huss, M.** (2010). Archazolid A binds to the equatorial region of the c-ring of the vacuolar H<sup>+</sup>-ATPase. *J. Biol. Chem.* **285**, 38304-14.
- Böhme, S., Steinhoff, H.-J. and Klare, J. P.** (2010). Accessing the distance range of interest in biomolecules: Site-directed spin labeling and DEER spectroscopy. *Spectroscopy* **24**, 283-288.
- Bowman, B. J. and Bowman, E. J.** (2002). Mutations in subunit c of the vacuolar ATPase confer resistance to bafilomycin and identify a conserved antibiotic binding site. *J. Biol. Chem.* **277**, 3965-72.
- Bowman, B. J., McCall, M. E., Baertsch, R. and Bowman, E. J.** (2006). A model for the proteolipid ring and bafilomycin/concanamycin-binding site in the vacuolar ATPase of *Neurospora crassa*. *J. Biol. Chem.* **281**, 31885-93.
- Bowman, E. J. and Bowman, B. J.** (2005). V-ATPases as drug targets. *J. Bioenerg. Biomembr.* **37**, 431-5.
- Bowman, E. J., Graham, L. A., Stevens, T. H. and Bowman, B. J.** (2004). The bafilomycin/concanamycin binding site in subunit c of the V-ATPases from *Neurospora crassa* and *Saccharomyces cerevisiae*. *J. Biol. Chem.* **279**, 33131-8.

- Bowman, E. J., Gustafson, K. R., Bowman, B. J. and Boyd, M. R.** (2003). Identification of a new chondropsin class of antitumor compound that selectively inhibits V-ATPases. *J. Biol. Chem.* **278**, 44147-52.
- Bowman, E. J., Siebers, A. and Altendorf, K.** (1988). Bafilomycins: a class of inhibitors of membrane ATPases from microorganisms, animal cells, and plant cells. *Proc. Natl. Acad. Sci. USA* **85**, 7972-6.
- Boyd, M. R., Farina, C., Belfiore, P., Gagliardi, S., Kim, J. W., Hayakawa, Y., Beutler, J. A., McKee, T. C., Bowman, B. J. and Bowman, E. J.** (2001). Discovery of a novel antitumor benzolactone enamide class that selectively inhibits mammalian vacuolar-type H<sup>+</sup>-atpases. *J. Pharmacol. Exp. Ther.* **297**, 114-20.
- Boyer, P. D.** (1997). The ATP synthase-a splendid molecular machine. *Annu. Rev. Biochem.* **66**, 717-49.
- Cantrell, C. L., Gustafson, K. R., Cecere, M. R., Pannell, L. K. and Boyd, M. R.** (2000). Chondropsins A and B: Novel Tumor Cell Growth-Inhibitory Macrolide Lactams from the Marine Sponge *Chondropsis* sp. *J. Am. Chem. Soc.* **122**, 8825-8829.
- Chadwick, C. C. and Thomas, E. W.** (1983). Inactivation of sarcoplasmic reticulum (Ca<sup>2+</sup>+Mg<sup>2+</sup>)-ATPase by *N*-cyclohexyl-*N'*-(4-dimethylamino- $\alpha$ -naphthyl)carbodiimide. *Biochim. Biophys. Acta* **730**, 201-6.
- Chadwick, C. C. and Thomas, E. W.** (1985). Inhibition of (Ca<sup>2+</sup> + Mg<sup>2+</sup>)-ATPase by carbodiimides. A structure-activity study. *Biochim. Biophys. Acta* **827**, 419-23.
- Chan, H., Babayan, V., Blyumin, E., Gandhi, C., Hak, K., Harake, D., Kumar, K., Lee, P., Li, T. T., Liu, H. Y. et al.** (2010). The p-type ATPase superfamily. *J. Mol. Microbiol. Biotechnol.* **19**, 5-104.
- Chavez, C., Bowman, E. J., Reidling, J. C., Haw, K. H. and Bowman, B. J.** (2006). Analysis of strains with mutations in six genes encoding subunits of the V-ATPase: eukaryotes differ in the composition of the V<sub>O</sub> sector of the enzyme. *J. Biol. Chem.* **281**, 27052-62.
- Crider, B. P., Xie, X. S. and Stone, D. K.** (1994). Bafilomycin inhibits proton flow through the H<sup>+</sup> channel of vacuolar proton pumps. *J. Biol. Chem.* **269**, 17379-81.
- Demain, A. L. and Fang, A.** (2000). The natural functions of secondary metabolites. *Adv. Biochem. Eng. Biotechnol.* **69**, 1-39.
- Diab, H., Ohira, M., Liu, M., Cobb, E. and Kane, P. M.** (2009). Subunit interactions and requirements for inhibition of the yeast V<sub>1</sub>-ATPase. *J. Biol. Chem.* **284**, 13316-25.
- Diakov, T. T. and Kane, P. M.** (2010). Regulation of vacuolar proton-translocating ATPase activity and assembly by extracellular pH. *J. Biol. Chem.* **285**, 23771-8.
- Diepholz, M., Borsch, M. and Böttcher, B.** (2008). Structural organization of the V-ATPase and its implications for regulatory assembly and disassembly. *Biochem. Soc. Trans.* **36**, 1027-31.
- Dixon, N., Páli, T., Ball, S., Harrison, M. A., Marsh, D., Findlay, J. B. and Kee, T. P.** (2003). New biophysical probes for structure-activity analyses of vacuolar-H<sup>+</sup>-ATPase enzymes. *Org. Biomol. Chem.* **1**, 4361-3.
- Dixon, N., Páli, T., Kee, T. P., Ball, S., Harrison, M. A., Findlay, J. B., Nyman, J., Vaananen, K., Finbow, M. E. and Marsh, D.** (2008). Interaction of spin-labeled inhibitors of the vacuolar H<sup>+</sup>-ATPase with the transmembrane V<sub>O</sub>-sector. *Biophys. J.* **94**, 506-14.
- Dixon, N., Páli, T., Kee, T. P. and Marsh, D.** (2004). Spin-labelled vacuolar-ATPase inhibitors in lipid membranes. *Biochim. Biophys. Acta* **1665**, 177-83.

- Doherty, R. D. and Kane, P. M.** (1993). Partial assembly of the yeast vacuolar H<sup>+</sup>-ATPase in mutants lacking one subunit of the enzyme. *J. Biol. Chem.* **268**, 16845-51.
- Dow, J. A.** (1984). Extremely high pH in biological systems: a model for carbonate transport. *Am. J. Physiol.* **246**, R633-6.
- Drory, O., Frolow, F. and Nelson, N.** (2004). Crystal structure of yeast V-ATPase subunit C reveals its stator function. *EMBO Rep.* **5**, 1148-52.
- Dröse, S. and Altendorf, K.** (1997). Bafilomycins and concanamycins as inhibitors of V-ATPases and P-ATPases. *J. Exp. Biol.* **200**, 1-8.
- Dröse, S., Bindseil, K. U., Bowman, E. J., Siebers, A., Zeeck, A. and Altendorf, K.** (1993). Inhibitory effect of modified bafilomycins and concanamycins on P- and V-type adenosinetriphosphatases. *Biochemistry* **32**, 3902-6.
- Dröse, S., Boddien, C., Gassel, M., Ingenhorst, G., Zeeck, A. and Altendorf, K.** (2001). Semisynthetic derivatives of concanamycin A and C, as inhibitors of V- and P-type ATPases: structure-activity investigations and developments of photoaffinity probes. *Biochemistry* **40**, 2816-25.
- Erickson, K. L., Beutler, J. A., Cardellina, J. H. and Boyd, M. R.** (1997). Salicylhalamides A and B, Novel Cytotoxic Macrolides from the Marine Sponge *Haliclona* sp. *J. Org. Chem.* **62**, 8188-8192.
- Fais, S., De Milito, A., You, H. and Qin, W.** (2007). Targeting vacuolar H<sup>+</sup>-ATPases as a new strategy against cancer. *Cancer Res.* **67**, 10627-30.
- Fares, C., Hassfeld, J., Menche, D. and Carlomagno, T.** (2008). Simultaneous determination of the conformation and relative configuration of archazolide a by using nuclear overhauser effects, J couplings, and residual dipolar couplings. *Angew. Chem. Int. Ed. Engl.* **47**, 3722-6.
- Fillingame, R. H. and Dmitriev, O. Y.** (2002). Structural model of the transmembrane F<sub>0</sub> rotary sector of H<sup>+</sup>-transporting ATP synthase derived by solution NMR and intersubunit cross-linking in situ. *Biochim. Biophys. Acta* **1565**, 232-45.
- Finbow, M. E., Eliopoulos, E. E., Jackson, P. J., Keen, J. N., Meagher, L., Thompson, P., Jones, P. and Findlay, J. B.** (1992). Structure of a 16 kDa integral membrane protein that has identity to the putative proton channel of the vacuolar H<sup>+</sup>-ATPase. *Protein Eng.* **5**, 7-15.
- Forgac, M.** (2007). Vacuolar ATPases: rotary proton pumps in physiology and pathophysiology. *Nat. Rev. Mol. Cell Biol.* **8**, 917-29.
- Frattoni, A., Orchard, P. J., Sobacchi, C., Giliani, S., Abinun, M., Mattsson, J. P., Keeling, D. J., Andersson, A. K., Wallbrandt, P., Zecca, L. et al.** (2000). Defects in TCIRG1 subunit of the vacuolar proton pump are responsible for a subset of human autosomal recessive osteopetrosis. *Nat. Genet.* **25**, 343-6.
- Gagliardi, S., Gatti, P. A., Belfiore, P., Zocchetti, A., Clarke, G. D. and Farina, C.** (1998a). Synthesis and structure-activity relationships of bafilomycin A1 derivatives as inhibitors of vacuolar H<sup>+</sup>-ATPase. *J. Med. Chem.* **41**, 1883-93.
- Gagliardi, S., Nadler, G., Consolandi, E., Parini, C., Morvan, M., Legave, M. N., Belfiore, P., Zocchetti, A., Clarke, G. D., James, I. et al.** (1998b). 5-(5,6-Dichloro-2-indolyl)-2-methoxy-2,4-pentadienamides: novel and selective inhibitors of the vacuolar H<sup>+</sup>-ATPase of osteoclasts with bone antiresorptive activity. *J. Med. Chem.* **41**, 1568-73.
- Gagliardi, S., Rees, M. and Farina, C.** (1999). Chemistry and structure activity relationships of bafilomycin A1, a potent and selective inhibitor of the vacuolar H<sup>+</sup>-ATPase. *Curr. Med. Chem.* **6**, 1197-212.
- Galinis, D. L., McKee, T. C., Pannell, L. K., Cardellina, J. H. and Boyd, M. R.** (1997). Lobatamides A and B, Novel Cytotoxic Macrolides from the Tunicate *Aplidium lobatum*. *J. Org. Chem.* **62**, 8968-8969.

- Gräf, R., Harvey, W. R. and Wieczorek, H.** (1996). Purification and properties of a cytosolic V<sub>1</sub>-ATPase. *J. Biol. Chem.* **271**, 20908-13.
- Green, R. C., Thumser, A. E., Povey, D., Saldanha, J. W., Potter, B. S., Palmer, R. A. and Howlin, B. J.** (2009). A comparative study of the single crystal X-ray determination and molecular modelling of the binding of oligomycin to ATP synthase. *Comput. Biol. Chem.* **33**, 189-95.
- Gregorini, M., Wang, J., Xie, X. S., Milligan, R. A. and Engel, A.** (2007). Three-dimensional reconstruction of bovine brain V-ATPase by cryo-electron microscopy and single particle analysis. *J. Struct. Biol.* **158**, 445-54.
- Grüber, G. and Marshansky, V.** (2008). New insights into structure-function relationships between archeal ATP synthase (A<sub>1</sub>A<sub>0</sub>) and vacuolar type ATPase (V<sub>1</sub>V<sub>0</sub>). *Bioessays* **30**, 1096-109.
- Hanada, H., Moriyama, Y., Maeda, M. and Futai, M.** (1990). Kinetic studies of chromaffin granule H<sup>+</sup>-ATPase and effects of bafilomycin A1. *Biochem. Biophys. Res. Commun.* **170**, 873-8.
- Hanahan, D.** (1983). Studies on transformation of *Escherichia coli* with plasmids. *J. Mol. Biol.* **166**, 557-80.
- Harrison, M., Powell, B., Finbow, M. E. and Findlay, J. B.** (2000). Identification of lipid-accessible sites on the *nephrops* 16-kDa proteolipid incorporated into a hybrid vacuolar H<sup>+</sup>-ATPase: site-directed labeling with *N*-(1-Pyrenyl)cyclohexylcarbodiimide and fluorescence quenching analysis. *Biochemistry* **39**, 7531-7.
- Harrison, M. A., Jones, P. C., Kim, Y. I., Finbow, M. E. and Findlay, J. B.** (1994). Functional properties of a hybrid vacuolar H<sup>+</sup>-ATPase in *Saccharomyces* cells expressing the *Nephrops* 16-kDa proteolipid. *Eur. J. Biochem.* **221**, 111-20.
- Harvey, W. R., Maddrell, S. H. P., Telfer, W. H. and Wieczorek, H.** (1998). H<sup>+</sup> V-ATPases Energize Animal Plasma Membranes for Secretion and Absorption of Ions and Fluids. *Amer. Zool.* **38**, 426-441.
- Harvey, W. R. and Wieczorek, H.** (1997). Animal plasma membrane energization by chemiosmotic H<sup>+</sup> V-ATPases. *J. Exp. Biol.* **200**, 203-16.
- Hassfeld, J., Fares, C., Steinmetz, H., Carlomagno, T. and Menche, D.** (2006). Stereochemical determination of Archazolid A and B, highly potent vacuolar-type ATPase inhibitors from the Myxobacterium *Archangium gephyra*. *Org. Lett.* **8**, 4751-4.
- Hennigan, B. B., Wolfersberger, M. G., Parthasarathy, R. and Harvey, W. R.** (1993). Cation-dependent leucine, alanine, and phenylalanine uptake at pH 10 in brush-border membrane vesicles from larval *Manduca sexta* midgut. *Biochim. Biophys. Acta* **1148**, 209-15.
- Hinton, A., Bond, S. and Forgac, M.** (2009). V-ATPase functions in normal and disease processes. *Pflugers Arch.* **457**, 589-98.
- Hirata, R., Graham, L. A., Takatsuki, A., Stevens, T. H. and Anraku, Y.** (1997). VMA11 and VMA16 encode second and third proteolipid subunits of the *Saccharomyces cerevisiae* vacuolar membrane H<sup>+</sup>-ATPase. *J. Biol. Chem.* **272**, 4795-803.
- Hirata, R., Umemoto, N., Ho, M. N., Ohya, Y., Stevens, T. H. and Anraku, Y.** (1993). VMA12 is essential for assembly of the vacuolar H<sup>+</sup>-ATPase subunits onto the vacuolar membrane in *Saccharomyces cerevisiae*. *J. Biol. Chem.* **268**, 961-7.
- Ho, M. N., Hill, K. J., Lindorfer, M. A. and Stevens, T. H.** (1993). Isolation of vacuolar membrane H<sup>+</sup>-ATPase-deficient yeast mutants; the VMA5 and VMA4 genes are essential for assembly and activity of the vacuolar H<sup>+</sup>-ATPase. *J. Biol. Chem.* **268**, 221-7.

- Hong, J., Ishihara, K., Zee, O. and Ohuchi, K.** (2005a). Induction of apoptosis by apicularen A in human promyelocytic leukemia cell line HL-60. *Planta Med.* **71**, 306-12.
- Hong, J., Sasaki, H., Niikura, K., Yanai, M., Nakano, Y., Yokomakura, A., Ishihara, K., Hirasawa, N., Kang, Y. S., Oh, J. S. et al.** (2007). Inhibition of bone resorption in cultures of mouse calvariae by apicularen A. *Planta Med.* **73**, 173-5.
- Hong, J., Yamaki, K., Ishihara, K., Ahn, J. W., Zee, O. and Ohuchi, K.** (2003). Induction of apoptosis of RAW 264.7 cells by the cytostatic macrolide apicularen A. *J. Pharm. Pharmacol.* **55**, 1299-306.
- Hong, J., Yokomakura, A., Nakano, Y., Ban, H. S., Ishihara, K., Ahn, J. W., Zee, O. and Ohuchi, K.** (2005b). Induction of nitric oxide production by the cytostatic macrolide apicularen A [2,4-heptadienamido, N-[(1E)-3-[(3S,5R,7R,9S)-3,4,5,6,7,8,9,10-octahydro-7,14-dihydroxy-1-oxo-5,9-epoxy-1H-2-benzoxacyclododecin-3-yl]-1-propenyl]-, (2Z,4Z)-(9CI)] and possible role of nitric oxide in apicularen A-induced apoptosis in RAW 264.7 cells. *J. Pharmacol. Exp. Ther.* **312**, 968-77.
- Hong, J., Yokomakura, A., Nakano, Y., Ishihara, K., Kaneda, M., Onodera, M., Nakahama, K., Morita, I., Niikura, K., Ahn, J. W. et al.** (2006). Inhibition of vacuolar-type H<sup>+</sup>-ATPase by the cytostatic macrolide apicularen A and its role in apicularen A-induced apoptosis in RAW 264.7 cells. *FEBS Lett* **580**, 2723-30.
- Horstmann, N., Essig, S., Bockelmann, S., Wieczorek, H., Huss, M., Sasse, F. and Menche, D.** (2011). Archazolid A-15-O- $\beta$ -D-glucopyranoside and iso-Archazolid B: Potent V-ATPase Inhibitory Polyketides from the Myxobacteria *Cystobacter violaceus* and *Archangium gephyra*. *J. Nat. Prod.* **74**, 1100-1105.
- Huss, M., Ingenhorst, G., König, S., Gassel, M., Dröse, S., Zeeck, A., Altendorf, K. and Wieczorek, H.** (2002). Concanamycin A, the specific inhibitor of V-ATPases, binds to the V<sub>O</sub> subunit c. *J. Biol. Chem.* **277**, 40544-8.
- Huss, M., Sasse, F., Kunze, B., Jansen, R., Steinmetz, H., Ingenhorst, G., Zeeck, A. and Wieczorek, H.** (2005). Archazolid and apicularen: novel specific V-ATPase inhibitors. *BMC Biochem.* **6**, 13.
- Huss, M. and Wieczorek, H.** (2007). Influence of ATP and ADP on dissociation of the V-ATPase into its V<sub>1</sub> and V<sub>O</sub> complexes. *FEBS Lett.* **581**, 5566-72.
- Huss, M. and Wieczorek, H.** (2009). Inhibitors of V-ATPases: old and new players. *J. Exp. Biol.* **212**, 341-6.
- Ikeda, M., Hinohara, M., Umami, K., Taguro, Y., Okada, Y., Wada, Y., Nakanishi, Y. and Maeshima, M.** (2001). Expression of V-ATPase proteolipid subunit of *Acetabularia acetabulum* in a VMA3-deficient strain of *Saccharomyces cerevisiae* and its complementation study. *Eur. J. Biochem.* **268**, 6097-104.
- Imamura, H., Nakano, M., Noji, H., Muneyuki, E., Ohkuma, S., Yoshida, M. and Yokoyama, K.** (2003). Evidence for rotation of V<sub>1</sub>-ATPase. *Proc. Natl. Acad. Sci. USA* **100**, 2312-5.
- Iwata, M., Imamura, H., Stambouli, E., Ikeda, C., Tamakoshi, M., Nagata, K., Makyio, H., Hankamer, B., Barber, J., Yoshida, M. et al.** (2004). Crystal structure of a central stalk subunit C and reversible association/dissociation of vacuole-type ATPase. *Proc. Natl. Acad. Sci. USA* **101**, 59-64.
- Jefferies, K. C. and Forgac, M.** (2008). Subunit H of the vacuolar H<sup>+</sup> ATPase inhibits ATP hydrolysis by the free V<sub>1</sub> domain by interaction with the rotary subunit F. *J. Biol. Chem.* **283**, 4512-9.
- Jeschke, G., Chechik, V., Ionita, P., Godt, A., Zimmermann, H., Banham, J., Timmel, C., Hilger, D. and Jung, H.** (2006). DeerAnalysis2006 - a comprehensive software package for analyzing pulsed ELDOR data. *Appl. Magn. Reson.* **30**, 473-498.

**Junge, W. and Nelson, N.** (2005). Structural biology. Nature's rotary electromotors. *Science* **308**, 642-4.

**Junge, W., Sielaff, H. and Engelbrecht, S.** (2009). Torque generation and elastic power transmission in the rotary  $F_0F_1$ -ATPase. *Nature* **459**, 364-70.

**Kane, P. M.** (1995). Disassembly and reassembly of the yeast vacuolar  $H^+$ -ATPase in vivo. *J. Biol. Chem.* **270**, 17025-32.

**Kane, P. M.** (2006). The where, when, and how of organelle acidification by the yeast vacuolar  $H^+$ -ATPase. *Microbiol. Mol. Biol. Rev.* **70**, 177-91.

**Karet, F. E., Finberg, K. E., Nelson, R. D., Nayir, A., Mocan, H., Sanjad, S. A., Rodriguez-Soriano, J., Santos, F., Cremers, C. W., Di Pietro, A. et al.** (1999). Mutations in the gene encoding B1 subunit of  $H^+$ -ATPase cause renal tubular acidosis with sensorineural deafness. *Nat. Genet.* **21**, 84-90.

**Kawasaki-Nishi, S., Nishi, T. and Forgac, M.** (2001). Arg-735 of the 100-kDa subunit a of the yeast V-ATPase is essential for proton translocation. *Proc. Natl. Acad. Sci. USA* **98**, 12397-402.

**Keeling, D. J., Herslof, M., Ryberg, B., Sjogren, S. and Solvell, L.** (1997). Vacuolar  $H^+$ -ATPases. Targets for drug discovery? *Ann. NY Acad. Sci.* **834**, 600-8.

**Kim, J. S., Lee, Y. C., Nam, H. T., Li, G., Yun, E. J., Song, K. S., Seo, K. S., Park, J. H., Ahn, J. W., Zee, O. et al.** (2007). Apicularen A induces cell death through Fas ligand up-regulation and microtubule disruption by tubulin down-regulation in HM7 human colon cancer cells. *Clin. Cancer Res.* **13**, 6509-17.

**Kitagawa, N., Mazon, H., Heck, A. J. and Wilkens, S.** (2008). Stoichiometry of the peripheral stalk subunits E and G of yeast  $V_1$ -ATPase determined by mass spectrometry. *J. Biol. Chem.* **283**, 3329-37.

**Klare, J. P. and Steinhoff, H.-J.** (2010). Site-directed Spin Labeling and Pulse Dipolar Electron Paramagnetic Resonance: Encyclopedia of Analytical Chemistry, John Wiley & Sons, Ltd.

**Klare, J. P. and Steinhoff, H. J.** (2009). Spin labeling EPR. *Photosynth. Res.* **102**, 377-90.

**Klionsky, D. J., Herman, P. K. and Emr, S. D.** (1990). The fungal vacuole: composition, function, and biogenesis. *Microbiol. Rev.* **54**, 266-92.

**Kühlbrandt, W.** (2004). Biology, structure and mechanism of P-type ATPases. *Nat. Rev. Mol. Cell Biol.* **5**, 282-95.

**Kunze, B., Jansen, R., Sasse, F., Hofle, G. and Reichenbach, H.** (1998). Apicularens A and B, new cytostatic macrolides from *Chondromyces* species (myxobacteria): production, physico-chemical and biological properties. *J. Antibiot. (Tokyo)* **51**, 1075-80.

**Kyhse-Andersen, J.** (1984). Electrophotting of multiple gels: a simple apparatus without buffer tank for rapid transfer of proteins from polyacrylamide to nitrocellulose. *J. Biochem. Biophys. Methods* **10**, 203-9.

**Laemmli, U. K.** (1970). Cleavage of structural proteins during the assembly of the head of bacteriophage T4. *Nature* **227**, 680-5.

**Lau, W. C. and Rubinstein, J. L.** (2010). Structure of intact *Thermus thermophilus* V-ATPase by cryo-EM reveals organization of the membrane-bound  $V_0$  motor. *Proc. Natl. Acad. Sci. USA* **107**, 1367-72.

**Lu, M., Sautin, Y. Y., Holliday, L. S. and Gluck, S. L.** (2004). The glycolytic enzyme aldolase mediates assembly, expression, and activity of vacuolar  $H^+$ -ATPase. *J. Biol. Chem.* **279**, 8732-9.

**Ludwig, J., Kerscher, S., Brandt, U., Pfeiffer, K., Getlawi, F., Apps, D. K. and Schagger, H.** (1998). Identification and characterization of a novel 9.2-kDa membrane

sector-associated protein of vacuolar proton-ATPase from chromaffin granules. *J. Biol. Chem.* **273**, 10939-47.

**Mandel, M., Moriyama, Y., Hulmes, J. D., Pan, Y. C., Nelson, H. and Nelson, N.** (1988). cDNA sequence encoding the 16-kDa proteolipid of chromaffin granules implies gene duplication in the evolution of H<sup>+</sup>-ATPases. *Proc. Natl. Acad. Sci. USA* **85**, 5521-4.

**Martin, R. E., Pannier, M., Diederich, F., Gramlich, V., Hubrich, M. and Spiess, H. W.** (1998). Determination of End-to-End Distances in a Series of TEMPO Diradicals of up to 2.8 nm Length with a New Four-Pulse Double Electron Electron Resonance Experiment. *Angew. Chem. Int. Edit.* **37**, 2833-2837.

**Meier, T., Ferguson, S. A., Cook, G. M., Dimroth, P. and Vonck, J.** (2006). Structural investigations of the membrane-embedded rotor ring of the F-ATPase from *Clostridium paradoxum*. *J. Bacteriol.* **188**, 7759-64.

**Meier, T., Polzer, P., Diederichs, K., Welte, W. and Dimroth, P.** (2005). Structure of the rotor ring of F-Type Na<sup>+</sup>-ATPase from *Ilyobacter tartaricus*. *Science* **308**, 659-62.

**Menche, D., Hassfeld, J., Li, J. and Rudolph, S.** (2007a). Total synthesis of archazolid A. *J. Am. Chem. Soc.* **129**, 6100-1.

**Menche, D., Hassfeld, J., Sasse, F., Huss, M. and Wieczorek, H.** (2007b). Design, synthesis, and biological evaluation of novel analogues of archazolid: a highly potent simplified V-ATPase inhibitor. *Bioorg. Med. Chem. Lett.* **17**, 1732-5.

**Menche, D., Hassfeld, J., Steinmetz, H., Huss, M., Wieczorek, H. and Sasse, F.** (2007c). Archazolid-7-O-β-D-glucopyranoside - Isolation, Structural Elucidation and Solution Conformation of a Novel V-ATPase Inhibitor from the Myxobacterium *Cystobacter violaceus*. *Eur. J. Org. Chem.* **2007**, 1196-1202.

**Menche, D., Hassfeld, J., Steinmetz, H., Huss, M., Wieczorek, H. and Sasse, F.** (2007d). The first hydroxylated archazolid from the myxobacterium *Cystobacter violaceus*: isolation, structural elucidation and V-ATPase inhibition. *J. Antibiot. (Tokyo)* **60**, 328-31.

**Merzendorfer, H., Huss, M., Schmid, R., Harvey, W. R. and Wieczorek, H.** (1999). A novel insect V-ATPase subunit M9.7 is glycosylated extensively. *J. Biol. Chem.* **274**, 17372-8.

**Merzendorfer, H., Reineke, S., Zhao, X. F., Jacobmeier, B., Harvey, W. R. and Wieczorek, H.** (2000). The multigene family of the tobacco hornworm V-ATPase: novel subunits a, C, D, H, and putative isoforms. *Biochim. Biophys. Acta* **1467**, 369-79.

**Miseta, A., Kellermayer, R., Aiello, D. P., Fu, L. and Bedwell, D. M.** (1999). The vacuolar Ca<sup>2+</sup>/H<sup>+</sup> exchanger Vcx1p/Hum1p tightly controls cytosolic Ca<sup>2+</sup> levels in *S. cerevisiae*. *FEBS Lett.* **451**, 132-6.

**Morth, J. P., Pedersen, B. P., Toustrup-Jensen, M. S., Sorensen, T. L., Petersen, J., Andersen, J. P., Vilsen, B. and Nissen, P.** (2007). Crystal structure of the sodium-potassium pump. *Nature* **450**, 1043-9.

**Muench, S. P., Huss, M., Song, C. F., Phillips, C., Wieczorek, H., Trinick, J. and Harrison, M. A.** (2009). Cryo-electron microscopy of the vacuolar ATPase motor reveals its mechanical and regulatory complexity. *J. Mol. Biol.* **386**, 989-99.

**Muench, S. P., Trinick, J. and Harrison, M. A.** (2011). Structural divergence of the rotary ATPases. *Q. Rev. Biophys.*, 1-46.

**Mulkidjanian, A. Y., Makarova, K. S., Galperin, M. Y. and Koonin, E. V.** (2007). Inventing the dynamo machine: the evolution of the F-type and V-type ATPases. *Nat. Rev. Microbiol.* **5**, 892-9.

- Müller, M. L. and Taiz, L. (2002). Regulation of the lemon-fruit V-ATPase by variable stoichiometry and organic acids. *J. Membr. Biol.* **185**, 209-20.
- Müller, V. and Grüber, G. (2003). ATP synthases: structure, function and evolution of unique energy converters. *Cell Mol. Life Sci.* **60**, 474-94.
- Munn, A. L. and Riezman, H. (1994). Endocytosis is required for the growth of vacuolar H<sup>+</sup>-ATPase-defective yeast: identification of six new END genes. *J. Cell. Biol.* **127**, 373-86.
- Murata, T., Yamato, I., Kakinuma, Y., Leslie, A. G. and Walker, J. E. (2005). Structure of the rotor of the V-Type Na<sup>+</sup>-ATPase from *Enterococcus hirae*. *Science* **308**, 654-9.
- Muroi, M., Shiragami, N. and Takatsuki, A. (1994). Destruxin B, a specific and readily reversible inhibitor of vacuolar-type H<sup>+</sup>-translocating ATPase. *Biochem. Biophys. Res. Commun.* **205**, 1358-65.
- Nadler, G., Morvan, M., Delimoge, I., Belfiore, P., Zocchetti, A., James, I., Zembryki, D., Lee-Rycakzewski, E., Parini, C., Consolandi, E. *et al.* (1998). (2Z,4E)-5-(5,6-dichloro-2-indolyl)-2-methoxy-N-(1,2,2,6,6-pentamethylpiperidin-4-yl)-2,4-pentadienamide, a novel, potent and selective inhibitor of the osteoclast V-ATPase. *Bioorg. Med. Chem. Lett.* **8**, 3621-6.
- Nelson, H. and Nelson, N. (1990). Disruption of genes encoding subunits of yeast vacuolar H<sup>+</sup>-ATPase causes conditional lethality. *Proc. Natl. Acad. Sci. USA* **87**, 3503-7.
- Niikura, K. (2006). Vacuolar ATPase as a drug discovery target. *Drug News Perspect.* **19**, 139-44.
- Nishi, T., Kawasaki-Nishi, S. and Forgac, M. (2003). The first putative transmembrane segment of subunit c" (Vma16p) of the yeast V-ATPase is not necessary for function. *J. Biol. Chem.* **278**, 5821-7.
- Noumi, T., Beltran, C., Nelson, H. and Nelson, N. (1991). Mutational analysis of yeast vacuolar H<sup>+</sup>-ATPase. *Proc. Natl. Acad. Sci. USA* **88**, 1938-42.
- Ohya, Y., Umemoto, N., Tanida, I., Ohta, A., Iida, H. and Anraku, Y. (1991). Calcium-sensitive cls mutants of *Saccharomyces cerevisiae* showing a Pet<sup>-</sup> phenotype are ascribable to defects of vacuolar membrane H<sup>+</sup>-ATPase activity. *J. Biol. Chem.* **266**, 13971-7.
- Páli, T., Dixon, N., Kee, T. P. and Marsh, D. (2004a). Incorporation of the V-ATPase inhibitors concanamycin and indole pentadiene in lipid membranes. Spin-label EPR studies. *Biochim. Biophys. Acta* **1663**, 14-8.
- Páli, T., Finbow, M. E., Holzenburg, A., Findlay, J. B. and Marsh, D. (1995). Lipid-protein interactions and assembly of the 16-kDa channel polypeptide from *Nephrops norvegicus*. Studies with spin-label electron spin resonance spectroscopy and electron microscopy. *Biochemistry* **34**, 9211-8.
- Páli, T., Finbow, M. E. and Marsh, D. (1999). Membrane assembly of the 16-kDa proteolipid channel from *Nephrops norvegicus* studied by relaxation enhancements in spin-label ESR. *Biochemistry* **38**, 14311-9.
- Páli, T., Whiteside, G., Dixon, N., Kee, T. P., Ball, S., Harrison, M. A., Findlay, J. B., Finbow, M. E. and Marsh, D. (2004b). Interaction of inhibitors of the vacuolar H<sup>+</sup>-ATPase with the transmembrane V<sub>O</sub>-sector. *Biochemistry* **43**, 12297-305.
- Pannier, M., Veit, S., Godt, A., Jeschke, G. and Spiess, H. W. (2000). Dead-time free measurement of dipole-dipole interactions between electron spins. *J. Magn. Reson.* **142**, 331-40.
- Parra, K. J., Keenan, K. L. and Kane, P. M. (2000). The H subunit (Vma13p) of the yeast V-ATPase inhibits the ATPase activity of cytosolic V<sub>1</sub> complexes. *J. Biol. Chem.* **275**, 21761-7.



- Plant, P. J., Manolson, M. F., Grinstein, S. and Demaurex, N.** (1999). Alternative mechanisms of vacuolar acidification in H<sup>+</sup>-ATPase-deficient yeast. *J. Biol. Chem.* **274**, 37270-9.
- Pogoryelov, D., Yildiz, O., Faraldo-Gomez, J. D. and Meier, T.** (2009). High-resolution structure of the rotor ring of a proton-dependent ATP synthase. *Nat. Struct. Mol. Biol.* **16**, 1068-73.
- Powell, B., Graham, L. A. and Stevens, T. H.** (2000). Molecular characterization of the yeast vacuolar H<sup>+</sup>-ATPase proton pore. *J. Biol. Chem.* **275**, 23654-60.
- Radermacher, M., Ruiz, T., Wieczorek, H. and Grüber, G.** (2001). The structure of the V<sub>1</sub>-ATPase determined by three-dimensional electron microscopy of single particles. *J. Struct. Biol.* **135**, 26-37.
- Rashid, M. A., Cantrell, C. L., Gustafson, K. R. and Boyd, M. R.** (2001). Chondropsin D, a new 37-membered-ring macrolide lactam from the marine sponge *Chondropsis* species. *J. Nat. Prod.* **64**, 1341-4.
- Rautiala, T. J., Koskinen, A. M. and Vaananen, H. K.** (1993). Purification of vacuolar ATPase with bafilomycin C1 affinity chromatography. *Biochem. Biophys. Res. Commun.* **194**, 50-6.
- Roberts, C. J., Raymond, C. K., Yamashiro, C. T. and Stevens, T. H.** (1991). Methods for studying the yeast vacuole. *Methods. Enzymol.* **194**, 644-61.
- Sagermann, M., Stevens, T. H. and Matthews, B. W.** (2001). Crystal structure of the regulatory subunit H of the V-type ATPase of *Saccharomyces cerevisiae*. *Proc. Natl. Acad. Sci. USA* **98**, 7134-9.
- Sambade, M. and Kane, P. M.** (2004). The yeast vacuolar proton-translocating ATPase contains a subunit homologous to the *Manduca sexta* and bovine e subunits that is essential for function. *J. Biol. Chem.* **279**, 17361-5.
- Sasse, F., Steinmetz, H., Hofle, G. and Reichenbach, H.** (2003). Archazolids, new cytotoxic macrolactones from *Archangium gephyra* (Myxobacteria). Production, isolation, physico-chemical and biological properties. *J. Antibiot. (Tokyo)* **56**, 520-5.
- Schweikl, H., Klein, U., Schindlbeck, M. and Wieczorek, H.** (1989). A vacuolar-type ATPase, partially purified from potassium transporting plasma membranes of tobacco hornworm midgut. *J. Biol. Chem.* **264**, 11136-42.
- Sennoune, S. R., Bakunts, K., Martinez, G. M., Chua-Tuan, J. L., Kebir, Y., Attaya, M. N. and Martinez-Zaguilan, R.** (2004). Vacuolar H<sup>+</sup>-ATPase in human breast cancer cells with distinct metastatic potential: distribution and functional activity. *Am. J. Physiol. Cell Physiol.* **286**, C1443-52.
- Sennoune, S. R. and Martinez-Zaguilan, R.** (2007). Plasmalemmal vacuolar H<sup>+</sup>-ATPases in angiogenesis, diabetes and cancer. *J. Bioenerg. Biomembr.* **39**, 427-33.
- Smardon, A. M., Tarsio, M. and Kane, P. M.** (2002). The RAVE complex is essential for stable assembly of the yeast V-ATPase. *J. Biol. Chem.* **277**, 13831-9.
- Smith, A. N., Skaug, J., Choate, K. A., Nayir, A., Bakkaloglu, A., Ozen, S., Hulton, S. A., Sanjad, S. A., Al-Sabban, E. A., Lifton, R. P. et al.** (2000). Mutations in ATP6N1B, encoding a new kidney vacuolar proton pump 116-kD subunit, cause recessive distal renal tubular acidosis with preserved hearing. *Nat. Genet.* **26**, 71-5.
- Sørensen, M. G., Henriksen, K., Neutzsky-Wulff, A. V., Dziegiel, M. H. and Karsdal, M. A.** (2007). Diphyllin, a novel and naturally potent V-ATPase inhibitor, abrogates acidification of the osteoclastic resorption lacunae and bone resorption. *J. Bone Miner. Res.* **22**, 1640-8.
- Stock, D., Gibbons, C., Arechaga, I., Leslie, A. G. and Walker, J. E.** (2000). The rotary mechanism of ATP synthase. *Curr. Opin. Struct. Biol.* **10**, 672-9.

**Sumner, J. P., Dow, J. A., Earley, F. G., Klein, U., Jager, D. and Wieczorek, H.** (1995). Regulation of plasma membrane V-ATPase activity by dissociation of peripheral subunits. *J. Biol. Chem.* **270**, 5649-53.

**Supek, F., Supekova, L., Mandiyan, S., Pan, Y. C., Nelson, H. and Nelson, N.** (1994). A novel accessory subunit for vacuolar H<sup>+</sup>-ATPase from chromaffin granules. *J. Biol. Chem.* **269**, 24102-6.

**Toei, M., Saum, R. and Forgac, M.** (2010). Regulation and isoform function of the V-ATPases. *Biochemistry* **49**, 4715-23.

**Tomashek, J. J. and Brusilow, W. S.** (2000). Stoichiometry of energy coupling by proton-translocating ATPases: a history of variability. *J. Bioenerg. Biomembr.* **32**, 493-500.

**Towbin, H., Staehelin, T. and Gordon, J.** (1979). Electrophoretic transfer of proteins from polyacrylamide gels to nitrocellulose sheets: procedure and some applications. *Proc. Natl. Acad. Sci. USA* **76**, 4350-4.

**Uchida, E., Ohsumi, Y. and Anraku, Y.** (1985). Purification and properties of H<sup>+</sup>-translocating, Mg<sup>2+</sup>-adenosine triphosphatase from vacuolar membranes of *Saccharomyces cerevisiae*. *J. Biol. Chem.* **260**, 1090-5.

**Umemoto, N., Ohya, Y. and Anraku, Y.** (1991). VMA11, a novel gene that encodes a putative proteolipid, is indispensable for expression of yeast vacuolar membrane H<sup>+</sup>-ATPase activity. *J. Biol. Chem.* **266**, 24526-32.

**Vazquez, M. J., Albarran, M. I., Espada, A., Rivera-Sagredo, A., Diez, E. and Hueso-Rodriguez, J. A.** (2005). A new destruxin as inhibitor of vacuolar-type H<sup>+</sup>-ATPase of *Saccharomyces cerevisiae*. *Chem. Biodivers.* **2**, 123-30.

**Venzke, D., Domgall, I., Kocher, T., Fethiere, J., Fischer, S. and Bottcher, B.** (2005). Elucidation of the stator organization in the V-ATPase of *Neurospora crassa*. *J. Mol. Biol.* **349**, 659-69.

**Visentin, L., Dodds, R. A., Valente, M., Misiano, P., Bradbeer, J. N., Oneta, S., Liang, X., Gowen, M. and Farina, C.** (2000). A selective inhibitor of the osteoclastic V-H<sup>+</sup>-ATPase prevents bone loss in both thyroparathyroidectomized and ovariectomized rats. *J. Clin. Invest.* **106**, 309-18.

**Vitavska, O., Merzendorfer, H. and Wieczorek, H.** (2005). The V-ATPase subunit C binds to polymeric F-actin as well as to monomeric G-actin and induces cross-linking of actin filaments. *J. Biol. Chem.* **280**, 1070-6.

**Vitavska, O., Wieczorek, H. and Merzendorfer, H.** (2003). A novel role for subunit C in mediating binding of the H<sup>+</sup>-V-ATPase to the actin cytoskeleton. *J. Biol. Chem.* **278**, 18499-505.

**Vollmar, M., Schlieper, D., Winn, M., Buchner, C. and Groth, G.** (2009). Structure of the c14 rotor ring of the proton translocating chloroplast ATP synthase. *J. Biol. Chem.* **284**, 18228-35.

**von Ballmoos, C., Cook, G. M. and Dimroth, P.** (2008). Unique rotary ATP synthase and its biological diversity. *Annu. Rev. Biophys.* **37**, 43-64.

**Voss, M., Vitavska, O., Walz, B., Wieczorek, H. and Baumann, O.** (2007). Stimulus-induced phosphorylation of vacuolar H<sup>+</sup>-ATPase by protein kinase A. *J. Biol. Chem.* **282**, 33735-42.

**Wagner, C. A., Finberg, K. E., Breton, S., Marshansky, V., Brown, D. and Geibel, J. P.** (2004). Renal vacuolar H<sup>+</sup>-ATPase. *Physiol. Rev.* **84**, 1263-314.

**Wang, Y., Cipriano, D. J. and Forgac, M.** (2007). Arrangement of subunits in the proteolipid ring of the V-ATPase. *J. Biol. Chem.* **282**, 34058-65.

**Wang, Y., Inoue, T. and Forgac, M.** (2005). Subunit a of the yeast V-ATPase participates in binding of bafilomycin. *J. Biol. Chem.* **280**, 40481-8.

**Wang, Y., Toei, M. and Forgac, M.** (2008). Analysis of the membrane topology of transmembrane segments in the C-terminal hydrophobic domain of the yeast vacuolar ATPase subunit a (Vph1p) by chemical modification. *J. Biol. Chem.* **283**, 20696-702.

**Wieczorek, H., Cioffi, M., Klein, U., Harvey, W. R., Schweikl, H. and Wolfersberger, M. G.** (1990). Isolation of goblet cell apical membrane from tobacco hornworm midgut and purification of its vacuolar-type ATPase. *Methods. Enzymol.* **192**, 608-16.

**Wieczorek, H., Grüber, G., Harvey, W. R., Huss, M., Merzendorfer, H. and Zeiske, W.** (2000). Structure and regulation of insect plasma membrane H<sup>+</sup> V-ATPase. *J. Exp. Biol.* **203**, 127-35.

**Wieczorek, H., Putzenlechner, M., Zeiske, W. and Klein, U.** (1991). A vacuolar-type proton pump energizes K<sup>+</sup>/H<sup>+</sup> antiport in an animal plasma membrane. *J. Biol. Chem.* **266**, 15340-7.

**Wieczorek, H., Weerth, S., Schindlbeck, M. and Klein, U.** (1989). A vacuolar-type proton pump in a vesicle fraction enriched with potassium transporting plasma membranes from tobacco hornworm midgut. *J. Biol. Chem.* **264**, 11143-8.

**Wieczorek, H., Wolfersberger, M. G., Cioffi, M. and Harvey, W. R.** (1986). Cation-stimulated ATPase activity in purified plasma membranes from tobacco hornworm midgut. *Biochim. Biophys. Acta* **857**, 271-81.

**Wilkins, S., Zhang, Z. and Zheng, Y.** (2005). A structural model of the vacuolar ATPase from transmission electron microscopy. *Micron* **36**, 109-26.

**Xie, X. S., Padron, D., Liao, X., Wang, J., Roth, M. G. and De Brabander, J. K.** (2004). Salicylilalamide A inhibits the V<sub>O</sub> sector of the V-ATPase through a mechanism distinct from bafilomycin A1. *J. Biol. Chem.* **279**, 19755-63.

**Xu, T. and Forgac, M.** (2001). Microtubules are involved in glucose-dependent dissociation of the yeast vacuolar H<sup>+</sup>-ATPase in vivo. *J. Biol. Chem.* **276**, 24855-61.

**Yokoyama, K. and Imamura, H.** (2005). Rotation, structure, and classification of prokaryotic V-ATPase. *J. Bioenerg. Biomembr.* **37**, 405-10.

**Yokoyama, K., Nakano, M., Imamura, H., Yoshida, M. and Tamakoshi, M.** (2003). Rotation of the proteolipid ring in the V-ATPase. *J. Biol. Chem.* **278**, 24255-8.

**Zhang, J., Feng, Y. and Forgac, M.** (1994). Proton conduction and bafilomycin binding by the V<sub>O</sub> domain of the coated vesicle V-ATPase. *J. Biol. Chem.* **269**, 23518-23.

**Zhang, J., Myers, M. and Forgac, M.** (1992). Characterization of the V<sub>O</sub> domain of the coated vesicle H<sup>+</sup>-ATPase. *J. Biol. Chem.* **267**, 9773-8.

**Zhang, Z., Zheng, Y., Mazon, H., Milgrom, E., Kitagawa, N., Kish-Trier, E., Heck, A. J., Kane, P. M. and Wilkins, S.** (2008). Structure of the yeast vacuolar ATPase. *J. Biol. Chem.* **283**, 35983-95.

## **7. Appendix**

### **7.1 Abbreviations**

ATP	Adenosine triphosphate
APS	Ammonium persulfate
BCIP	5-bromo-4-chloro-3-indolyl-phosphate
bp	Base pair
BSA	Bovine serum albumin
Da	Dalton
DMF	Dimethyl formamide
DMSO	Dimethyl sulfoxide
DNA	Deoxyribonucleic acid
dNTP	2-Deoxynucleoside-5-triphosphate
DTT	Dithiothreitol
EDTA	Ethylenediaminetetraacetic acid
IC <sub>50</sub>	half maximal inhibitory concentration
LB	Lucia Bertani
MES	2-(N-morpholino)ethanesulfonic acid
MOPS	3-(N-morpholino)propanesulfonic acid
NBT	Nitro blue tetrazolium
OD	Optical density
rpm	Rounds per minute
SD	Synthetic defined
SDS	Sodium dodecyl sulfate
TAE	Tris acetate EDTA
TCA	Trichloric acid
TE	Tris EDTA
TEMED	Tetramethylethylenediamine
Tris	tris(hydroxymethyl)aminomethane
U	Unit
v/v	Volume per volume percentage
w/v	Weight per volume percentage
x g	Times gravitational acceleration

## 7.2 Vector maps

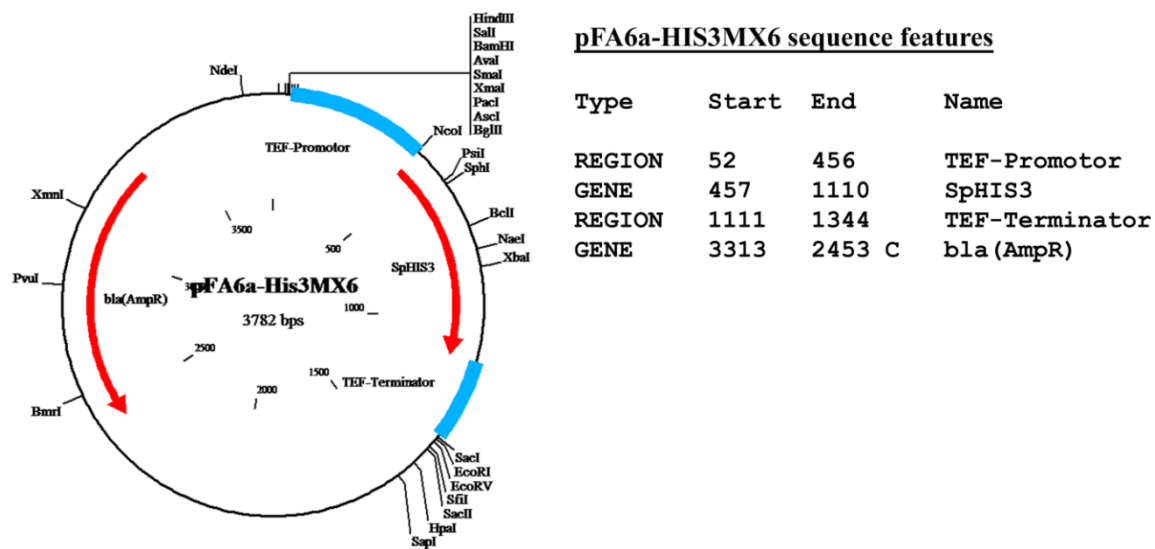


Figure 7.1: Vector map and features of pFA6a-HIS3MX6

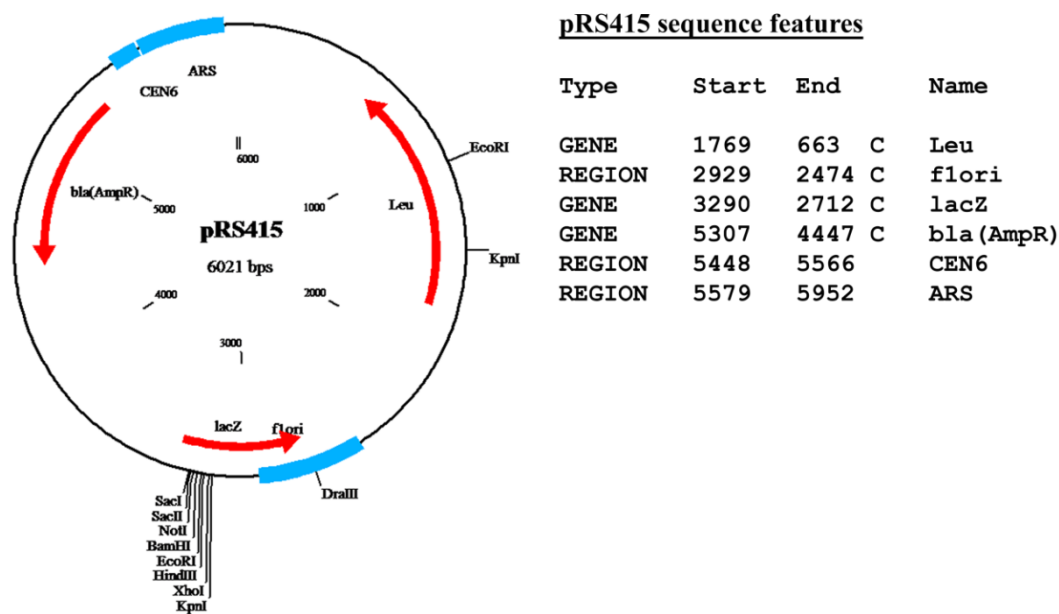


Figure 7.2: Vector map and features of pRS415

### 7.3 Curriculum Vitae

#### Personal Data

Name:	Svenja Bockelmann
Address:	Küsterskamp 12 49134 Wallenhorst
Contact:	05407/8139865 svenjabockelmann@aol.com
Day of Birth:	04.07.1981
Birth place:	Lüneburg
Marital status:	unmarried

#### Studies and education

2007-2011	PhD student at the University of Osnabrück, Section of animal physiology supported by the VolkswagenStiftung funding initiative “Interplay between Molecular Conformations and Biological Function” Thesis titel: “Molecular interactions of archazolid with the V-ATPase”
2000-2006	Studies in biology at the University of Osnabrück, Diploma in biology Diploma thesis at the Department of Biology/Chemistry, Section of animal physiology, Thesis title: “Heterologe Expression von V-ATPase-Untereinheiten in <i>Saccharomyces cerevisiae</i> “
1993 - 2000	Wilhelm-Raabe-Schule Lüneburg, Abitur (High school graduation)

#### 7.4 Publications

**Bockelmann, S., Menche, D., Rudolph, S., Bender, T., Grond, S., von Zezschwitz, P., Muench, S. P., Wieczorek, H. and Huss, M.** (2010). Archazolid A binds to the equatorial region of the c-ring of the vacuolar H<sup>+</sup>-ATPase. *J. Biol. Chem.* **285**, 38304-14.

**Horstmann, N., Essig, S., Bockelmann, S., Wieczorek, H., Huss, M., Sasse, F. and Menche, D.** (2011). Archazolid A-15-O- $\beta$ -d-glucopyranoside and iso-Archazolid B: Potent V-ATPase Inhibitory Polyketides from the Myxobacteria *Cystobacter violaceus* and *Archangium gephyra*. *J. Nat. Prod.* **74**, 1100-1105.

**Huss, M., Vitavska, O., Albertmelcher, A., Bockelmann, S., Nardmann, C., Tabke, K., Tiburcy, F. and Wieczorek, H.** (2011). Vacuolar H<sup>+</sup>-ATPases: Intra- and intermolecular interactions. *Eur. J. Cell Biol.* **90**, 688-695.

### 7.5 Erklärung über die Eigenständigkeit der erbrachten wissenschaftlichen Leistung

Ich erkläre hiermit, dass ich die vorliegende Arbeit ohne unzulässige Hilfe Dritter und ohne Benutzung anderer als der angegebenen Hilfsmittel angefertigt habe. Die aus anderen Quellen direkt oder indirekt übernommenen Daten und Konzepte sind unter Angabe der Quelle gekennzeichnet.

Bei der Auswahl und Auswertung folgenden Materials haben mir die nachstehend aufgeführten Personen in der jeweils beschriebenen Weise entgeltlich / unentgeltlich geholfen.

1. Im Rahmen von Abschlussarbeiten wurden einige Laborarbeiten gemeinsam mit Studenten durchgeführt. Dabei haben folgende Personen zu den angegebenen Abbildungen und Tabellen beigetragen:  
Johanna Bahr (Diplom) und Katja Finsterbusch (Master): Fig. 3.1 und 3.2  
Lena Dieckmann (Bachelor): Fig. 3.8 und 3.9  
Maren Oude Lansink (Bachelor): Fig. 3.8, 3.9 sowie Tab. 3.3 und 3.4  
Nicole Meyer (Diplom): Fig. 3.8, 3.9, 3.10 sowie Tab. 3.3 und 3.4  
Mareike Nolte (Bachelor): Fig. 3.11, 3.12, 3.13 sowie Tab. 3.5 und 3.6
2. Im Rahmen von Großpraktika haben folgende Personen zu den angegebenen Abbildungen und Tabellen beigetragen:  
Denise Beckmann: Fig. 3.8 und 3.9 sowie Tab. 3.3 und 3.4  
Mareike Fröhling: Fig. 3.12 und 3.13
3. Die Aufnahmen zur Electron Paramagnetic Resonance Spektroskopie (Fig. 3.18, 3.19 und 3.20) wurden im Rahmen einer Kooperation mit der Abteilung Makromolekülstruktur des Fachbereichs Physik der Universität Osnabrück von Dr. J. P. Klare angefertigt.

Weitere Personen waren an der inhaltlichen materiellen Erstellung der vorliegenden Arbeit nicht beteiligt. Insbesondere habe ich hierfür nicht die entgeltliche Hilfe von Vermittlungs- bzw. Beratungsdiensten (Promotionsberater oder andere Personen) in Anspruch genommen. Niemand hat von mir unmittelbar oder mittelbar geldwerte Leistungen für Arbeiten erhalten, die im Zusammenhang mit dem Inhalt der vorgelegten Dissertation stehen. Die Arbeit wurde bisher weder im In- noch im Ausland in gleicher oder ähnlicher Form einer anderen Prüfungsbehörde vorgelegt.

.....  
(Ort, Datum)

.....  
(Unterschrift)



## **8. Acknowledgements**

Zuallererst danke ich Prof. Dr. Helmut Wieczorek für die Betreuung während meiner Promotion sowie für Anregungen und Ratschläge, die für den experimentellen wie auch den theoretischen Bereich dieser Arbeit sehr wertvoll waren.

Bei Prof. Dr. Karlheinz Altendorf bedanke ich mich für die Übernahme des Zweitgutachtens und für viele interessante Vorlesungen, die mein Biologiestudium bereichert haben.

Prof. Dr. Heinz-Jürgen Steinhoff danke ich für die bereitwillige Teilnahme an der Prüfungskommission sowie für alle Anregungen und Ratschläge zu den EPR Messungen.

Dr. Markus Huss gilt ebenfalls besonderer Dank für die Betreuung meiner Promotion, seine beständige Hilfsbereitschaft hat mir über manche Tiefschläge im Labor hinweggeholfen. Außerdem danke ich ihm für die hilfreichen Anmerkungen zu dieser Arbeit und die Teilnahme an der Prüfungskommission.

Mein besonderer Dank gilt Dr. Johann P. Klare dafür, dass er mich auf meinen ersten Schritten durch die Wirren der EPR Spektroskopie begleitet und diese für mich verständlich gemacht hat. Danke auch für die Beharrlichkeit, wenn das Protein (oder der Inhibitor) mal wieder nicht so wollte wie die Wissenschaftler.

Prof. Dr. Dirk Menche und Dr. Teresa Carlomagno danke ich für die anregenden Diskussionen und die gute Zusammenarbeit im Rahmen des Projektes „Conformation-activity relationship of the Archazolids: Development of a novel class of highly potent V-ATPase inhibitors“ (VolkswagenStiftung). Sandra Dreisigacker danke ich für den sehr hilfreichen Informationsaustausch über neueste Forschungsergebnisse.

Mein Dank gilt allen Studenten die ich während meiner Promotion betreut habe, davon im Besonderen Johanna Bahr, Katja Finsterbusch und Nicole Meyer, die mir sehr dabei geholfen haben, die nicht enden wollende Fülle an Aktivitätstests zu bewältigen.

Im Besonderen danke ich auch Martin Dransmann für seine unermüdliche Hilfsbereitschaft und Motivation, die mich aus mancher misslichen Lage befreien konnten und mir die Arbeit sehr erleichtert haben. Martin, du kannst den Spitznamen „Raupenschlichter“ mit Stolz tragen! An dieser Stelle danke ich auch Gundula Key für die beständige Versorgung mit Hefevakuolen.

Bei apl. Prof. Dr. Hans Merzendorfer bedanke ich mich für die vielen Gespräche und Anregungen, die mir bei der Planung meines wissenschaftlichen Lebens sehr hilfreich waren, sowie für die unterhaltsamen Gespräche, die den Laboralltag aufgelockert haben.

I thank Dr. Seléne van der Poel and Dr. Gunnar Bröhan for helpful comments on the manuscript. Seléne I also thank for the numberless encouraging visits at the Pizzaria and the Ratskeller during her time in Osnabrück as well as for the kind accommodation during my visit in Utrecht. Gunnar danke ich besonders für die sehr lustigen Jahre im Labor, aber auch für die Auseinandersetzungen, wenn unsere Temperamente sich mal wieder nicht vertragen haben. Danke auch für die vielen Ratschläge und Hilfestellungen, die mir das Laborleben sehr erleichtert haben.

Meiner Kollegin Christin Nardmann danke ich herzlich für die äußerst harmonische Zusammenarbeit und die vielen lustigen Unterhaltungen und Unternehmungen wäh-

rend der letzten Jahre. Herzlicher Dank gebührt auch Felix Tiburecy, der mich gnädig als Büro-Mitbewohnerin aufgenommen (und erduldet) hat und wider alle Hindernisse immer um eine heitere Stimmung im Labor bemüht war. Katharina Tabke, Dr. Derek Meissner, Dr. Olga Vitavska, Dr. Andrea Albertmelcher, PD Dr. Thomas Krüppel und Harald Mikoleit danke ich ebenfalls für die gute Zusammenarbeit im Laboralltag.

Herzlicher Dank gilt meinen Line Dance-Freundinnen Margret Düvel und Gundula Key, die neben dem Laboralltag auch meine Freizeit bereichern haben. Ich danke euch sehr für die jahrelange Unterstützung und hoffe, dass wir auch in Zukunft noch den einen oder anderen Tanz aufs Parkett bringen. Hallelujah! Oder Yee-Haw?

Ein großes „Danke!“ auch an Manuela Teske, Tanja Mundt-Kempen, Katrin Blawat und Anne Saure, die mich in den letzten Jahren besonders in schwierigen Phasen unterstützt und ermutigt haben.

Großer Dank gilt auch meinen Eltern, die mich in allen Lebenslagen bedingungslos unterstützt und somit maßgeblichen Anteil an der Entstehung dieser Arbeit haben.